

DESIGN & FABRICATION OF A MICROFLUIDIC
DEVICE FOR CLINICAL OUTCOME
PREDICTION OF SEVERE SEPSIS

DESIGN & FABRICATION OF A MICROFLUIDIC DEVICE
FOR CLINICAL OUTCOME PREDICTION OF
SEVERE SEPSIS

By

JUN YANG, B.ENG.

B. Eng. (Tianjin University, Tianjin, China)

A Thesis

Submitted to the School of Graduate Studies

In Partial Fulfillment of the Requirements

For the Degree

Master of Applied Science

McMaster University

© Copyright by Jun Yang, December 2014

MASTER OF APPLIED SCIENCE (2014)

McMaster University

(Biomedical Engineering)

Hamilton, Ontario, Canada

TITLE

DESIGN & FABRICATION OF A MICROFLUIDIC
DEVICE FOR CLINICAL OUTCOME PREDICTION OF
SEVERE SEPSIS

AUTHOR

JUN YANG, B.Eng.

SUPERVISOR

Professor P. R. Selvaganapathy, Associate Professor

Department of Mechanical Engineering

NUMBER OF PAGES

xviii, 155

Abstract

Sepsis is an uncontrolled response to infection. Severe sepsis is associated with organ dysfunction, and has mortality rate of 30-50%. Identification of severity of sepsis and prediction on mortality is crucial in making clinical decisions. Recently, cell-free DNA (cfDNA) in blood was found to have high discriminative power in predicting ICU mortality in patients with severe sepsis. In an analysis of 80 severely septic patients, the mean cfDNA level in survivors ($1.16 \pm 0.13 \mu\text{g/ml}$) was similar to that of healthy volunteers ($0.93 \pm 0.76 \mu\text{g/ml}$), while that of non-survivors ($4.65 \pm 0.48 \mu\text{g/ml}$) was notably higher. Therefore, rapid quantification of cfDNA concentration in blood will enable physicians to quickly predict mortality of sepsis and decide on treatment.

Current methods for quantification of cfDNA involve multiple steps including centrifugation, DNA-extraction from plasma, and its quantification either through spectroscopic methods or quantitative PCR. The whole process is time consuming, thus is not suitable for immediate bedside assessment. To solve the problems, a microfluidic device is designed and fabricated in this thesis, which is potential for cfDNA quantification directly using blood in 5 minutes. The goal is to use this device for distinguishing survivors or healthy donors from non-survivors in patients with severe sepsis.

The two-layer device consists of a sample channel (top) and an accumulation channel (bottom) that intersect each other. The accumulation channel is preloaded with 1% agarose gel, and the blood containing cfDNA and intercalating fluorescent dye is loaded in the sample channel. Fluorescently labeled DNA is able to be trapped and concentrated at the intersection using a DC electric field, and fluorescent intensity of the accumulated DNA is representative of its concentration in the blood. The simulated electric field in the sample channel reveals that both the magnitude and the gradient of electric field reach their maximum values at the intersection. Force analysis shows that DNA was driven into the gel by the dominate electrophoretic force, while red blood cells moved away from the gel due to a strong dielectrophoretic force.

In this thesis, 4 types of samples have been used to characterize the performance of the device. It showed that DNA was efficiently accumulated at the intersection, and the fluorescent intensity could be measured using a fluorescent microscope. Samples from healthy donors were able to be distinguished from that of severely septic patients in 5 minutes. However, better resolution was needed for differentiating various cfDNA concentrations in patient samples. The discussion on the effect of applied voltage showed that 9V is an optimized setting compared with 3V and 15V. In addition, it has been proved that the fluorescent reagent could be immobilized in the device and the sample preparation could be absolutely eliminated.

In summary, the device proposed in this thesis is capable of distinguishing severely septic patients from healthy donors using clinical plasma in 5 minutes, and is potential to be applied in clinical blood samples. It has low cost, and is ready to be developed into a fully functioned system. This tool can be a valuable addition to the ICU to rapidly assess the severity of sepsis for informed decision making.

Acknowledgement

It has been a long and tough process to complete this thesis, but it has also proved to be a great reflection period and learning process. I have had many great memories during the past two years at McMaster University, which I've shared with the amazing people around me. It would have been impossible for me to complete my master's studies without them.

Dr. P. Ravi Selvaganapathy has been an incredible supervisor who not only helped me through my thesis writing, but also guided me on various project directions as well as improving my poster/oral presentation skills. He provided me with a free and flexible research environment, and made himself readily available whenever I had any problems. I sincerely appreciate his guidance, patience and tolerance throughout my Master's, which has led to my growth.

I am also very grateful for my colleagues who have continuously supported me as well. Many thanks to Leo Hsu, Allison Yeh, Chao Zhu, Wen-I Wu and Bo Dang for their endless aid during experiments and my daily life as an international student. I will never forget Rana Attalla and Rahul Sadavarte who helped me to polish up my thesis and provide insight on my various projects. I also want to thank Sarah Nangle, Stephen Woo, Conrad P. Rockel, Jieting Shang, Celine Ling, Scott Campbell, Nehad Hirmiz, and Yujie

Zhu, who generously provided me with useful suggestions and ideas. I really enjoyed working with all my CAMEF lab mates who are creative, funny and always ready to help. I will miss this fantastic working atmosphere where I have spent the past 2 years of my life.

My thesis is based on a collaborative project with another group from Department of Medicine at McMaster University. My sincere gratitude goes to Dr. Dhruva Dwivedi, Dr. Alison Fox-Robichaud and Dr. Patricia C. Liaw who provided me with their lab resources to complete this project.

Finally, outside of my work, I would really like to thank my girlfriend Joyce Yeh who brightened up my tough days and made them more bearable. Thanks to my parents, Guangming Yang and Houxian Chen, for their support, both spiritually and financially. None of this could have been possible without them. I would also thank my friends who brought me so much amazing memories.

To all these people, I am forever grateful. It's not that I met them during the best of times, but it is them that helped make this the best of times. My gratitude goes to all who guided, helped and cared about me.

Table of Contents

Abstract	ii
Acknowledgement	v
Table of Contents	vii
List of Figures	xi
List of Tables	xviii
Chapter 1. Motivation and Organization	1
1.1 Motivation.....	1
1.2 Organization of the Chapters.....	2
Chapter 2. Introduction	5
2.1 Sepsis.....	5
2.2 Severe Sepsis and Mortality Rate among Patients.....	6
2.3 Current Methods to Evaluate Disease Severity: Scoring Systems.....	7
2.3.1 General Scoring Systems.....	8
2.3.2 Disease or Organ-specific Scoring Systems.....	9
2.3.3 Organ Dysfunction (OD) Scoring Systems.....	9
2.4 Biomarkers for Severe Sepsis Prognostication.....	11
2.4.1 Sepsis Biomarkers.....	11
2.4.2 Current State of Sepsis Biomarkers Development.....	11
2.4.3 Circulating Cell-free (cfDNA).....	13
2.4.4 Cell-free DNA for Severe Sepsis Prognostication.....	14
2.5 Current Methods for DNA Quantification.....	16
2.5.1 Sample Preparation Prior to DNA Quantification.....	16
2.5.2 DNA Quantification Methods.....	19

2.5.3 A Direct DNA Quantification Method.....	24
2.5.5 Summary of Current DNA Quantification Methods.....	26
2.6 Microfluidic Sample Preparation	27
2.6.1 Microfluidics	28
2.6.2 Advantages of Microfluidics.....	29
2.6.3 Current Microfluidic Devices for DNA Extraction and Concentration.....	32
2.7 Summary	44
Chapter 3. Device Design and Working Principle	46
3.1 Forces Affecting Transport of DNA and Cells	46
3.1.1 Hydrodynamic drag force	47
3.1.2 Electrophoretic (EP) Force.....	47
3.1.3 DC Dielectrophoretic (DEP) Force.....	50
3.1.4 Electro osmotic force	52
3.2 Device Design and Working Principle	54
3.2.1 Design Criteria	54
3.2.2 Device Design.....	56
3.3 Modeling and Force Analysis	60
3.3.1 Numerical Simulation of the Electric Field	60
3.3.2 Force Analysis	65
3.4 Summary	68
Chapter 4. Device Fabrication and Experimental Preparation.....	70
4.1 Device Fabrication	70
4.1.1 Materials Used	70
4.1.2 Fabrication Steps and Methods	73
4.2 Sample Preparation	76
4.2.1 Materials	76

4.2.2 Sample preparation	81
4.3 Sample Loading and Experimental Setup.....	82
4.3.1 Sample loading.....	82
4.3.2 Experimental setup.....	82
4.4 Image Processing Methods	83
4.4.1 Average gray scale measurement.....	84
4.4.2 Relative Gray scale measurement	84
4.5 Summary	85
Chapter 5. DNA Accumulation and Characterization	87
5.1 Demonstration of DNA Accumulation	87
5.2 DNA Concentration from Complex Samples	91
5.2.1 Sample Type 1- DNA in Buffer.....	91
5.2.2 Sample Type 2- DNA Spiked Plasma.....	94
5.2.3 Sample Type 3- Clinical Plasma.....	100
5.2.4 Sample Type 4- DNA Spiked Whole Blood.....	105
5.3 Effect of Applied Voltage on DNA Accumulation.....	107
5.4 Immobilization of Reagents and Elimination of Sample Preparation.....	112
5.5 Summary	115
Chapter 6. Contributions and Future Work	117
6.1 Contributions.....	117
6.1.1 A Direct DNA Quantification Method.....	117
6.1.2 A Low Cost Device.....	118
6.1.3 A Variety of Potential Applications.....	119
6.2 Future Work	120
6.3 Summary	121
Reference.....	123

Appendix A: Model Setup in COMSOL Simulation	137
Appendix B: Mesh Dependence Test in COMSOL Simulation.....	143
Appendix C: Device Fabrication	147
Appendix D: Force Calculation	152

List of Figures

Figure 2.1 The relationship between SIRS, sepsis, and infection [8].....	5
Figure 2.2 Sepsis hospitalization rate in Canada; Source: Discharge Abstract Database, Canadian Institute for Health Information [9].	7
Figure 2.3 The mechanism of DNA release [18].....	14
Figure 2.4 Temporal changes in levels of cfDNA in 50 patients with severe sepsis [5]. Survivors are shown by white circles (o), and non-survivors are shown by black circles (●). The number of patients at each time point is indicated. The mean levels of cfDNA in healthy volunteers (n= 14) is shown by the arrows. Error bars represent standard error of mean (SEM).	15
Figure 2.5 DNA isolation procedures using a commercial kit (Norgen Biotek Corp., ON, Canada): DNA is bound to Norgen's column under optimized salt concentrations (BIND), and other contaminants can be washed and flow away (WASH). Purified DNA is finally eluted into clean buffer (ELUTE). https://norgenbiotek.com/display-product-blood-genomic-dna.php?ID=495	18
Figure 2.6 Fluorescent staining quantification method: (a) an example of DNA mass ladder with low DNA size range [31]. The dye was ethidium bromide. Electrophoresis was conducted in 2% agarose gel. (b) Fluorescent intensity increase in a typical qPCR process [32].....	22

Figure 2.7 Various microfluidic devices using silica absorptive extraction method. Different silica microstructures like (a) micropillars [46][48]; (b) microbeads, silica particles, sol-gels or their combination[49]; and (d) porous monoliths [50] have been developed.	34
Figure 2.8 Microfluidic devices using both AC EOS flow and EP/DEP force to concentrate DNA onto the surface of electrodes with various geometries: (a) design of an electrokinetic concentrator [52][53]; (b) two identical half-quadrupole electrode sets [54]; (c) coplanar plate microelectrode array and the experimental setup [55][56].	36
Figure 2.9 (a) A microfluidic device extracting DNA onto microtips in human buccal swab or saliva samples; (b) the working principle of DNA extraction with the microtip [59][60].	38
Figure 2.10 Microfluidic devices for DNA concentration using DC electric fields with various structures: (a) micro electrode arrays [61]; (b) permeable polymer barriers [62]; and (c) hydrogel microplug [63].	39
Figure 2.11 Other DNA extraction devices: (a) pH-induced electrostatic extraction with various channel geometries [64][65]; (b) filtration using a porous AlO _x membrane [66]; (c) a PPC microfluidic chip with a DNA immobilization bed [69].	43

Figure 3.1 Schematic of a negatively charged particle in solution where mobile ions exist. The size of ions and EDL is exaggerated for the purpose of the figure. The yellow circle represents the Stern Layer.	48
Figure 3.2 Generation of a negative dielectrophoretic force in a non-uniform DC electric field. The dash lines represent electric field.	51
Figure 3.3 Schematic of the electrical double layer (EDL, the yellow area) and generation of the electroosmotic flow.....	53
Figure 3.4 Schematic of the device: (a) an overview of the device; (b) a top-view and cross-sectional view of the intersection.	57
Figure 3.5 Schematic of the model built in COMSOL: (a) the geometry of the model; (b) the ground boundary condition definition; (c) the positive charge boundary condition definition.	62
Figure 3.6 Simulated results of: (a) potential drop between the two electrodes; (b) potential drop at the intersection. The difference between each line is 0.05V; (c)&(d) the electric field strength at the intersection. The difference between each line in (c) is 0.5mV/ μm	63
Figure 3.7 Electric field magnitudes of the selected sites in the sample channel. The plane selected was 1 μm above the bottom of the sample channel: (a) the locations of the 3 lines along which the magnitude of electric field was simulated. The yellow area	

represents the intersection; (b) the simulated electric field strength along the 3 lines.	
The red area along the x-axis indicates the accumulation channel location.	65
Figure 3.8 Directions of EP force (red arrows) and DEP force (black arrows) in a plane 1 μ m above the bottom of sample channel. The arrow sizes are proportional to the magnitude of EP force and DEP forces respectively. The yellow area represents the intersection.	66
Figure 3.9 Electrokinetic forces analysis for (a) a DNA molecule and (b) a red blood cell in the sample channel close to the intersection. <i>E</i> represents electric field strength.	67
Figure 4.1 Schematic of Device Fabrication Process	71
Figure 4.2 Device assembly	75
Figure 4.3 Gel filling process: agarose gel is represented in yellow.	76
Figure 4.4 Properties of PicoGreen reagent: the emission fluorescence was measured at 520nm using a spectrofluorometer. (a) linearity and sensitivity of PicoGreen at low dsDNA concentration range (<1 μ g/ml); (b) fluorescence enhancement of PicoGreen upon binding dsDNA, ssDNA, and RNA; (c) PicoGreen fluorescence excitation spectra (dash line) and emission spectra (green area).....	79
Figure 4.5 Sample loading and experimental setup: sample is represented in red.	83
Figure 4.6 A 4-minute DNA accumulation result with DNA in buffer sample in the device: the dash lines are the outline of accumulation channel; (a) RGB fluorescent	

image; (b) 8-digit gray scale image. Mean gray scale value is measured and calculated in the area enclosed by red lines.	85
Figure 4.7 A 5-minute DNA accumulation result with clinical plasma sample in the device: the dash lines label the boundary of accumulation channel; <i>M1</i> and <i>M2</i> represent areas for gray scale value calculation.	85
Figure 5.1 Experiment demonstrating DNA accumulation: (a) fluorescent images taken at time points of 0, 5, and 10min. The dash lines represent the outlines of the sample channel and the accumulation channel; (b) fluorescent intensity curve with no voltage applied (blue) and with 9V applied (red). Error bars represent standard deviation (SD).	89
Figure 5.2 Experimental results using DNA in buffer sample: error bars represent standard deviation (SD). 9V was applied; (a) fluorescent images taken at time intervals of 0, 1, 2, and 4min demonstrating the DNA accumulation process at the intersection with 1 μ g/ml and 5 μ g/ml DNA concentration; (b) fluorescent intensity curves during DNA accumulation; (c) fluorescent intensity values at the beginning (0 min) and the end (4 min) of DNA accumulation.	92
Figure 5.3 Experimental results using DNA spiked plasma sample: error bars represent standard deviation (SD). 9V was applied; (a) fluorescent images taken at time intervals of 0, 1, 2, and 4min demonstrating the DNA accumulation process at the intersection with 0.8 μ g/ml and 4.2 μ g/ml DNA concentration; (b) fluorescent	

intensity curves during DNA accumulation; (c) fluorescent intensity values at the beginning (0 min) and the end (4 min) of DNA accumulation.....96

Figure 5.4 Experimental results using the clinical plasma sample: error bars represent standard deviation (SD). 9V was applied; (a) fluorescent images taken at time intervals of 0, 1, 3, and 5min demonstrating the DNA accumulation process at the intersection with samples from healthy donors (healthy samples, 0 μ g/ml) and samples from severe septic patients with various concentration (patient samples, 6 μ g/ml, 10 μ g/ml and 4.2 μ g/ml); (b) fluorescent intensity at the beginning (0 min) and the end (4 min) of DNA accumulation; (c) a zoom-in-view of the data in (b). 101

Figure 5.5 Experimental results using DNA spiked whole blood sample: error bars represent SD. 9V was applied. The concentration of 0 μ g/ml represents whole blood with no extraneous DNA added. (a) fluorescent images taken at time intervals of 0, 1, 3, and 5min demonstrating the DNA accumulation process at the intersection with samples of no DNA added, 1 μ g/ml and 5 μ g/ml DNA added; (b) fluorescent intensity at the beginning (0 min) and the end (5 min) of DNA accumulation. 106

Figure 5.6 Experimental results using 1.6 μ g/ml DNA spiked plasma sample with 3V, 9V, and 15V applied on the device: error bars represent SD. (a) fluorescent images at the intersection after applying various voltages for 5 minutes; (b) fluorescent intensity values at the beginning (0 min) and the end (5 min) of DNA accumulation; (c) fluorescent intensity curves during DNA accumulation. 109

Figure 5.7 Fluorescent images taken at time intervals of 0, 1, 3, and 5min with PicoGreen-integrated device (with PicoGreen) and regular device (without PicoGreen); 9V was applied. The sample was 5 μ g/ml DNA spiked plasma with no PicoGreen added in the solution. 114

List of Tables

Table 2.1 Comparison of DNA extraction and concentration methods with regards to the fast DNA quantification purpose in this thesis.	45
Table 4.1 Effects of contaminants on the fluorescent intensity of PicoGreen in the presence of 500ng/mL calf thymus DNA: a. the change in fluorescence signal observed with the indicated concentration of assay contaminant relative to the presence of no contaminant in the assay; b. volume/volume; c. weight/volume [93].	78
Table 5.1 The electric current variation in the device with different voltages applied. The initial current implies the current upon applying the electric field; the final current represents the current at the end of DNA accumulation; the current drop indicates the decreased value between the initial current and final current. The total time for electric field application is 5 minutes.	111

Chapter 1.

Motivation and Organization

1.1 Motivation

Sepsis is defined as a systemic inflammatory syndrome in response to infection. When acute organ dysfunction happens on the patient, the condition is specified as severe sepsis [1]. According to the Surviving Sepsis Campaign in 2008, the sepsis-associated mortality rate is at 30-50% in Canada [2]. With such a high mortality rate, identification of severity of sepsis is crucial in making clinical decisions. Current commonly used scoring systems only focus on physiological variables and do not have sufficient discriminative power [3]. Therefore, biomarkers that can serve as prognostic indicators have been actively sought. Although various biomarkers such as C-reactive protein, procalcitonin, serum amyloid A, mannan and IFN- γ -inducible protein 10 are being investigated, none of them have been accepted as highly reliable clinical outcome predictor of severe sepsis [4].

Recently, cell-free DNA (cfDNA) in blood was found to have high discriminative power in predicting ICU mortality in patients with severe sepsis [5]. In an analysis of 80 severely septic patients, the mean cfDNA levels in survivors ($1.16 \pm 0.13 \mu\text{g/ml}$) was

similar to that of healthy volunteers ($0.93\pm 0.76\mu\text{g/ml}$), while that of non-survivors ($4.65\pm 0.48\mu\text{g/ml}$) was notably higher [5]. As a result, rapid quantification of cfDNA concentration in blood will enable physicians to quickly assess severity of sepsis and decide on treatment.

Current commonly used methods for quantifying cfDNA requires the sample preparation which involves multiple steps including centrifugation, plasma separation from blood cells, and DNA isolation from plasma [6]. The quantification is completed either through spectroscopic methods or quantitative PCR [7]. The whole process is time-consuming and complicated, thus is not suitable for immediate bedside assessment. Therefore, a device which can perform rapid quantification of cfDNA directly in whole blood is in need.

This thesis focuses on developing a microfluidic device which can fast distinguish blood samples of non-survivors and that of survivors in severe septic patients, and the device is potential to quantify cfDNA directly in blood. This thesis also provides proof-of-concept experiments to show the possibility of a zero sample preparation process in which a droplet of blood can be directly loaded into the device and be quantified.

1.2 Organization of the Chapters

The thesis is organized in the following chapters:

Chapter 2 provides a comprehensive background review on the thesis. Sepsis and its mortality rate are introduced. Current scoring systems and biomarkers on study are evaluated. Cell-free DNA (cfDNA) is introduced and the correlation between sepsis prognosis and cfDNA is emphasized. Current commonly used DNA quantification approaches are summarized, which provides a strong reference for developing the device in the thesis.

Chapter 3 presents the device design and the working principle of the device. The forces acting on a particle in a DC electric field are introduced. The device developed is displayed, and the electric field in the channels is simulated using COMSOL. Principle forces on DNA and cells, such as the electrophoretic force, are calculated and compared which illustrates in Appendix D.

Chapter 4 describes the device fabrication and experimental setup in detail. Techniques including photolithography and soft-lithography are described. Materials used for device assembly and sample preparation are introduced. Experimental setup and steps are demonstrated, and image processing methods for characterizing the fluorescent intensity of labelled DNA are listed at the end of this chapter. A step-by-step device fabrication procedure is summarized in Appendix C.

Chapter 5 includes all the experimental data obtained using the device. A proof-of-concept experiment is shown to demonstrate the DNA accumulation in the device. Experimental results with various samples and different voltages applied are presented

and discussed. At the end of the this chapter, a preliminary experiment realizing a zero sample preparation is shown, in which the sample can be directly loaded and measured in the device.

Chapter 6 highlights the conclusions of the results and the contribution of the device. Future work is pointed out in the end.

Chapter 2.

Introduction

2.1 Sepsis

Sepsis is defined as a type of Systemic Inflammatory Response Syndrome (SIRS) developed from infection [8]. As shown in **Figure 2.1**, an uncontrolled inflammatory response to infection causes sepsis which is one among the various types of SIRS.

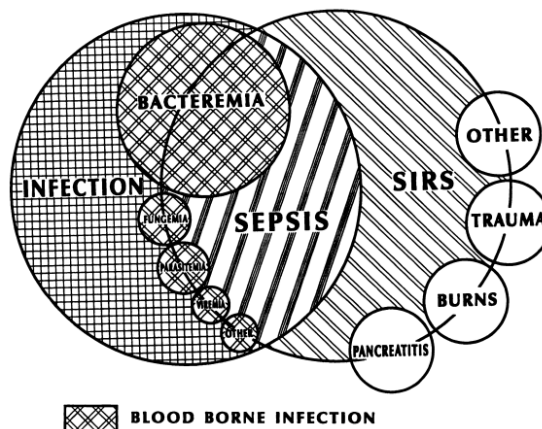


Figure 2.1 The relationship between SIRS, sepsis, and infection [8]

In clinical practice, sepsis is characterized by several physiological abnormal changes including temperature ($<36^{\circ}\text{C}$ or $>38^{\circ}\text{C}$), heart rate (>90 beats/min), white blood

cell count ($<4000/\text{cumm}$ or $>12,000/\text{cumm}$), and so on [8]. Being an increasingly common cause of morbidity and mortality in patients, especially in elderly, prognosis and treatment of sepsis is becoming increasingly important [9].

2.2 Severe Sepsis and Mortality Rate among Patients

Progression of septic condition may lead to severe sepsis in which one or more organ dysfunction, such as renal failure, is evident in addition to inflammation and infection [8].

Based on reviews in Canada, both the hospitalization rate and mortality rate are remarkably high. Figure 2.2 demonstrates the hospitalization rates of septic patients from 2004 to 2009 in Canada, among which elderly groups and young children amounted for the majority [9]. According to the Surviving Sepsis Campaign in 2008, the sepsis-associated mortality rate is at 30-50% [10]. For severe septic patients, the mortality rate was slightly above 38% based on a prospective observational study of 12 Canadian community and teaching hospital critical care units [10].

In addition, due to the large number of septic patients and the necessity of using intensive care units (ICUs) for severe sepsis patients, the personal and social resource costs of sepsis are high, especially for severe sepsis [10].

Due to the reasons mentioned above, mortality prediction of severe sepsis patients and evaluation of their severity is of great significance. It helps in clinical decision making and better allocation of hospitals' resources [9]. With a relatively clear and precise assessment on the risk of death, a more comprehensive and timely treatment can be arranged for a patient. Therefore, intensive efforts have been made to determine reliable predictors to evaluate the severity of septic patients' condition. These predictors could also be quite useful in monitoring the effect of treatment on patients [5].

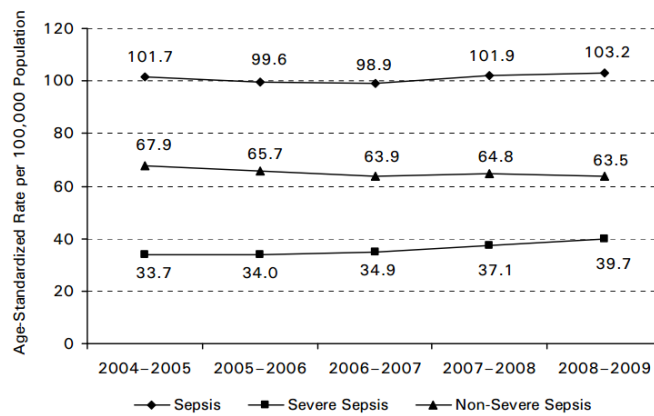


Figure 2.2 Sepsis hospitalization rate in Canada; Source: Discharge Abstract Database, Canadian Institute for Health Information [9].

2.3 Current Methods to Evaluate Disease Severity: Scoring Systems

In order to decide on the severity of illness for patients in ICU, various scoring systems have been developed and widely applied in clinical practice today. These scoring

systems are currently a crucial tool for disease severity evaluation, but have a number of limitations. Based on specificity and emphasis of the patient's condition, there are 3 main categories of scoring systems [11].

2.3.1 General Scoring Systems

The basic idea of this type of scoring system is to evaluate the abnormality of patients' physiological variables, which is assumed to be related with disease severity. More sophisticated models have been applied in these systems recently to make the evaluation more precise [12]. Several commonly used scoring systems belong to this category, such as *Acute Physiology and Chronic Health Evaluation (APACHE)*, *mortality prediction model (MPM)*, and *Simplified Acute Physiology Score (SAPS)* scoring systems [11].

Although these systems have been validated and widely used, there are some limitations [11] including 1) all of the systems are only focused on patients' physiological abnormalities, ignoring other potential measurable variables; 2) the discriminative power and predictive ability varies among patients with distinct individual conditions, and discrimination and calibration of the systems remains to be improved [13].

2.3.2 Disease or Organ-specific Scoring Systems [11]

Similar to general scoring systems, the main objective of specific scoring systems is also to assess the degree of physiologic abnormality in patients. This type of scoring systems is more focused on single-organ failure or a specific disease, such as pancreatitis, hepatic failure and so on. As a result, they have strong discrimination on certain cases. The disease or organ-specific scoring systems are often used outside of ICU but can be of great assistance for prognostication and treatment. Scoring systems like *Glasgow Coma Scale (GCS)*, *Child–Pugh (CP)*, and *Risk, injury, failure, loss and end-stage kidney (RIFLE) classification* belong to this category [11].

Specific scoring systems share most of the shortcomings with general scoring systems since they are rooted on the same principle. Besides, for the purposes of this thesis, there is no specific scoring system exclusive for severe sepsis prognostication and monitoring.

2.3.3 Organ Dysfunction (OD) Scoring Systems [11]

The objective of this type of scoring system is to assign scores based on the severity of organ failure. Each crucial organ gets scored independently, and multi-scores from different organs are considered comprehensively. The goal is to monitor the change of organ functions on a daily basis. Currently, there are 3 main systems under this

category: *Sequential Organ Failure Assessment (SOFA)*, *Multiple Organ Dysfunction Score (MODS)*, and *Logistic Organ Dysfunction System (LODS)* [11].

It should be noted that even though OD scoring systems fulfill a dynamic evaluation of organ functions in ICU patients, they are not as developed as disease severity scoring systems [11]. Since organ dysfunction is one aspect of patients' condition, OD scoring systems are not comprehensive enough in evaluation of the severity or the improvement in condition.

In addition, since all of the current scoring systems are developed based on the certain patient population and demographic, it may not be useful outside this demographic [14]. For example, most of the general scoring systems were established based on patients older than 16 years old in ICU units [11], thus the prediction may not be accurate when applied to patients younger than 16. Current data also shows that the reliability and consistency of scoring systems vary with local population among patients [11][14]. Therefore more studies need to be conducted to validate various scoring systems.

To sum up, current severity scoring systems are of great significance in helping disease severity evaluation and providing predictive information on patients' condition. However, due to lack of comprehensive assessment and consistency among various populations, the scoring systems have considerable limitations.

2.4 Biomarkers for Severe Sepsis Prognostication

As discussed above, current scoring systems do not provide a comprehensive evaluation of severe sepsis or its prognosis. Hence, alternative approaches are required to provide detailed and accurate evaluation of sepsis severity in patients. A wide variety of biomarkers have been considered for this purpose.

2.4.1 Sepsis Biomarkers

A biomarker is generally defined as an objectively measured indicator of certain biological or pathogenic processes, or pharmacologic response to a therapeutic intervention [15]. Compared to the scoring systems, biomarkers have some obvious benefits: 1) they have an indicative ability to tell the absence or presence, or severity of sepsis; 2) by detecting certain biomarkers, the source (bacterial, viral, or fungal infection, etc.) of sepsis can be identified, which helps in formulating treatment [16]; 3) biomarkers monitoring can be an easy and continuous process, thus provide an option on evaluation of patient response to therapy [17].

2.4.2 Current State of Sepsis Biomarkers Development

According to a review work in 2010, a total of 178 biomarkers had been studied associated with the sepsis process. However, the reliability of these biomarkers in actual

clinical application has not been established [17]. In fact, the research on seeking a highly discriminative biomarker is extremely challenging mainly due to two aspects:

1) The pathophysiology of sepsis is a complex process involving multiple mechanisms. A large amount of mediators, such as cytokines, cell-surface markers, acute phase proteins, coagulation factors and apoptosis mediators, participate in the septic process, which can be potentially studied as biomarkers in sepsis [17]. However, most of the mediators do not participate in the whole septic process; thus they can hardly reflect an overview pathological development in sepsis patients. Instead, most of the biomarkers are relevant for only one aspect of sepsis. For example, some biomarkers were shown to be effective in distinguishing septic patients with non-septic patients who have SIRS; some were identified to be useful in early diagnosis of sepsis; and most of the biomarkers were analyzed to distinguish patients who likely to survive (survivors) with those who have high probability to die (non-survivors) [17].

2) It is extremely difficult to build up an experimental model for sepsis biomarker studies, thus current way to find a reliable biomarker is through clinical practice or animal trials, which have high cost and long duration [17]. As mentioned above, the pathological process of sepsis is complicated and the factors may vary among patients, hence biomarkers research based on an accurate sepsis model is extremely difficult. Most of the results from current studies are validated by comparing with the methods used in everyday clinical practice [17].

In summary, numerous biomarkers have been investigated as diagnostic indicators of sepsis and its various stages. However, none of them have been demonstrated to be suitably accurate and sensitive to be used in clinical practice. Although a combination of several biomarkers has been proposed for sepsis prognostication or diagnosis, there is insufficient data to validate this approach. Based on review and analysis, it is unlikely to get a single ideal predictor can be used for sepsis diagnosis due to the complexity of sepsis, but biomarkers can be useful in improving sepsis prognostication and severity assessment.

In this thesis, one of the most promising biomarker, circulating cell-free DNA in blood, has been investigated and reviewed in greater detail.

2.4.3 Circulating Cell-free (cfDNA)

Circulating cell-free DNA (cfDNA) broadly refers to extracellular DNA present in blood. It was first discovered in 1948 [18], and since 2000, has been increasingly investigated for application in disease diagnosis and prognosis [19]. Increased level of cfDNA reflects some pathological processes, including tumor, malignant lesions, inflammatory diseases, trauma, sepsis, and so on [18]. Additionally, higher level of cfDNA can be detected in certain non-pathological results, such as after intense exercise [20] or women with pregnancy [21]. Indeed, cfDNA always exists in blood of healthy people, but is at a relatively low level.

The sources of cfDNA in blood and the mechanism by which its concentration increases are not well understood. Upon review, the main source of cfDNA in blood is due to programmed cell death (apoptosis) and necrosis of cell. Apart from this, some of it is generated by secretion (Figure 2.3) [18].

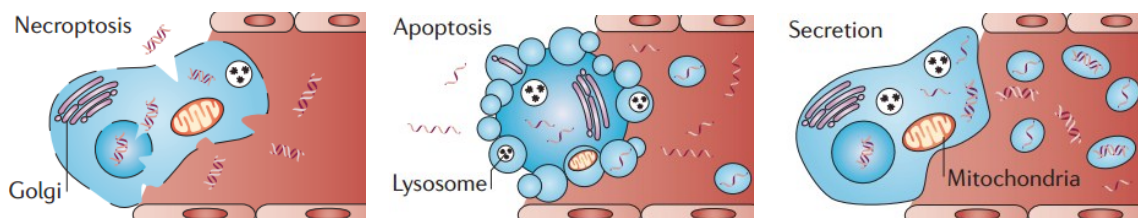


Figure 2.3 The mechanism of DNA release [18]

CfDNA can stay in blood circulating system for several hours at most, and then will be cleared by liver and kidney efficiently [18]. The mechanism of cfDNA generation has not yet been completely understood. A growing consensus to explain the increased level of cfDNA in some patients' blood is through elevated levels of necrosis or decreased clearance efficiency [22], but more investigations are required to verify this hypothesis.

2.4.4 Cell-free DNA for Severe Sepsis Prognostication

Recently, cfDNA concentration in blood has been found to be a reliable indicator for predicting mortality in ICU patients. In combination with current scoring systems (e.g. MODS) and some other sepsis biomarkers (e.g. Protein C), cfDNA levels can potentially

have stronger predictive power [5][22]. The study concludes that cfDNA concentration in blood is much higher in patients who died in ICU (non-survivors) compared with those who survived (survivors) based on data collected from 80 severely septic patients. The mean cfDNA levels in survivors ($1.16 \pm 0.13 \mu\text{g/ml}$) was similar to that of healthy volunteers ($0.93 \pm 0.76 \mu\text{g/ml}$) ($P=0.426$), while that of non-survivors ($4.65 \pm 0.48 \mu\text{g/ml}$) was notably higher ($P<0.001$) (Figure 2.4) [5].

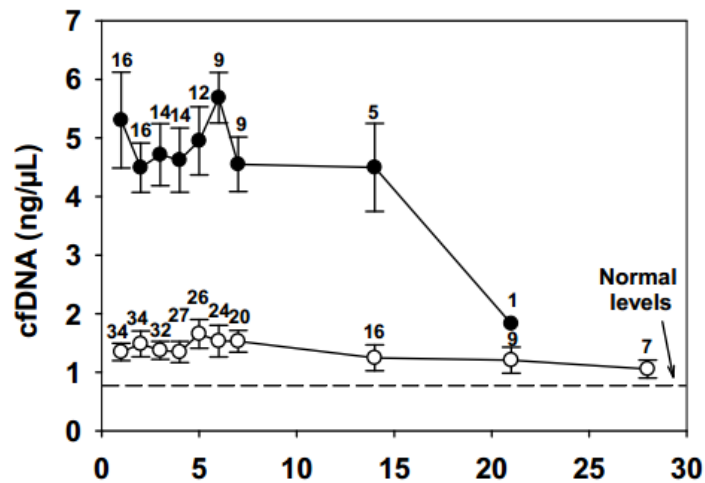


Figure 2.4 Temporal changes in levels of cfDNA in 50 patients with severe sepsis [5]. Survivors are shown by white circles (○), and non-survivors are shown by black circles (●). The number of patients at each time point is indicated. The mean levels of cfDNA in healthy volunteers (n= 14) is shown by the arrows. Error bars represent standard error of mean (SEM).

The cfDNA concentrations in blood of a number of non-survivors were found to be much higher than $5 \mu\text{g/ml}$ [5]. The DNA concentration difference between survivors

and non-survivors (approximately 1µg/ml versus 5µg/ml) in ICU could be used to select out patients with much higher risk of death (non-survivors), and specific treatment can be provided.

Therefore, rapid quantification of cfDNA in severe septic patients in ICU can be of great help in mortality prediction and disease prognosis.

2.5 Current Methods for DNA Quantification

DNA quantification is the measurement of the concentration of DNA from a biological sample, such as human blood and cell lysate. It plays a crucial role not only in this sepsis prognosis, but also many other molecular biology-based studies. There are two mainstream nucleic acid quantification approaches, both of which require sample preparation (i.e. DNA extraction and purification) as the first step. Lately, a direct DNA quantification method has been carried out but remains research stage.

2.5.1 Sample Preparation Prior to DNA Quantification

Existing DNA quantification methods require DNA to be extracted and purified before analysis. The cells, proteins and other biological contents in the sample can have a significant effect on the accuracy of the measurement depending on the technique used. In quantification of cfDNA in human blood, the sample is centrifuged to separate blood cells from plasma followed by cfDNA isolation from the plasma. There are two main

approaches to isolate DNA from complex samples. One method is based on the selective absorption of DNA on silica in the presence of chaotropic salt (e.g. guanidine hydrochloride or guanidine thiocyanate) [23]. In this method, the proteins and other debris in sample solution can be washed away while DNA is still attached to the surface of silica structure. Subsequently, the DNA can be eluted using a buffer that does not contain the chaotropic salt.

The other way of extracting DNA is to take advantage of the different solubility of DNA and proteins in phenol:chloroform mixture [24]. During sample preparation, equal volume of phenol/chloroform is mixed with aqueous blood plasma, resulting in separation of upper aqueous phase and lower organic phase rich in phenol. While DNA stays in aqueous phase, proteins separate into the organic phase. With a following ethanol precipitation step, pure DNA can be separated with processing chemicals.

The cfDNA concentrations in blood of a number of non-survivors were found to be much higher than $5\mu\text{g/ml}$ [5]. The DNA concentration difference between survivors and non-survivors (approximately $1\mu\text{g/ml}$ versus $5\mu\text{g/ml}$) in ICU could be used to select out patients with much higher risk of death (non-survivors), and specific treatment can be provided.

Therefore, rapid quantification of cfDNA in severe septic patients in ICU can be of great help in mortality prediction and disease prognosis.



Figure 2.5 DNA isolation procedures using a commercial kit (Norgen Biotek Corp., ON, Canada): DNA is bound to Norgen's column under optimized salt concentrations (BIND), and other contaminants can be washed and flow away (WASH). Purified DNA is finally eluted into clean buffer (ELUTE). <https://norgenbiotek.com/display-product-blood-genomic-dna.php?ID=495>

Due to the extensive sample preparation required to isolate DNA from complex samples, current DNA quantification methods have some common issues:

1) The required sample volume can be large. Because conventional detector sizes are very large with regards to biosamples like DNA, a certain amount of DNA is required to meet the sensitivity and accuracy of detection. But DNA concentration in most sample liquids is small, thus a relatively large volume may need to extract a certain amount of DNA for detection. For instance, in a DNA extraction utilizing NaI, only about 40~50 μ g DNA can be obtained from 1ml whole blood [25].

2) The process is time-consuming. Multiple steps involved in the DNA purification process each of which takes significant time makes quantification of DNA into a time consuming process. For instance, it can take up to 30 minutes to complete a

DNA preparation process as demonstrated in [Figure 2.5](#) to extract DNA out of 100 µl of blood.

3) The additional purification process increases the risk of contamination and may introduce errors in sample handling [\[26\]](#). For instance, chemicals used during DNA isolation if not washed properly can lead to errors in subsequent quantification. Similarly, a multi-step manual process can introduce operator dependent errors in sample handling.

4) Loss of DNA can also happen during the sample preparation process [\[27\]](#). It is typically not possible to collect all DNA present in a complex sample. Also, the amount of DNA left uncollected is difficult to determine and may vary according to the procedure used which may eventually affect the quantification process.

2.5.2 DNA Quantification Methods

After DNA isolation from original samples, the concentration of a purified DNA solution is measured mainly by two approaches as listed below.

2.5.2.1 Ultraviolet (UV) Spectrometry Method

UV spectrometry method is the most popular and simplest way to measure DNA concentrations in a pure solution [\[28\]](#). DNA has a dominant absorbance peak to UV light at 260nm; thus the intensity of the absorbed UV light at 260nm is dependent on the concentration as per Lambert-Beer's law [\[28\]](#):

$$A = \epsilon cl \quad \text{Eq. 2.1}$$

In the equation, ϵ stands for molar absorption coefficient, c is DNA concentration in the sample, and l represents the light path length in the solution. In a measuring system, the concentration can be calculated if the other parameters are fixed or precisely measured. In principle, the amount of light absorbed is proportional to the DNA concentration in solution. Since proteins, phenol or other contaminants absorb UV light strongly at or near 280nm, the ratio of the absorbance at 260 and 280nm ($A_{260/280}$) is used to assess the purity of DNA, which is an indispensable parameter for checking the accuracy of measurement [28]. For pure DNA, $A_{260/280}$ is around 1.8. Current commonly used spectrophotometers are all dependent on this method. In this thesis, spectrophotometric measurement of the cfDNA concentration in clinical plasma was used as a reference.

The UV spectrometry method has other issues besides those mentioned in the DNA isolation process: 1) the measured result is highly dependent on the purity of the sample, which sets a high requirement for DNA purification process. The readings can be misleading if the sample contains proteins, chemicals or other contaminants; 2) Most of the instruments using UV spectrometry method are only applicable to concentrations higher than $2\mu\text{g/ml}$ [28], which is a significant limitation because many samples have DNA concentrations lower than $2\mu\text{g/ml}$. In this thesis, the cfDNA concentration in non-survivors blood samples ($>5\mu\text{g/ml}$) of severe septic patients were measured using UV

spectrometry as a reference, while the cfDNA in healthy donor samples ($<2\mu\text{g/ml}$) were not quantified with this technique due to the low concentration.

2.5.2.2 Fluorescent Staining Method

Compared with the UV spectrometry method, this DNA quantification approach is able to detect much lower concentration of DNA (in the order of ng/ml) [28]. The idea is to characterize DNA concentration using fluorescence emitted by fluorophore bound to the DNA. The fluorescent intensity is directly proportional to the total mass of DNA present. Although this method is relatively more expensive due to the use of fluorescent dyes, the result can be more reliable and accurate [29]. Two primary techniques are used in this method:

One of the techniques is electrophoresis and band quantification [30]. It estimates the unknown DNA mass by comparing with the fluorescent bands of a DNA ladder (Figure 2.6(a)) with known mass. During quantification, the same volume of sample solution and DNA mass ladder was loaded into the same gel but in adjacent lanes [31]. Then the intensity of the bands is compared between the sample and the DNA mass ladder after electrophoresis. The DNA concentration in the sample solution is then estimated by adding up the masses of various bands (total mass) and dividing the sample volume. The biggest problem of this method is its estimated result depends significantly on the distribution of bands in the ladder. If an unmatched band appears in the sample

electrophoresis, the estimation of DNA mass for that band will potentially introduce errors. Also, the comparison between the DNA ladder and the sample DNA mass may not be accurate. This method is also time-consuming.

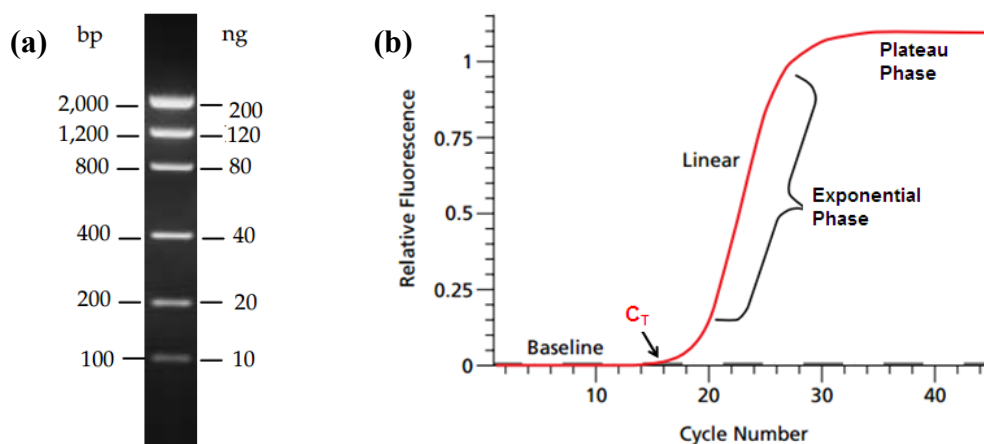


Figure 2.6 Fluorescent staining quantification method: (a) an example of DNA mass ladder with low DNA size range [31]. The dye was ethidium bromide. Electrophoresis was conducted in 2% agarose gel. (b) Fluorescent intensity increase in a typical qPCR process [32].

The other technique more widely used is quantitative polymerase chain reaction (qPCR) [28]. It is a method combining conventional PCR amplification technique and fluorescent quantification to measure DNA concentrations. During DNA amplification in a PCR process, the fluorescent signal from the fluorescently labelled DNA will change as shown in **Figure 2.6(b)**. After several cycles of amplification, the fluorescence reaches a pre-set fluorescence baseline, at which the amplification cycle is called threshold cycle

(C_T). The fluorescent signal increases exponentially (*Exponential Phase*) after C_T , and eventually become saturated (*Plateau Phase*) [32]. In theory, with a fixed fluorescence baseline, the higher the original concentration of sample DNA, the sooner the amplified product will be detected, thus the C_T value is lower. The relationship of C_T and the concentration of sample DNA can be established in a standard curve by using multiple dilutions of a known amount of standard DNA [32]. Therefore DNA in sample is quantified by recording C_T under a pre-fixed fluorescence baseline in the instrument.

The qPCR method can be made highly accurate with careful design, optimization and validation [33]. This technique can also be used to quantify a targeted sequence of DNA by selectively labelling it with a fluorophore. The operation of qPCR instruments is simple and relatively fast; however, there is also much room for errors. The primary problem is the inconsistency of DNA amplification efficiency which can lead to various C_T values even though the original sample DNA concentration is the same. The DNA amplification efficiency can be affected by many factors including the presence of inhibitors in the sample, the design of primers, and so on. Another big issue is the protocol for qPCR quantification varies with different instruments used or research groups, which leads to an unclear standard. Thus the evaluation between different qPCR quantification results is difficult. In addition, for a sample concentration that can be directly measured, there is no need to amplify DNA before quantification. The process

can be significantly simplified by directly measuring the fluorescent intensity which has a linear relationship with DNA concentration in sample.

To sum up, although the fluorescent staining method is a promising way for quantifying cfDNA in human blood samples, current procedure and equipment still remain to be optimized, simplified and standardized.

2.5.3 A Direct DNA Quantification Method

As mentioned above, some of the deficiencies in current DNA quantification methods stem from the need for DNA isolation. Therefore, one approach in making quantification better could be development of direct quantification approaches from raw samples without DNA purification process. This requires measurement of DNA concentrations directly in plasma or serum, or even whole blood. Recently, a direct DNA quantification method from blood plasma or serum has been published [26][34][35]. In this method, specific PCR primers targeting DNA repeats that are commonly interspersed throughout the human genome were used to produce an amplified product that was proportional to the amount of cfDNA originally present in the sample.

There are two groups who have applied this modified qPCR quantification in their research. One group targeted on amplifying ALU repeats with an ALU115 primers [34][35]. The results obtained after quantification represent the total DNA concentration in the serum sample. For the other group, a primer established for 90bp L1PA2 repeat

was used [26]. The quantification results from this group were compared with that from traditional methods, and validated. In the studies, it was claimed that due to the high sensitivity of the primers applied in the qPCR process, the interference of proteins and other material in the unpurified plasma/serum was limited.

Although the DNA isolation procedure can be avoided when using this method, there are some disadvantages should be noted. First of all, it is built on the conventional qPCR technique hence the cost is still relatively high. Secondly, the research group using ALU primers did not fulfill a real direct quantification method because it still requires a sample pre-treatment including preparation of a specifically designed buffer and proteinase K, centrifugation and some other work [26]. Although these sample preparation procedures are much simpler than conventional sample preparation requirements, it is not a one-step quantification approach. Thirdly, the time required for the quantification is long. It takes more than 40 minutes to just amplify DNA, and more time is needed for sample pre-treatment and concentration measurement. Last but not least, the published direct quantification method has not been demonstrated in whole blood. It is possible that the presence of blood cells and other contents in whole blood samples can inhibit the qPCR process. Therefore blood cells removal from whole blood is indispensable. Studies have shown a cfDNA loss in the blood cells removal process, and the quantification results can be significantly affected depending on the blood processing protocols chosen [36].

There is another major problem for using qPCR-based methods to quantify cfDNA in samples of severe septic patients. The total amount of DNA can be underestimated because certain degraded target-gene copies (e.g. β -globin) may not be amplified using the PCR process [5].

2.5.5 Summary of Current DNA Quantification Methods

DNA isolation from original samples is an essential procedure for current commonly used quantification methods; however, this procedure is time consuming, sample and reagent consuming, and is difficult to operate. It can introduce errors into the final quantification results due to DNA loss and inconsistency in the isolation steps. One of the techniques for absolute DNA quantification in purified samples is UV spectrometry. It is a simple and relatively cheap method, but the measured result is extremely dependent on the sample purity, and the detection range is limited. The other technique applied is through fluorescent staining (mainly qPCR technique). This principle can be applied to a wide-range measurement, and the result relies less on the sample purity. However, the calibration and DNA amplification efficiency varies, which leads to inconsistent results. A modified qPCR method has been realized to directly quantify cfDNA from plasma or serum, but it provides no theoretical analysis or preliminary experimental results to show the potential of direct quantification from whole blood.

Studies have shown that qPCR based methods may underestimate the DNA levels in samples of severe septic patients, thus is not an ideal technique to be used. The DNA

amplification before concentration measurement in qPCR is not necessary as long as DNA in blood can be selectively labeled by a fluorophor and the concentration is over the detection threshold.

In general, an ideal method for cfDNA quantification should be 1) minimum sample preparation process which means the quantification can be carried out directly in whole blood sample; 2) high sensitivity and repeatability which implies a limited interference by other contents in blood (e.g. proteins and blood cells); 3) fast analysis (within several minutes); 4) low cost, including fabrication/operation cost and sample/reagents consumption.

Based on the criteria mentioned above, the fluorescent staining method is the best option for DNA quantification due to its linearity and high sensitivity. The other requirements can be met by applying microfluidic technology.

2.6 Microfluidic Sample Preparation

Sample preparation refers to the isolation and/or concentration of some target analytes (e.g. DNA, proteins and cells) from various matrices (e.g. blood and cell lysate) [37], which is a prerequisite for following sample processing in most cases. Microfluidic sample preparation refers to completing sample preparation in a microfluidic scale (in or below the order of microliter). Generally, sample preparation for DNA-related analysis

involves two phases: cell lysis and DNA extraction/concentration [38]. But in this thesis, the target analyte is cfDNA (extracellular DNA) in human blood, which means the sample preparation should focus on separating extracellular DNA from blood cells, proteins, and other contaminants in whole blood without lysing the cells. Then the isolated DNA should be concentrated for quantification purpose. Based on the goal of this thesis, existing microfluidic devices developed for DNA isolation and concentration have been reviewed in the following sub sections.

2.6.1 Microfluidics

Microfluidics is the science and technology of processing or manipulating small amount of liquids using structures (e.g., channels, pumps, valve, etc.) with sub-millimeter dimensions. It has been applied in various research areas like chemical synthesis, multiphase flows control, drug delivery, and cell biology [39]. A large body of work in microfluidics has focused on microanalysis and in particular automation of molecular diagnostics so that these assays can be performed at the point of care. These devices have been labelled using various terms , including micro Total Analysis Systems (μ TAS), Lab-on-a-chip platforms (LOC), and Point-of-care testing (POC [40]).

Despite the significant developments in microfluidics over the past several decades in the area of molecular analysis, the adoption of these devices has been stymied primarily due to the complexity of human (e.g. blood) or environmental (e.g. soil)

samples and the need for external sample preparation prior to the use of the devices[39]. Therefore, better solutions than those currently available for sample preparations are required.

2.6.2 Advantages of Microfluidics

Although the current microfluidic devices remain to be improved, they still have remarkable advantages compared with large scale devices. [39][41][42].

- 1) Small size and weight which makes microfluidic devices portable. They are an ideal candidate for bedside or on-site analytical devices.
- 2) Low cost in fabrication due to the small size of the device and the development of parallelization fabrication technique. Also, the commonly used materials in microfluidics, like polydimethylsiloxane (PDMS), can be cheap, which further decreases the device cost.
- 3) Low sample and reagents consumption. The channel dimension of general microfluidic devices is in sub-millimeter, thus the capacity for sample liquid is in the order of microliter or even smaller, which is approximately the volume of a droplet. In clinical analysis, this would be beneficial for minimum-invasive test. The reagents cost can be lowered or eliminated as well, which realizes a reagent-free process.

- 4) Low energy consumption [43]. For those devices requiring power supply, by scaling down their geometry, smaller voltage is needed to generate the same strength of electric field. A direct current (DC) electrostatic field (E) is defined as the negative gradient of electric potential (Φ):

$$E = -\nabla\Phi \quad \text{Eq. 2.2}$$

With a fixed potential drop, a smaller distance between the two electrodes can lead to a greater potential gradient (i.e. a stronger electric field). Therefore a simpler power supply could be used to deliver the same electric field.

- 5) Automation and integration of components with various functions. Take the area of bio-sample analysis as an example, the best scenario is “raw sample in, clear answer out”, which cannot be realized using current macroscale instruments. In a microfluidic device, the components with different roles can be integrated more easily, which makes the analyzing process automated [44].
- 6) High resolution and sensitivity in detection. The comparison between microfluidic devices and the conventional approaches shows a similar or higher resolution, which means the scaling down of the size does not sacrifice the detection effect but increase the resolution in some cases [39].

- 7) Short analysis time. When applied to microanalysis, the sample preparation and detection steps are simplified in most of the microfluidic devices, which enables a faster processing or a higher throughput than macroscale systems.
- 8) Limited temperature variations. With an electric field in a conductive liquid, heat can be generated and further affect the distribution of electric field. Heat can also be harmful to contents in the sample in some cases when viability matters. When fluorescent dye is used, the increased temperature can lead to an accelerated photodegradation of the dye [45], which ultimately decreases the accuracy on fluorescence measurement. Therefore a limited temperature increase in the sample is crucial. Following the scaling law of temperature variation [43]:

$$\Delta T \sim \sigma V^2 L^3 \quad \text{Eq. 2.3}$$

where σ is the conductivity of the medium; V is the voltage added; and L stands for the length scale. It can be seen that the scaling down of system dimension and voltage applied can significantly decrease the temperature variation.

In summary, microfluidic technology is advantageous in human sample analysis and molecular diagnostic applications. Many benefits listed above endorse realizing cfDNA quantification in a microfluidic device.

2.6.3 Current Microfluidic Devices for DNA Extraction and Concentration

In this thesis, sample preparation refers to cfDNA isolation and concentration in whole blood. Therefore current microfluidic devices with similar capabilities have been reviewed. Based on various mechanisms applied in the extraction and concentration, the microfluidic devices can be divided into 3 principal categories.

2.6.3.1 Silica-based Absorptive Extraction

This method is also known as *Solid Phase Extraction* (SPE). It has been commercialized and widely applied in current sample preparation methods. The basic principle is based on a selective “absorption” between silica surface and DNA in presence of chaotropic salts, such as guanidine hydrochloride. The selective “absorption” is mainly rooted in the hydrogen bonding, the increased entropy of the ionic environment formed by the chaotropic salts, and the decreased negative charge at the silica surface due to the solution pH [46]. A 3-step extraction procedure is usually required in this method [47]: 1) Bind: DNA is selectively bound to the silica structure in the presence of a buffer with a chaotropic salt; 2) Wash: contaminants, like proteins and cells that do not bind under these conditions, are removed using ethanol or isopropanol; 3) Elute: captured and purified DNA is ultimately eluted using a low-ionic strength buffer which reduces the binding between the DNA and the silica.

With the advance of micromachining technologies, many microfluidic devices have been developed with various silica microstructures (Figure 2.7), and the common goal of these silica microstructures is to maximize the surface area so that more contact area is available for DNA binding. Majority of the devices using silica absorptive extraction method have been tested with plasma or blood sample, in which most of the devices show good extraction efficiencies ($> 70\%$) [46]. Also, high purity of the isolated DNA can be achieved with this method in a shorter time ($< 15\text{min}$) compared with using conventional macroscale extraction kit [47]. In addition, it is easy for this type of device to be integrated with other components, such as cell lysis and DNA detection.

There are some conspicuous deficiencies of the silica absorptive extraction method: 1) the device fabrication is relatively difficult and expensive compared with other methods [47]; 2) the DNA extraction efficiency is highly dependent on the silica surface area available within the device, which can vary in some fabrication processes used. For instance, the sol-gel structure has low reproducibility on the pore size among devices, which leads to a relatively low and unstable extraction efficiency [46]; 3) multiple wash and elution steps that are necessary in these device require complex fluidic control in the device; 4) although there are no hazardous chemicals involved, it is not absolutely reagent-free method. The chaotropic salts and organic solvent used are potent PCR inhibitors which should be subsequently removed [46]; 5) extracted DNA cannot be

concentrated and quantified before the elution step, which means a one-step DNA quantification cannot be realized using this method.

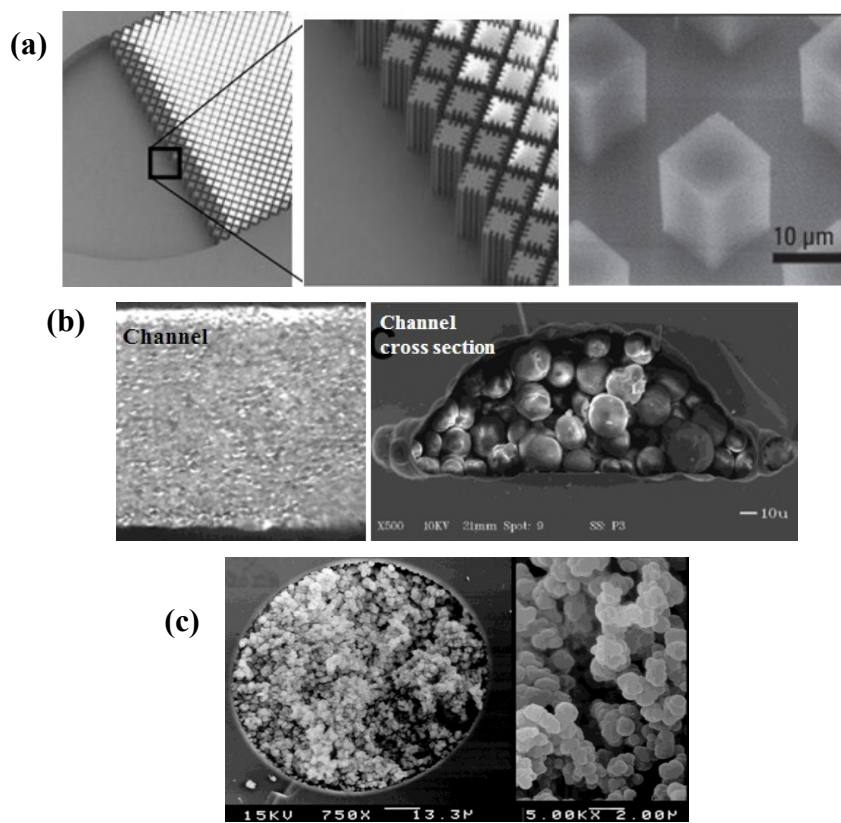


Figure 2.7 Various microfluidic devices using silica absorptive extraction method. Different silica microstructures like (a) micropillars [46][48]; (b) microbeads, silica particles, sol-gels or their combination[49]; and (d) porous monoliths [50] have been developed.

As analyzed above, the device cost needs to be reduced and the DNA extraction efficiency should be more consistent. More importantly, the operation for extraction,

concentration and quantification process must be significantly simplified, and a reagent-free approach needs to be carried out. Therefore, the silica absorptive extraction method is not appropriate for the intended application in this thesis.

2.6.3.2 Electrokinetic Extraction and Concentration

The working principle of this method is to extract and concentrate DNA using electrokinetic forces on the DNA in an electric field. It has been shown that electrokinetic forces such as electrophoretic force, dielectrophoretic force can be used to manipulate biological objects effectively [51]. The motion of an object in the electric field is primarily determined by 1) the property of the object (e.g. negative/ positive/ neutral charge, dielectric tendency, size, and shape) and 2) the property of the electric field (e.g. Alternating Current (AC)/ Direct Current (DC) electric field, frequency, magnitude, and distribution). Therefore, DNA can have distinct behaviour as compared with other contents like proteins and cells in the same electric field. A detailed analysis on the electrokinetic effect on DNA and cells in a complex sample will be done in [chapter 3](#).

The biggest advantage of electrokinetic extraction and concentration method is that it is reagent free. It can simplify the sample preparation process and decrease the reagent consumption.

Several groups have used AC electroosmosis (EOS) flow to focus DNA onto the surface of the electrodes, while a DC EP or DEP force was generated to keep DNA from being dragged away by the EOS flow (Figure 2.8) [51]-[58].

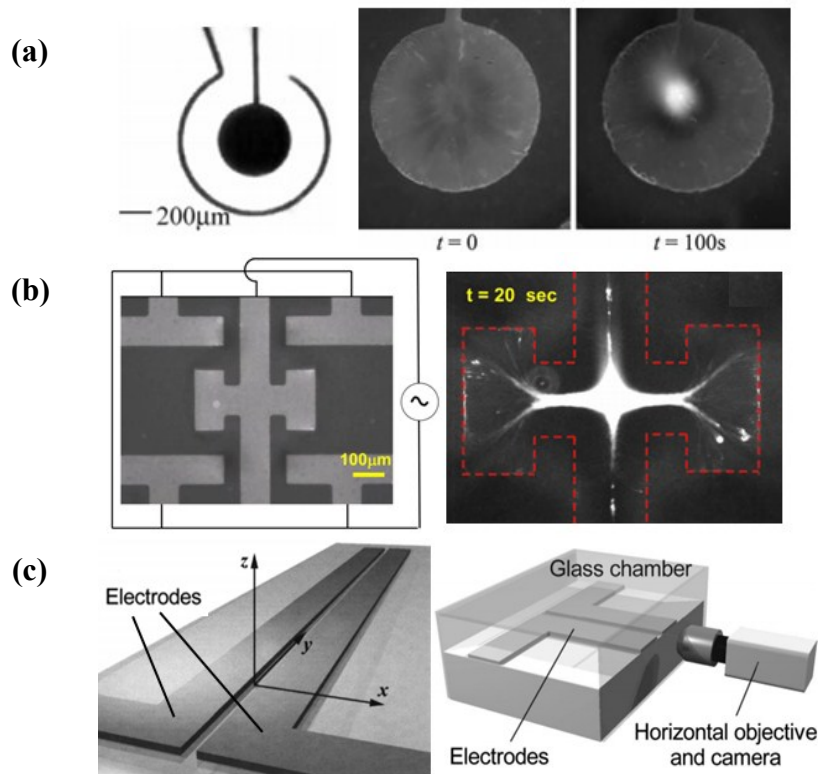


Figure 2.8 Microfluidic devices using both AC EOS flow and EP/DEP force to concentrate DNA onto the surface of electrodes with various geometries: (a) design of an electrokinetic concentrator [52][53]; (b) two identical half-quadrupole electrode sets [54]; (c) coplanar plate microelectrode array and the experimental setup [55][56].

By using these devices, DNA can be rapidly focused to a certain area on the surface of electrodes and gets concentrated, but some disadvantages make them not suitable for the fast quantification application: 1) the flow in the channel can cause removal of accumulated DNA on the surface of the electrodes, thus the fluorescent intensity is significantly affected; 2) the focused DNA is in direct contact with electrodes which could lead to irreversible binding. Therefore these expensive electrodes cannot be re-used due to contamination from previous experiments; 3) the device configuration is not convenient for fluorescence monitoring in whole blood as the fluorescent signals can be impaired due to non-transparency of blood, and the metallic electrodes block fluorescent signals as well; 4) none of the devices have been tested with plasma or whole blood. It is not clear if these devices can concentrate DNA in the presence of proteins, cells and other materials in the sample.

Using the similar mechanism, one group has successfully collected DNA to a microtip electrode in human buccal swab and saliva samples (Figure 2.9). Experiments using more complex human samples, such as blood, have not been carried out, but it claimed that DNA extraction from blood may work by modifying the extraction protocol [59][60]. One of the shortcomings of this device is that DNA must be eluted after extraction, which adds another step before quantification. Also, due to the direct contact between DNA and electrodes, fluorescence contamination must be eliminated by

thoroughly washing the electrodes or replacing electrodes for each experiment. The cost of device and operation is increased due to the reasons mentioned.

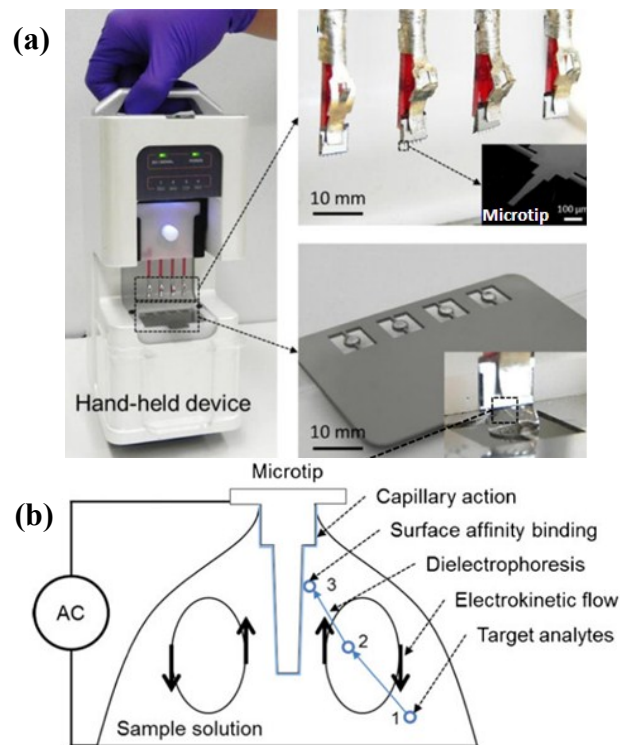


Figure 2.9 (a) A microfluidic device extracting DNA onto microtips in human buccal swab or saliva samples; (b) the working principle of DNA extraction with the microtip [59][60].

So in summary, some common problems are shared by the microfluidic devices listed above including: 1) flow induced variations can be significant as flow can remove the accumulated DNA at the surface of the electrodes; 2) the electrodes cannot be reused due to direct contact between fluorophore and electrodes; 3) AC power supply is used to

produce electrokinetic forces and to avoid bubble generation at the surface of electrodes; however, it increases the cost and decrease the portability of the device because low-cost batteries cannot be used.

Some microfluidic devices using DC power supply (Figure 2.10) have been developed, but none of them were tested using plasma or whole blood samples.

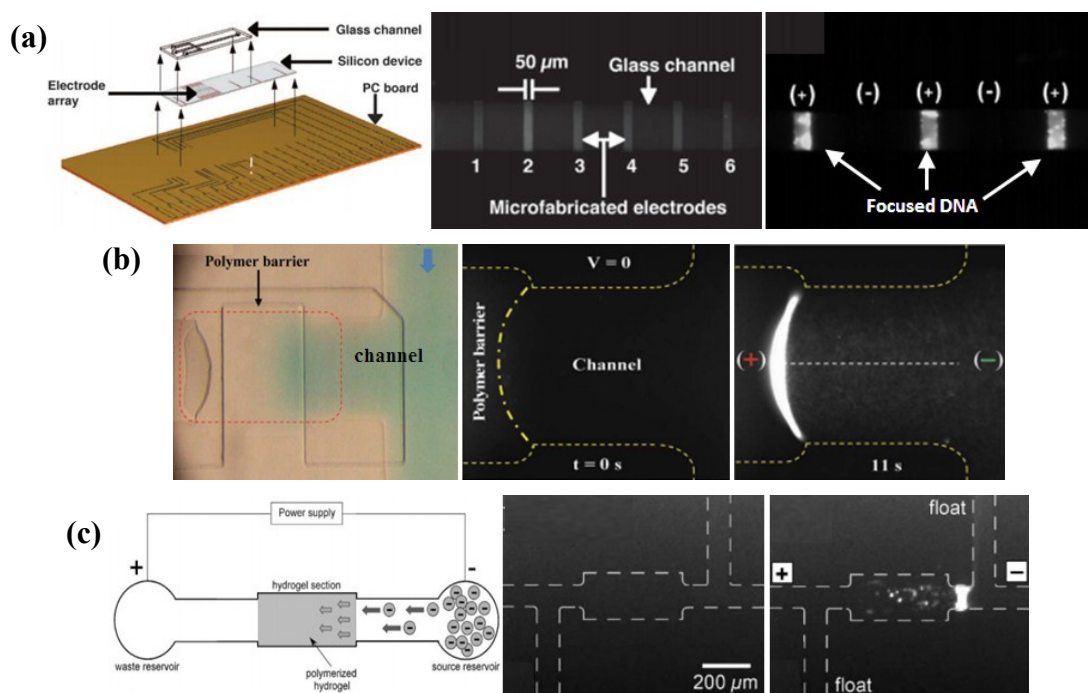


Figure 2.10 Microfluidic devices for DNA concentration using DC electric fields with various structures: (a) micro electrode arrays [61]; (b) permeable polymer barriers [62]; and (c) hydrogel microplug [63].

Figure 2.10(a) shows a device to focus DNA onto the surface of a micro electrodes array using sequential capture-release processes with 1V [61]. Although only a low DC voltage is required in this device, there are some issues with this device: 1) the operation of the device are very complicated which does not meet the requirement of low-cost; 2) flow induced variations can be significant as flow can remove the accumulated DNA at the surface of the electrodes; 3) concentrated DNA has direct contact with the electrodes thus electrodes cannot be reused; 4) the device design is not suitable for DNA quantification because fluorescent signals can be blocked by the electrodes and be interfered by the blood in the channel.

In Figure 2.10(b) & (c), porous material was pre-loaded in the channel, and DNA was accumulated in the gel using a simple DC electric field.

This type of devices can be easily applied for DNA quantification since the fluorescent signals can pass the transparent gel-like material even with the presence of blood, and the DNA collection site can be easily located and monitored. However, there are some disadvantages of the devices: 1) the device configuration is complicated and the experimental operation is difficult. UV light is used in both of the devices to polymerize the porous monomers in the device, which involves an additional photolithographic step; 2) the device geometry is not beneficial to an easy introduction of the sample solution to the DNA accumulation site; 3) DNA is accumulated in a plane that is parallel to the direction of fluorescent excitation and detection, which is not suitable for quantification

because DNA can be stacked and fluorescence intensity can be easily saturated. Quantification errors may be introduced in this case; 4) The DC voltage applied in these two devices are 20V and 100V respectively, which are still high and may not be suitable in a low-cost and portable device.

2.6.3.3 Other Extraction Methods

Some other DNA extraction methods have been developed which focus on modifying the surface properties of the channel and the interactions between DNA and the device.

One of the methods is a pH-induced DNA capture which takes advantage of the electrostatic interaction between DNA and the modified channel surface at different pH intervals. Amine-group surface coating [64] and Chitosan coating [65] have been tried by different groups, and proved to be successful in DNA extraction from whole blood (Figure 2.11(a)). In these microchannels, DNA can be electrostatically immobilized on the channel surfaces in a pH below 6, and be eluted with buffers in a pH over 7.5. Due to the limitation of contact area, DNA extraction efficiency varies with the channel dimensions, and the time cost is longer compared with other methods in microfluidic devices. Besides, this pH-induced extraction method shares a similar problem with the silica absorptive extraction method, which is a requirement of the binding-wash-elution

process. Therefore DNA quantification can only be done after DNA elution and concentration.

Some other devices employing a nanoporous aluminium oxide (AlO_x) membrane [66], functionalized microparticles with increased DNA binding affinity [67][68], and a photoactivated polycarbonate (PPC) DNA immobilization bed [69] have also been developed and tested with human blood samples or bacterial cell lysates. DNA has been successfully extracted from the complex samples, although the extraction efficiency and purity vary among different devices. Two of the devices are illustrated in Figure 2.11(b) & (c), while not all of the devices published are listed. But based on review, most of the devices in this category have complicated structures, and the fabrication process is difficult.

All the devices mentioned above are more applicable to be used for DNA extraction in complex samples, but not for a simple quantification usage because of the requirement of an elution step which usually involves large volume of elution buffers. Most importantly, none of the devices are reagent free, and require extra chemicals consumption.

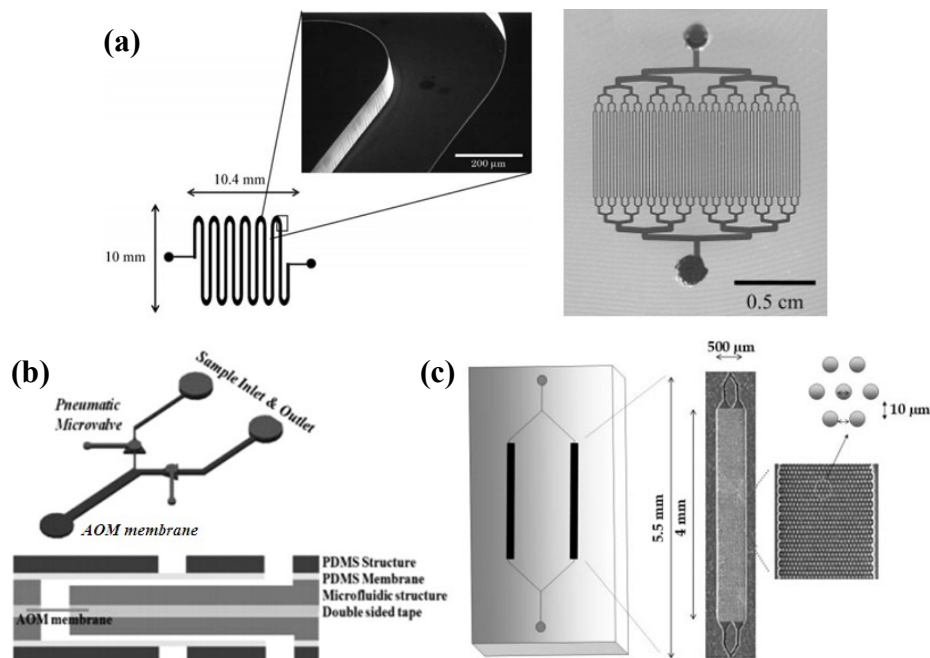


Figure 2.11 Other DNA extraction devices: (a) pH-induced electrostatic extraction with various channel geometries [64][65]; (b) filtration using a porous AlO_x membrane [66]; (c) a PPC microfluidic chip with a DNA immobilization bed [69].

2.6.3.4 Summary on DNA Extraction and Concentration Methods

Based on the review and analysis above, some advantages and disadvantages of current microfluidic DNA extraction and concentration devices are listed with regards to the DNA quantification objective of thesis (Table 2.1).

In comparison, electrokinetic DNA concentration method is most promising due to its fast concentration speed and reagent-free process. DC power supply for device design is preferable due to the portability and low-cost consideration, and a gel-like material can be applied to assist DNA accumulation. A challenge for using electrokinetic

DNA concentration method is the possible failure in whole blood sample since no previous experiments have shown a DNA concentration process using whole blood. Also, the device configuration and experimental operation must be simplified.

2.7 Summary

In this chapter, the background of the thesis is introduced. A rapid and accurate method to predict the mortality of severe sepsis patients is critically needed for clinical practice. Because current commonly used scoring systems are not accurate and sensitive enough on this task, lots of biomarkers have been studied as assistive indicator in severe sepsis prognostic utility. In a recent study, the concentration of cfDNA in blood was found to be an effective indicator for ICU mortality in patients with severe sepsis. But current DNA quantification techniques are time-consuming and involve extensive sample preparation. This can be a barrier for developing cfDNA quantification into a point-of-care test, which can be quite useful in assessing severity of sepsis and for physicians to decide on treatment. To solve this problem, a low-cost microfluidic device capable of rapid quantification of cfDNA concentration directly from blood plasma is needed. Based on review and analysis, a fluorescence-based DNA quantification approach and an electrokinetic DNA concentration method are advantageous to be applied on developing the new device.

Methods	Advantages	Disadvantages
Silica absorptive	Can extract DNA from whole blood with relatively high efficiencies; extracted DNA has high purity.	Device configurations are not compatible with quantification; DNA extraction (binding) and concentration (elution) steps are separated; device fabrication is complicated; not reagent-free.
Electrokinetic	Reagent-free DNA concentration; DNA can be concentrated rapidly. For devices using DC power supply and gel-like materials, the concentrated DNA can be easily located and quantified.	<p>Devices using AC+DC electric field: The AC power supply increases cost and decreases the portability of the device; direct contact of the electrodes and DNA; device structures are not compatible with DNA quantification needs; fluid flowing can impair DNA accumulation at the surface of electrodes.</p> <p>Devices using DC electric field and porous materials: Device structures and operations are complicated. Additional UV photolithography step is required; voltage applied is high; the orientation of the accumulation plane is not beneficial for quantification.</p>
Other extraction methods	Can extract DNA from whole blood.	DNA extraction (binding) and concentration (elution) steps are separated; not reagent-free; relatively long extraction time; most of the devices have complex configurations.

Table 2.1 Comparison of DNA extraction and concentration methods with regards to the fast DNA quantification purpose in this thesis.

Chapter 3.

Device Design and Working Principle

The device presented in this thesis should be able to quantify cfDNA concentrations with minimal sample pre-processing. This chapter will focus on the device design and its working principle. COMSOL[®] Multiphysics has been used to simulate the electric field distribution in the device and to analyze the forces on various particles in blood plasma or whole blood samples.

3.1 Forces Affecting Transport of DNA and Cells

Previous studies have shown that DNA has one intrinsic negative charge per base due to its sugar-phosphate backbone at most solution pH [70]. Phosphate groups in the DNA backbone are negatively charged above pH 2. However at pH 5 and below, the nucleotide bases attached to the backbone can accept protons which creates positive charged sites and can reduce the overall negative charge of DNA. At a pH above 5, DNA has a net negative charge and can be regarded as a polyanion [71]. Therefore, electrokinetic forces can be used to transport DNA in a fluid or concentrate it in a particular location by modulating the electric field profile. In general, for a particle in a DC electric field, there are four primary forces acting on it as described below.

3.1.1 Hydrodynamic drag force

Drag force originates from the viscous interaction between the particle and the fluid. Any particle moving in a fluid is subjected to drag force [72]. In a regular microfluidic channel, the liquid flow is laminar [73], and the governing equation is [72]:

$$F_{drag} = 6\pi\eta r\nu \quad \text{Eq. 3.1}$$

where η is the viscosity of the suspending medium, r is the particle radius, and ν is the relative velocity of the particle moving rate and the flow rate. The direction of the force is opposite to the relative motion of the particle with respect to the surrounding medium. Eq. 3.1 is an approximation built on the assumption that the object is a sphere, while in reality the configuration of objects in blood sample varies which can affect the magnitude of the drag force [72]. A particle in a static fluid under an electric field will move due to electrokinetic forces, which generates a drag force due to its motion.

3.1.2 Electrophoretic (EP) Force

When an electric field is applied to a conductive medium in which a charged particle is suspended, an electrical double layer (EDL) will be formed as shown in Figure 3.1, and an electrophoretic (EP) force will be exerted on the charged particle. In the case of a negatively charged particle, due to Coulomb attraction, a layer of positive ions from the conductive medium will be attracted to its surface forming the double layer. The

double layer consists of an inner layer, known as the Stern Layer, where the attracted ions are essentially immobile and an outer layer, called the diffuse layer, where the ions remain mobile [74]. Accordingly, the particle's charge is partially screened by the Stern Layer. The potential at the stern-diffuse layer interface, which is called zeta potential (ζ), represents the net charge on the particle after screening and is useful for determining the transport properties of the particle [74]. When an external DC electric field is applied, the charged particle and surrounding ions will experience a Coulomb force which results in a net EP force (F_{ep}) on the particle.

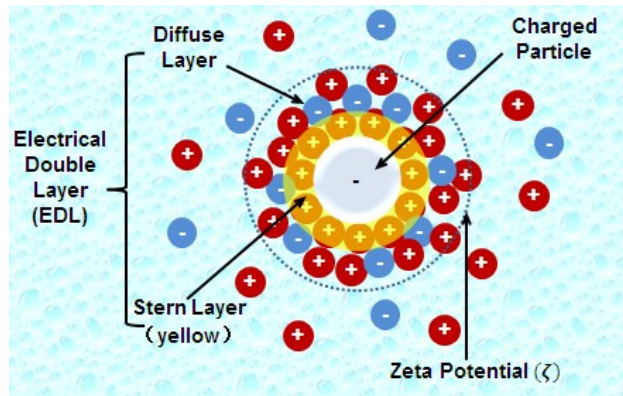


Figure 3.1 Schematic of a negatively charged particle in solution where mobile ions exist. The size of ions and EDL is exaggerated for the purpose of the figure. The yellow circle represents the Stern Layer.

For a DNA molecule, the magnitude of EP force (F_{ep}) and the drift velocity (v_{ep}) originating from EP force follows Eq. 3.2 as below [74]:

$$F_{ep} = qE \quad \text{Eq. 3.2}$$

where q is the particle charge, and E represents the strength of external electric field.

Based on the *Huckel* model, in a free-solution, the EP force is opposed by a friction force (Eq. 3.3), which is contributed by the drag force due to the hydrodynamic interactions between the fluid and the particle [75]. The EP velocity can be approximately calculated by equating the EP force and the drag force [75]:

$$v_{ep} = \mu_{ep}E = \frac{q}{6\pi\eta r}E \quad \text{Eq. 3.3}$$

where μ_{ep} is the EP mobility, q is the particle charge, η is the viscosity of the suspending medium, r is the particle radius, and E represents the electric field strength. EP mobility defines the ability of a charged particle to move in a medium in an applied electric field.

Due to the relationship between zeta potential and particle charge as shown in Eq. 3.4, another form of equation for EP velocity is shown in Eq. 3.5 [75][76]:

$$\zeta = \frac{q}{4\pi r \epsilon_m} \quad \text{Eq. 3.4}$$

$$v_{ep} = \frac{2\epsilon_m \zeta}{3\eta} E \quad \text{Eq. 3.5}$$

where ζ is the zeta potential, ϵ_m and η are the permittivity and viscosity of the suspending medium respectively, q is the particle charge, r is the radius of the particle, and E is the electric field strength.

In the *Smoluchowski* model, a similar definition for EP velocity is achieved with a slight difference in the numeric factor of $\frac{2}{3}$ [75]:

$$v_{ep} = \frac{\varepsilon_m \zeta}{\eta} E \quad \text{Eq. 3.6}$$

3.1.3 DC Dielectrophoretic (DEP) Force

A particle in an electric field will experience a dielectrophoretic (DEP) force if the following 3 requirements are met simultaneously: 1) the particle is dielectric, which means the particle is polarizable in an electric field; 2) the electric field is non-uniform with respect to space or time and 3) the conductivity of the particle and the suspending medium are different. As illustrated in [Figure 3.2](#), the charges that may be present in a neutral dielectric particle are balanced and evenly distributed without an electric field. After applying a DC electric field, the charges in the particle will be redistributed (*polarization*) which generates a separation between positive and negative charges (*dipole*). The direction of the dipole depends on the electric conductivity of the particles relative to the medium conductivity. Since the electric field is not uniform, the positive charges will experience a greater Coulomb force than the negative charges ($F_+ > F_-$), which results in a net force directed towards the weaker electric field region. This net force is called dielectrophoretic force.

The magnitude of the DC DEP force (F_{dep}) can be described by [Eq. 3.7](#) [77]:

$$F_{dep} = 2\pi\varepsilon m r^3 \frac{\sigma_p - \sigma_m}{\sigma_p + 2\sigma_m} \nabla E^2 \quad \text{Eq. 3.7}$$

where ϵ_m is the permittivity of the suspending medium, r is the radius of the particle, σ_p and σ_m are conductivity of the particle and the medium respectively, and E represents the strength of external electric field. The component ∇E^2 stands for the gradient of the electric field squared.

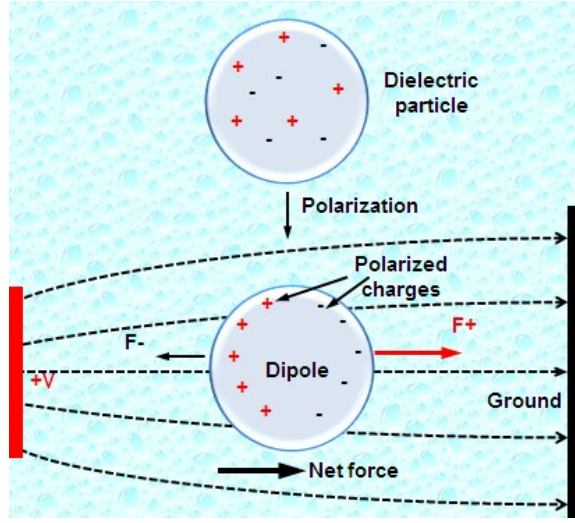


Figure 3.2 Generation of a negative dielectrophoretic force in a non-uniform DC electric field. The dash lines represent electric field.

Similarly with the EP velocity calculation in 3.1.2, the DEP velocity can be estimated by balancing the DEP force and the drag force (Eq. 3.8).

$$v_{dep} = \mu_{dep} \nabla E^2 = \frac{r^2 \epsilon_m}{3\eta} \frac{\sigma_p - \sigma_m}{\sigma_p + 2\sigma_m} \nabla E^2 \quad \text{Eq. 3.8}$$

where the DEP mobility (μ_{dep}) is defined as the relative DEP velocity per unit ∇E^2 [78]. η is the viscosity of the medium, while other parameters are the same as in Eq. 3.7.

Based on the equation, the dielectrophoretic force is proportional to the particle volume and the gradient of the electric field squared. Therefore the magnitude of force reduces significantly with the scaling of the particle size as compared to other forces that are dependent on size. Consequently, DEP is usually ignored in the analysis of forces on small biomolecules such as DNA [78]. Also, the direction of the DEP force is determined by the relative value of σ_p and σ_m : if $\sigma_p < \sigma_m$, the DEP force is directed towards the local electric field minimum, and this phenomenon is called negative DEP force (Figure 3.2); if $\sigma_p > \sigma_m$, a positive DEP force exists, which is directed to the local electric field maximum. In most cases, since the particle being analyzed is insulating, the conductivity of the particle is much smaller than that of the suspending medium, and a negative dielectrophoretic force is exerted on the particle.

3.1.4 Electro osmotic force

For a charged solid surface in a conductive liquid medium, an electrical double layer (EDL) will be formed at the two phase interface. Upon application of an electric field that is parallel to the solid surface, an electroosmotic flow can be generated. As shown in Figure 3.3, an electrical double layer forms on the negatively charged surface (e.g. PDMS). When applying a DC electric field directed from anode to cathode, the Coulomb force induces a movement of the charged EDL, which can lead to the electroosmotic (EOS) flow [79]. The bulk of the solution is electro-neutral, but is

transported along with the EDL due to the viscous drag between lamellas. This convective movement of the fluid will also move DNA, cells, and other items suspended in the bulk solution.

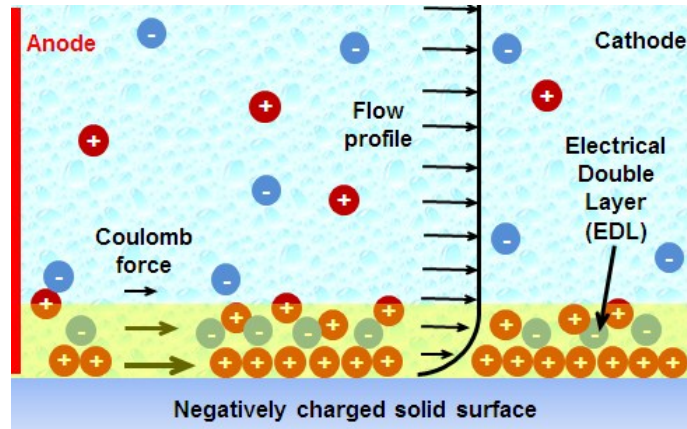


Figure 3.3 Schematic of the electrical double layer (EDL, the yellow area) and generation of the electroosmotic flow.

It should be noted that the flow induced by the EOS effect exhibits a “plug flow” velocity profile, which is distinct from a parabolic profile flow caused by pressure-driven flow. The velocity of the EOS flow is given by Eq. 3.9 [80]:

$$v_{eos} = \mu_{eos} E = \frac{\zeta \epsilon_m}{\eta} E \quad \text{Eq. 3.9}$$

where ζ represents zeta potential, ϵ_m and η are the permittivity and viscosity of the suspending medium respectively, and E represents the strength of external electric field.

μ_{eos} is the EOS mobility whose general value tends to be on the order of $10^{-8} \text{ m}^2\text{V}^{-1}\text{s}^{-1}$ [80]. Thus, a relatively high electric field is required to generate a significant EOS flow.

In summary, in a PDMS microfluidic channel under a spatially non-uniform DC electric field, a particle is potentially affected by 4 forces, among which the EP force and the DEP force are two of the most important forces because of their close connection with the electric field and the particle properties. The net Force acting on the particle is given by Eq. 3.10:

$$\vec{F}_{net} = \vec{F}_{ep} + \vec{F}_{dep} + \vec{F}_{eos} + \vec{F}_{drag} \quad \text{Eq. 3.10}$$

in which the force vectors, \vec{F}_{ep} , \vec{F}_{dep} , \vec{F}_{eos} and \vec{F}_{drag} represent the EP, DEP, EOS, and drag force respectively. The EOS force refers to the force acting on the particle because of the EOS flow. The net velocity of the particle is determined by the net force. In addition, the net velocity is affected by the particle size, the conductivity of the particle and the medium.

3.2 Device Design and Working Principle

3.2.1 Design Criteria

Because cfDNA, proteins, and cells in a blood sample have different sizes and electrical properties, their motion will be influenced differently by the various forces acting on them. Also, the electric field distribution and strength can be tailored by suitable

channel structures and dimensions, which can be designed to manipulate the contents in the sample.

The goal of this thesis is to design a device which can perform rapid quantification of cfDNA directly in whole blood. To realize this objective, several tasks must be completed: first of all, cfDNA in blood has to be isolated from the rest of the constituents; especially those that may significantly influence quantification results, such as red blood cells. Next, a mechanism to concentrate DNA needs to be carried out because its concentration in the blood may be low, making it difficult to detect. Meanwhile, the amount of concentrated DNA must be directly proportional to the original DNA concentration in the sample. Finally, the chemical concentration needs to be transduced into an optical or an electrical signal which can be easily recorded and quantified. Several key design criteria include:

- 1) Developing a device that can be used to differentiate between survivors ($1\mu\text{g/ml}$) and non-survivors ($5\mu\text{g/ml}$) in severe sepsis patients based on respective cfDNA concentration in blood, as described in [Chapter 2.4.4](#).

- 2) Achieving fast quantification, where the measurement time is less than 10 minutes. It is important to optimize both time efficiency and quantification accuracy.

- 3) Using a reagent-free process in order to simplify device operation.

- 4) Realizing a minimally invasive point-of-care system. The blood volume required in the quantification process should only be around $50\mu\text{l}$.

5) Maximizing the portability of the device. A low DC power supply (<10V) is required, which can be simply provided by batteries.

Based on the design criteria listed above and the methods for DNA extraction and concentration reviewed ([Chapter 2](#)), electrokinetic concentration was determined to be the most appropriate for this application because it is reagent-free. Subsequently, the fluorescent staining method was selected to enable DNA quantification by transducing chemical signals into optical signals. The fluorescent dye must be able to selectively label DNA molecules and maintain fluorescent linearity relative to DNA concentration despite other contaminants that may exist in the blood. Therefore, PicoGreen was selected ([Chapter 4](#)). The short detection time, low power supply, and small sample volume consumption means that small sample channel dimensions and short distances between the two electrodes are required. Also, for easier electrode placement and fluorescent measurement, the distance between the anode and cathode should be around 5mm. In addition, a porous material is necessary for assisting in DNA trapping as well as avoiding direct contact between the sample and the electrode.

3.2.2 Device Design

Based on the design criteria and analysis above, the microfluidic device designed is displayed in [Figure 3.4](#).

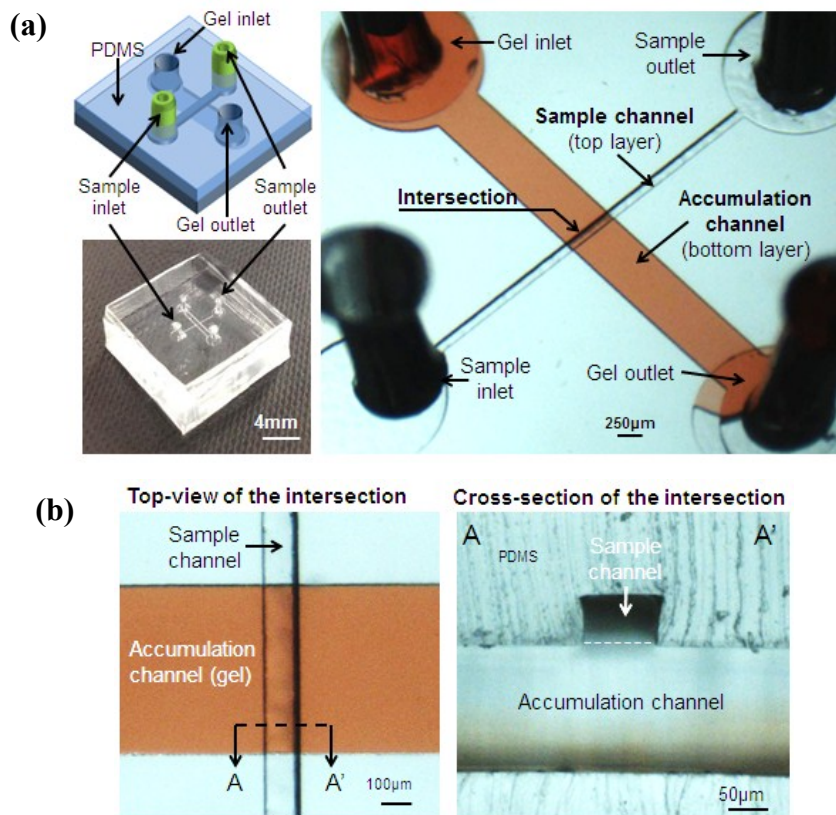


Figure 3.4 Schematic of the device: (a) an overview of the device; (b) a top-view and cross-sectional view of the intersection.

The device is comprised of two PDMS layers with a single microchannel in each layer (Figure 3.4(a)). The top layer consists of a sample channel with a dimension of 4mm (L) \times 100µm (W) \times 60µm (D), and in the bottom layer locates an accumulation channel with a dimension of 4mm (L) \times 500µm (W) \times 160µm (D). The total size of the device is as small as a dime. The two channels are positioned perpendicular to each other as shown in Figure 3.4(b). The top and bottom channels meet at an intersection where the

two channels are fully connected. The electrodes (not shown in the figure) are placed at the sample outlet and the gel inlet. The accumulation channel is pre-filled with 1% agarose gel which works as the porous material mentioned in 3.2.1. The gel will be exposed to the sample channel only at the intersection where the DNA is collected and concentrated. The intersection is also the location where fluorescent intensity is measured.

Agarose gel is used in the device because it is low-cost and easy to prepare although heating is required to melt agarose in buffer. Most importantly, agarose gel has been widely applied in electrophoresis due to its conductivity; hence it is a good choice for this application. A gel concentration of 1% is used in the device. This is because in previous electrophoresis experiments using 2% gel, no band was visualized for DNA over 300bp, which is a principal size for cfDNA in blood [5]. This means that larger DNA molecules were being blocked out of the gel. Therefore, the gel concentration must be decreased in order to allow for most of the DNA in the blood sample to pass through, while other contaminants like proteins and cells would be blocked.

The sample volume consumed is determined by the volume of the sample channel, which in this device is much smaller than 1 μ l. Thus the total sample volume required is far less than a droplet (~50ul) even considering the extra consumption in the inlet and outlet of the channel, and the possible waste during sample loading.

The length of the sample channel and the accumulation channel are both set as 4mm so that the distance between the two electrodes will be approximately 4mm along the channels. Based on the dimension of the channels, the volume of the accumulation channel is designed to be much larger than that of the sample channel due to two main reasons. Firstly, the smaller sample channel can lead to a relatively strong electric field compared with that in the accumulation channel (3.3.1). A stronger electric field in the sample channel is necessary so that more DNA can be driven to the intersection and is subsequently forced into the gel in the accumulation channel. Meanwhile a relatively weak electric field in the accumulation channel will slow down the migration speed of DNA in the gel, thus concentrated DNA at the intersection can be kept longer. Secondly, a smaller sample channel and a larger accumulation channel is key to the gel filling process (Chapter 4.1.2.5). Some preliminary gel filling tests have shown that the melted agarose gel entered and blocked the sample channel during the gel filling process if the accumulation channel was smaller than or equal to the sample channel.

In summary, the goal of this device is to quickly quantify cfDNA in a droplet of whole blood, based on which 5 key criteria have been set including a differentiation of 1µg/ml and 5µg/ml concentrations, a maximum measuring time of 10min, a maximum sample volume of 50µl, a maximum DC power supply of 10V, and a reagent-free process. A device is designed which can potentially meet the criteria, and a detailed experimental results will be shown in Chapter 5.

3.3 Modeling and Force Analysis

To better study the working principle of the device, the DC electric field in the device channels were simulated with a finite element analysis software, COMSOL[®] Multiphysics.

3.3.1 Numerical Simulation of the Electric Field

This simulation is carried out to investigate the DC electric field strength and its distribution at the intersection area when a potential difference was applied between the sample channel and the accumulation channel. The *Electrostatics* Module in COMSOL[®] Multiphysics 4.3 (COMSOL Inc., MA, USA) was used to build the model. A step-by-step model building up process is described in [Appendix A](#).

The model geometry and dimension is shown in [Figure 3.5\(a\)](#). The material parameters, including relative permittivity (ϵ) and electrical conductivity (σ), were set as blood plasma ($\epsilon=70$, $\sigma=0.01S/m$) for the sample channel [81], and water ($\epsilon=78$, $\sigma=5.5\times 10^{-6}S/m$) for the accumulation channel [82]. Properties for silver (Ag) electrodes were chosen from the material library in the software.

For the electrostatic simulation, key parameters were set as below:

- 1) Assumptions:

- a. Charge conservation;
 - b. Uniform temperature at 293.15K.
- 2) Boundary conditions: the electrode in the sample channel was set at ground boundary condition (Figure 3.5(b)), and the other electrode in the accumulation channel was set at positive potential (Figure 3.5(c)). All the other channel surfaces were set to zero charge boundary condition ($n \cdot D = 0$) because of the insulating property of the PDMS channel walls.
- 3) Initial input: 0V.

According to the setup above, the governing equations of the simulation are illustrated in Eq. 3.11 to Eq. 3.13:

$$E = -\nabla V \quad \text{Eq. 3.11}$$

$$D = \varepsilon_0 \varepsilon_r E \quad \text{Eq. 3.12}$$

$$\nabla \cdot D = \rho_v \quad \text{Eq. 3.13}$$

where E is the electric field strength; V is the potential difference between the two electrodes; D is the electric displacement field; and ε_0 is the vacuum permittivity ($\varepsilon_0 \approx 8.85 \times 10^{-12}$ F/m); ε_r is the relative permittivity of the material, which is set as 70 in this model; and ρ_v refers to the volume charge density of free charges in the material.

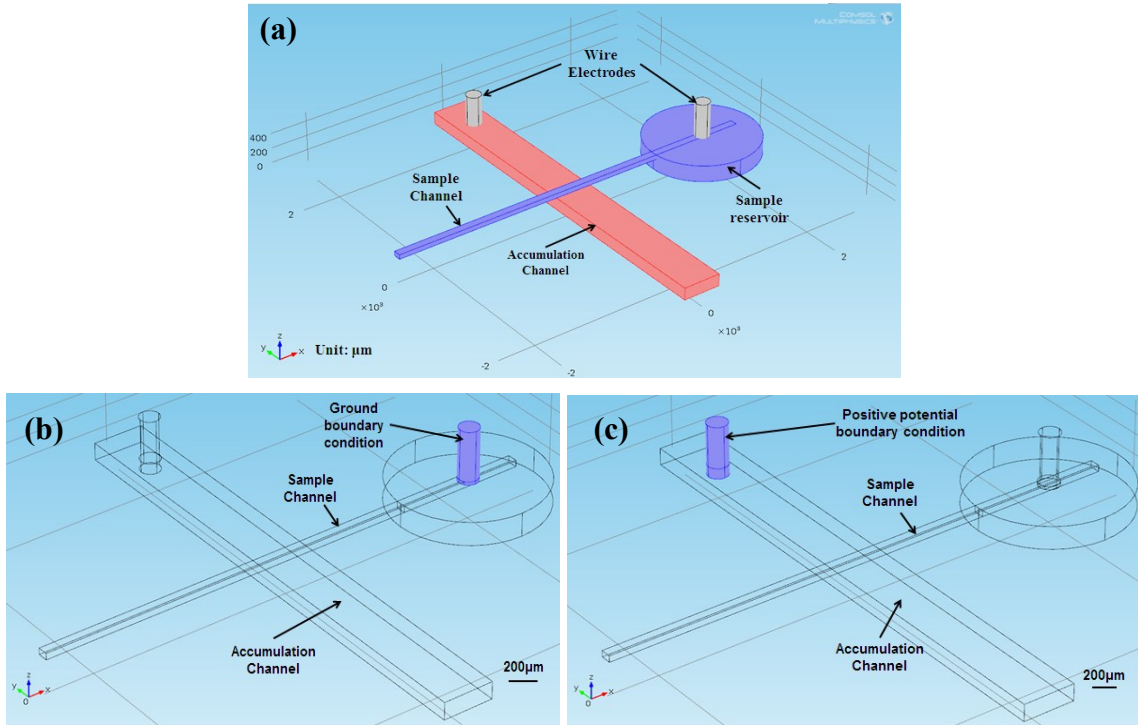


Figure 3.5 Schematic of the model built in COMSOL: (a) the geometry of the model; (b) the ground boundary condition definition; (c) the positive charge boundary condition definition.

To solve the model, a *Free Tetrahedral* mesh was used with a maximum mesh size of $15\mu\text{m}$. The simulated result is shown in [Figure 3.6](#), which is independent of the meshing resolution based on the mesh dependence test ([Appendix B](#)).

[Figure 3.6\(a\) & \(b\)](#) presents the potential drop between the two electrodes. It can be observed that most of the potential drop occurs in the sample channel between the ground electrode and the intersection while in the accumulation channel, the potential drop is very small (less than 1V). Therefore the electric field strength is much lower in

the accumulation channel than in the sample channel. Figure 3.6(c) & (d) shows that the magnitude of the electric field is highest at the intersection region, and the electric field strength in the sample channel (6 - 8 mV/ μm) is much higher than that in the accumulation channel (<1 mV/ μm).

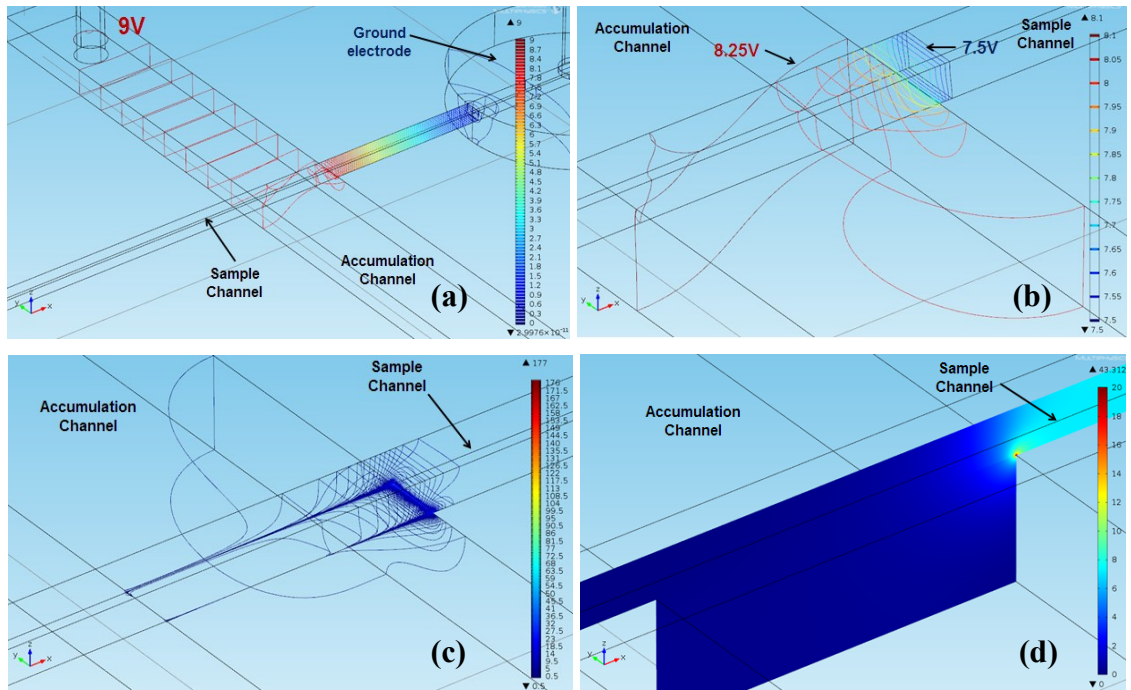


Figure 3.6 Simulated results of: (a) potential drop between the two electrodes; (b) potential drop at the intersection. The difference between each line is 0.05V; (c)&(d) the electric field strength at the intersection. The difference between each line in (c) is 0.5mV/ μm .

A noticeably higher electric field gradient is also generated at the intersecting channel junction, which is reflected by denser contours compared with other regions. But

in the regions of the sample channel and accumulation channel that are away from the intersection, the gradient of electric field significantly drops.

To better characterize the electric field distribution in the sample channel, several locations were chosen to graph the electric field magnitude. In COMSOL[®], a plane was first selected which is 1 μ m above the bottom of the sample channel. This height was chosen to show a typical electric field distribution along the sample channel. Other layers share a similar electric field pattern as well. Three lines that run the entire length of the intersection were then selected along this plane for analysis (Figure 3.7(a)). The distances between the lines and the channel wall were defined as 5, 50, and 95 μ m respectively, which were chosen to be representative of areas close to the channel walls and along the center of the channel. The electric field strength along these 3 lines is shown in Figure 3.7(b).

These results reaffirm the conclusions drawn from the data previously discussed in Figure 3.6. The electric field forms a peak around the edge ($x=550\mu$ m) of the intersection, where both the magnitude and the gradient of the electric field reach the maximum.

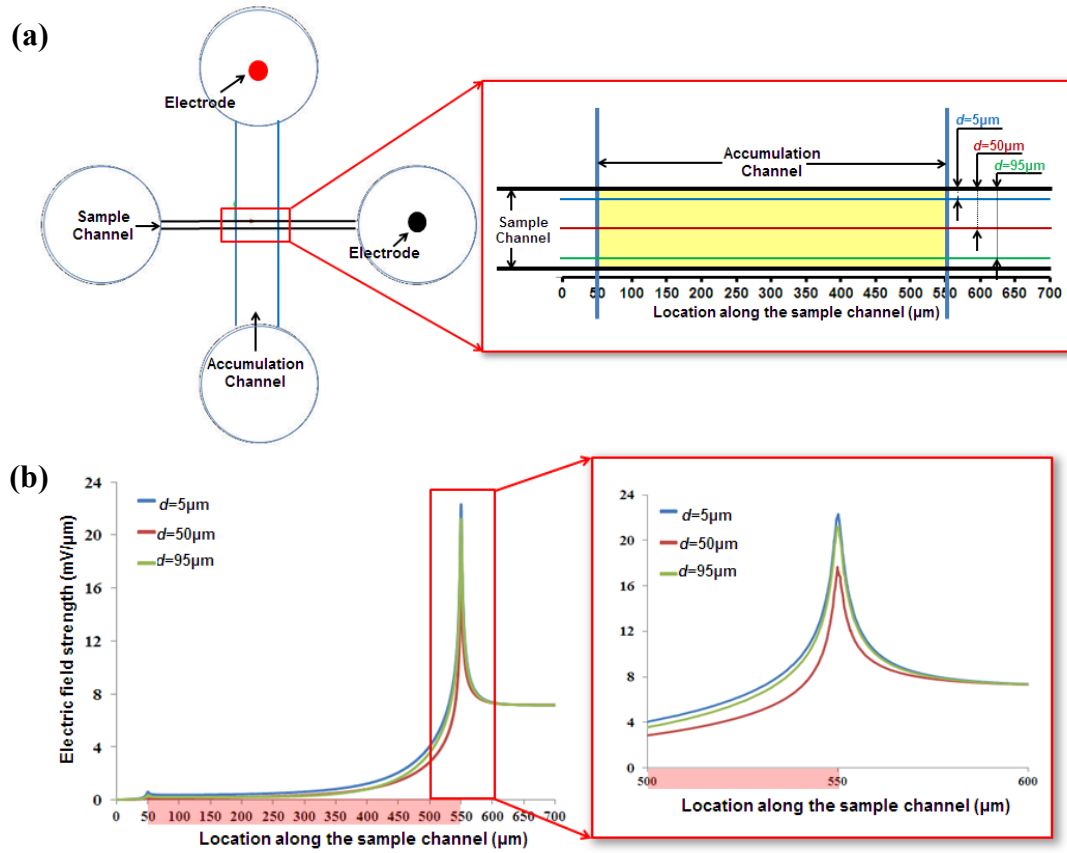


Figure 3.7 Electric field magnitudes of the selected sites in the sample channel. The plane selected was $1\mu\text{m}$ above the bottom of the sample channel: (a) the locations of the 3 lines along which the magnitude of electric field was simulated. The yellow area represents the intersection; (b) the simulated electric field strength along the 3 lines. The red area along the x-axis indicates the accumulation channel location.

3.3.2 Force Analysis

Based on the analysis introduced in 3.1.2 and 3.1.3, and the electric field distribution demonstrated in 3.3.1, the electrophoretic (EP) force and dielectrophoretic (DEP) force both reach maximum values at the intersection.

Figure 3.8 illustrates the directions of EP force and DEP force encountered by the objects in the sample channel along a plane that is located $1\mu\text{m}$ above the bottom of the sample channel. The object (e.g. DNA, red blood cell) is negatively charged, and is subjective to a negative DEP effect.

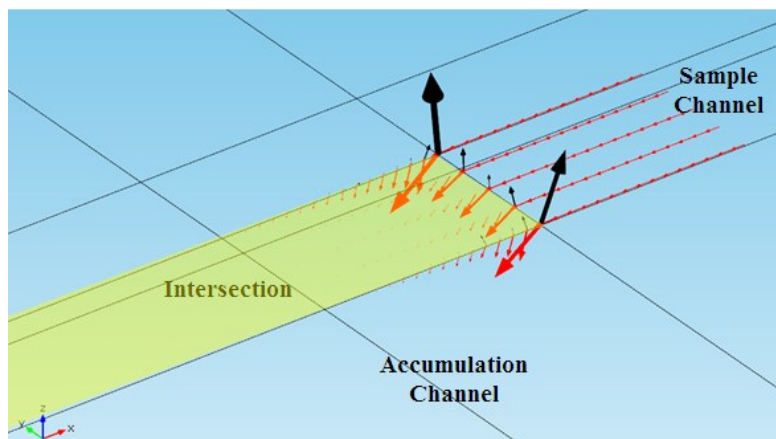


Figure 3.8 Directions of EP force (red arrows) and DEP force (black arrows) in a plane $1\mu\text{m}$ above the bottom of sample channel. The arrow sizes are proportional to the magnitude of EP force and DEP forces respectively. The yellow area represents the intersection.

As shown in the figure above, the EP force is directed away from the sample channel and into the accumulation channel while the DEP force points in the opposite direction. The magnitude of the forces is larger at the locations that are close to the channel walls compared with the center of the channel.

Considering the difference of the charge and size between DNA and blood cells in the sample, the electrokinetic forces vary as shown in Figure 3.9.

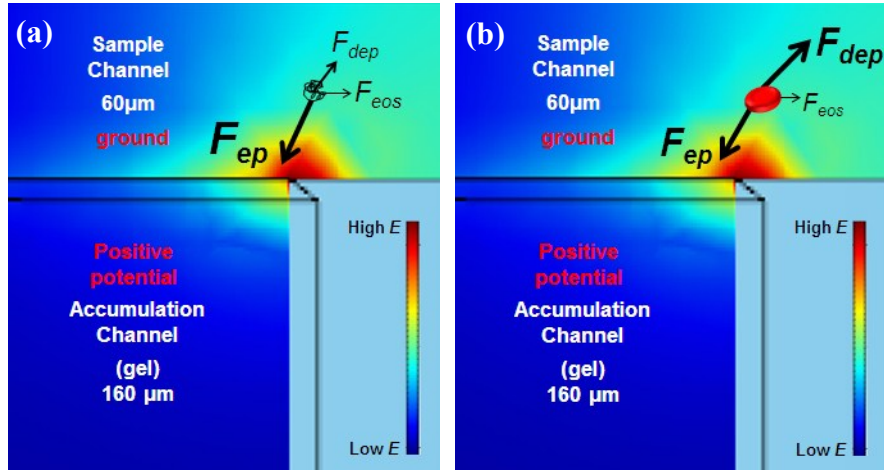


Figure 3.9 Electrokinetic forces analysis for (a) a DNA molecule and (b) a red blood cell in the sample channel close to the intersection. E represents electric field strength.

Since the EP force and the DEP force are directed in different direction, their relative magnitude determines the direction of the particle's motion. For the cfDNA in the samples from severe septic patients, two principal chain lengths were found to be around 150bps and 300bps. There are also cfDNA fragments with multiples of 180bps, and over $\sim 10,000$ bps [5]. Based on the force calculation (Appendix D), the ratio of EP velocity and DEP velocity ($\frac{v_{ep}}{v_{dep}}$) is in the order of 1×10^8 when 9V is applied on the device. Therefore cfDNA will move towards and into the gel. Meanwhile, red blood cells will move in the opposite direction ($\frac{v_{ep}}{v_{dep}} < 1$).

The electroosmotic flow generated in the sample channel is expected to be around $200\mu\text{m/s}$ [79]. However, in the plasma or blood sample, the electric double layer formed at the surface of PDMS channel walls can be severely affected by the absorption and interaction between the proteins or cells and the channel surface. The areas covered by proteins are treated as zero effective electric charge [78]. As a result, the electroosmotic flow generated will be much smaller than the expected value.

In summary, based on the force calculation and analysis above, the cfDNA in the blood sample is dominated by EP force which drives it into the gel at the intersection. But the DEP force on blood cells is able to overcome the EP force, thus moves them away from the gel.

3.4 Summary

A charged particle experiences 4 primary forces in a non-uniform DC electric field. The trajectory of the particle in the sample channel depends on its property (e.g. size, charge) and the electric field. Based on the goal of this thesis, 5 design criteria have been set, and the device and experiments have been designed. The simulated electric field revealed that both the magnitude and the gradient of electric field formed their maximum values at the intersection of the sample and accumulation channels in the device. Force

analysis concluded that DNA was driven into the gel by the dominating EP force, while red blood cells moved away from the gel due to a larger DEP force.

The device designed is beneficial for DNA accumulation in whole blood samples, which is key for subsequent quantification. The next step is to fabricate the device and conduct experiments.

Chapter 4.

Device Fabrication and Experimental Preparation

In this chapter, the device fabrication process will be described in detail. Experimental preparation will also be introduced, including sample preparation, device preparation, and experimental setup. Fluorescent image processing methods are shown in the end for data analysis.

4.1 Device Fabrication

The device is fabricated in multiple steps. A schematic of device fabrication process is shown in [Figure 4.1](#).

4.1.1 Materials Used

4.1.1.1 Silicon wafer

A silicon wafer serves as a substrate to make the mold for the devices using photolithography process. Silicon wafer bonds well with a negative photoresist SU-8 at a low temperature [83], which increases the lifetime of the mold. In this process, 3-inch silicon wafers (University Wafers, MA, USA) are used.

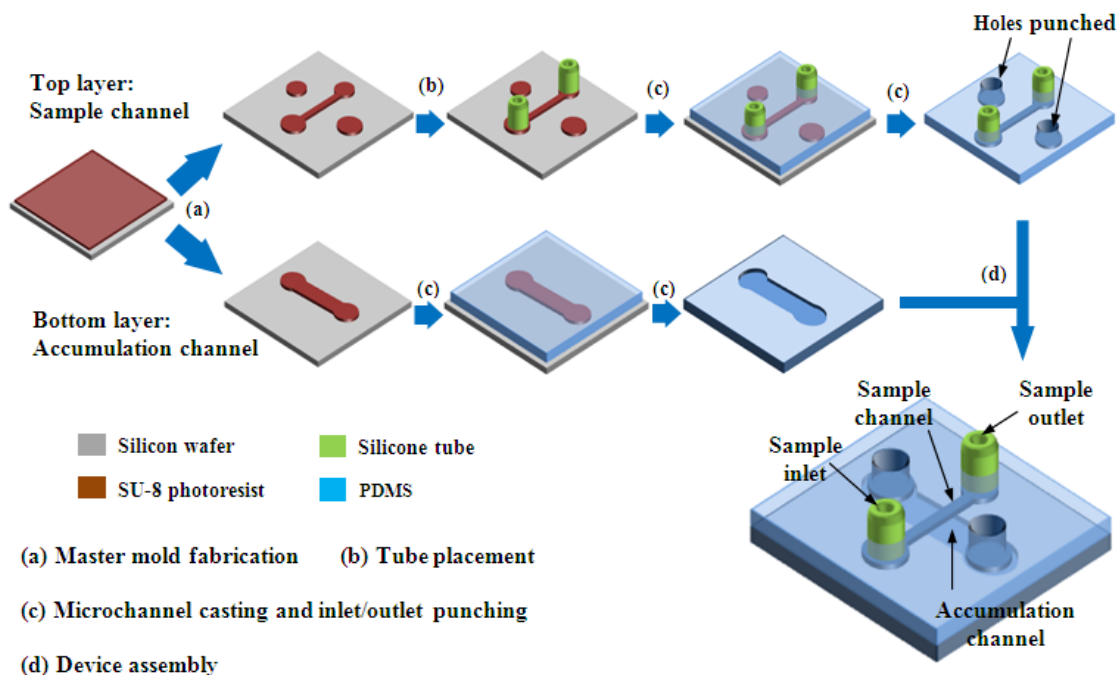


Figure 4.1 Schematic of Device Fabrication Process

4.1.1.2 SU-8 Photoresist

SU-8 Photoresist is an epoxy-based negative photoresist commonly used in micromachining and other microelectromechanical system (MEMS) applications. With a single coating process, it can be spun into thicknesses ranging from around 1 micron to 200 microns [84]. After exposed to near UV light (350-400 nm), SU-8 photoresist is polymerized and has highly stable thermal, chemical and mechanical properties. It has been widely used in fabrication of microstructured mold even with high aspect ratio. In this process, SU-8 2000 series products from *MicroChem Corp.* are used to fabricate PDMS molds.

4.1.1.3 Polydimethylsiloxane (PDMS)

Polydimethylsiloxane (PDMS) is a type of silicone rubber which is commercially available and widely used in industry and laboratory research. The chemical formula is $\text{CH}_3[\text{Si}(\text{CH}_3)_2\text{O}]_n\text{Si}(\text{CH}_3)_3$. It has several desirable properties, such as being transparent, hydrophobic, nontoxic and biocompatible, ability to replicate submicron features, easy bonding to itself or glass, and has low cost [85][86]. Thus PDMS has been widely used in rapid prototyping of microfluidic devices.

To make PDMS elastomer, *Sylgard*[®] 184 Silicone Elastomer kit was purchased from *Dow Corning Corp.* in USA. The kit contains two liquid components: a base and a curing agent. After thoroughly mixing the base and curing agent with a weight ratio of 10:1, the mixture solidifies into a flexible elastomer with 24 hours polymerization time in room temperature. Flexibility of the final product can be modified with different base/curing agent ratio, and curing time of the mixture can be largely shortened by heating [87].

4.1.1.4 Silicone tube

Silicone tubes are flexible tubes made of silicone polymers. PDMS is one type of silicone, and their physical and chemical properties are similar [88]. Silicone tubes are used in the fabrication as bond strongly with PDMS at room temperature due to their

similar structures. *Masterflex* platinum-cured silicone tubing was purchased from *Cole-Parmer*®, and used as the inlet and outlet of sample channel.

4.1.2 Fabrication Steps and Methods

The device fabrication includes the following 5 steps:

1) Master mold fabrication

The molds of channels for PDMS casting are fabricated using photolithography method. Photomasks with desired channel patterns and dimensions were completed with *AutoCAD* (Autodesk Inc., San Francisco, USA), followed by sending to *CAD/Art Services Inc.* for ultra-high-resolution printing on transparency sheet. Based on the manuscript provided by *MicroChem Corp.*, the molds were completed following the process in [Appendix C](#).

2) Tubing placement

Silicon tubes were cut flat into small length (about 8mm), and were placed on two ends of the sample channel mold as show in [Figure 4.1\(b\)](#). The tubes with clear and smooth inner surface were used as the inlet and outlet of the sample channel.

3) Microchannel casting and inlets/outlets punching

The PDMS microchannels were fabricated using a soft-lithography method ([Figure 4.1\(c\)](#)). PDMS pre-polymer was prepared and poured into molds, and left to cure

at room temperature for 24 hours. Then the solidified pieces were peeled off from the molds. Two holes were punched (1.2mm punch, Harris Uni-Core™) in the top layer piece as shown in [Figure 4.1\(c\)](#), and were used to fill gel into the accumulation channel.

4) Device assembly

The top layer and bottom layer of PDMS were finally assembled to one piece by plasma bonding ([Figure 4.1\(d\)](#)). The two PDMS parts were exposed to air plasma generated by 18W RF for 120s (Harrick Plasma, NY, USA), after which they were aligned and bonded as shown in [Figure 4.2](#), to form sealed channels with inlets/outlets, and an intersection between the top and bottom channels were formed. The completed devices were then put in the oven for 4 hours at 70°C to strengthen the bonding.

The next step which is filling gel selectively in the bottom accumulation channel cannot be performed immediately right after assembly, as the plasma bonding process makes PDMS hydrophilic [89]. Hydrophobic surfaces are needed at the intersection between the top and bottom channels to prevent the flow of the gel that is filled in the accumulation channel from entering the sample channel through capillary pinning. As a result, newly assembled device should be left for overnight before gel filling since PDMS regains its hydrophobicity as it ages [89].

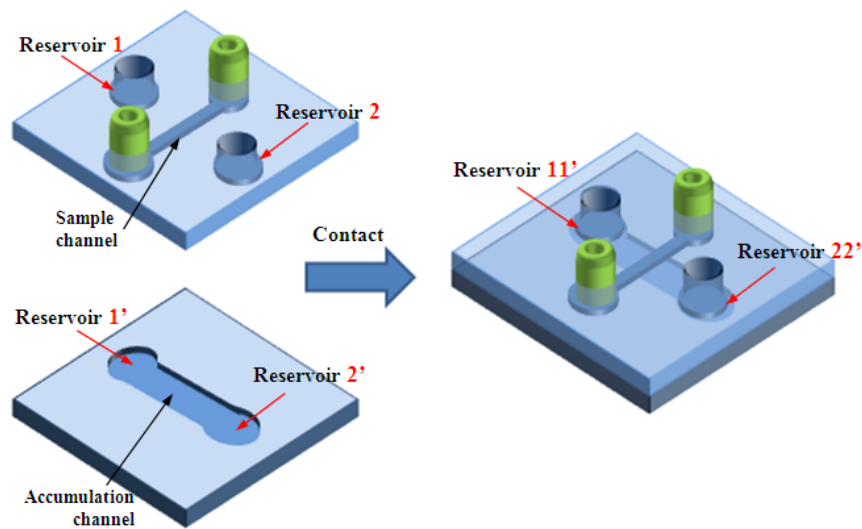


Figure 4.2 Device assembly

5) Gel filling and electrodes placement

Before loading sample in the sample channel, gel must be filled in the accumulation channel as steps shown in Figure 4.3. A droplet of heated liquid gel was dropped at one of the open ends of accumulation channel. Then an empty syringe was used to aspirate the heated 1% agarose solution from the other end of the channel. During the aspiration, liquid agarose solution fills the accumulation channel completely, while the sample channel stays clear due to aspiration of air from it. After ~30 seconds, the agarose solution cooled down and gelled, following which silver wire electrodes (0.2mm diameter, Warner Instruments) were inserted in the sample channel and accumulation channel respectively.

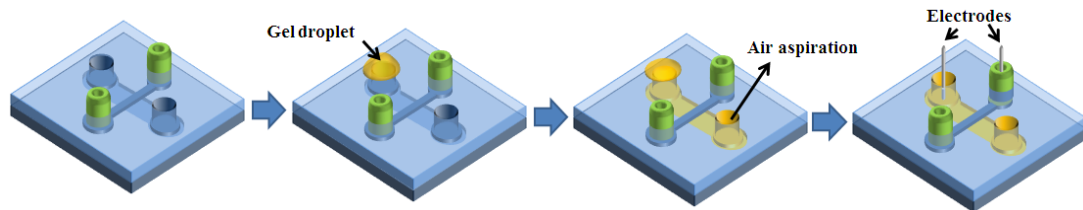


Figure 4.3 Gel filling process: agarose gel is represented in yellow.

4.2 Sample Preparation

4.2.1 Materials

4.2.1.1 *Quant-iT™ PicoGreen® dsDNA Reagent and Kits*

Purchased from *Invitrogen™, Life Technologies*, the kit includes standard lambda DNA solution, fluorescent probe solution, and buffer solution for DNA quantification and other applications. The specific details about the three components in the kit are detailed below [90]:

1) Component 1: Lambda DNA Standard (λ -DNA)

λ -DNA in this kit is linear double-strand DNA with size range of 125bp–23.1kb. It is prepared from λ -DNA (cIind1ts857 Sam7) that has been digested to completion with Hind III [91]. Studies have shown that cfDNA are mostly double-stranded DNA [92], and the molecular size ranges from ~150bp to over ~10kbp [5]. Therefore this λ -DNA sample can be a reasonable simulant for cfDNA in clinical blood samples.

2) Component 2: PicoGreen dsDNA reagent

PicoGreen reagent is a fluorophore specifically intercalates with double-strand DNA (dsDNA) molecules. Characterization studies have shown that the fluorescence of PicoGreen enhances over 1000-fold upon binding with dsDNA. The fluorescent linearity can be maintained even in the presence of most salts, proteins, agarose, and other contaminants. However, the intensity of the fluorescent signals may be affected as shown in [Table 4.1](#) [93]. It shows that the baseline of fluorescent signals may change due to the presence of contaminants in blood samples. However, levels of contaminants between individuals are similar and the signal changes resulting from these contaminants are minimal. In addition, the cfDNA concentrations in patient samples are much higher than 500ng/mL, thus the fluorescence of DNA will be more dominating in the quantification.

[Figure 4.4\(a\)](#) shows the linear increasing relationship between PicoGreen fluorescent intensity and dsDNA concentration in the pg/ml and ng/ml range. [Figure 4.4\(b\)](#) provides information of PicoGreen specificity on dsDNA among a sample containing single-strand DNA (ssDNA) and RNA. These properties make PicoGreen a suitable fluorophore for cfDNA quantification in this application. Based on the excitation/emission spectra of PicoGreen ([Figure 4.4\(c\)](#)), a fluorescent microscope with 457-492nm band excitation and 508-551nm band emission will be used. The binding mechanism between a PicoGreen molecule and the DNA is shown in [Figure 4.4\(d\)](#). It shows that intercalation is the principal mechanism.

Compound	Concentration	Signal change ^a
Ammonium acetate	50 mM	-3%
Sodium acetate	30 mM	+3%
Sodium chloride	200 mM	-30%
Zinc chloride	5 mM	-43%
Magnesium chloride	50 mM	-64%
Urea	2 M	+9%
Phenol	0.1% ^b	+13%
Ethanol	10% ^b	+12%
Chloroform	2% ^b	+14%
Sodium dodecyl sulfate	0.01% ^c	-1%
Triton X-100	0.1% ^b	+7%
Bovine serum albumin	2% ^c	-16%
IgG	0.1% ^c	+19%
Poly(ethylene glycol)	2% ^c	+8%
Agarose	0.1% ^c	+4%

Table 4.1 Effects of contaminants on the fluorescent intensity of PicoGreen in the presence of 500ng/mL calf thymus DNA: *a.* the change in fluorescence signal observed with the indicated concentration of assay contaminant relative to the presence of no contaminant in the assay; *b.* volume/volume; *c.* weight/volume [93].

3) Component 3: 20X TE buffer

The buffer solution consists of 200 mM Tris-HCl and 20 mM EDTA with a pH of 7.5 at room temperature. It is used to dilute the original DNA solution and PicoGreen reagent to desired concentrations.

4.2.1.2 Clinical blood plasma

Clinical plasma samples used in the experiments come from both healthy donors and septic patients. They were prepared by spinning fresh whole blood in a centrifuge and were separated from blood cells at bottom layer.

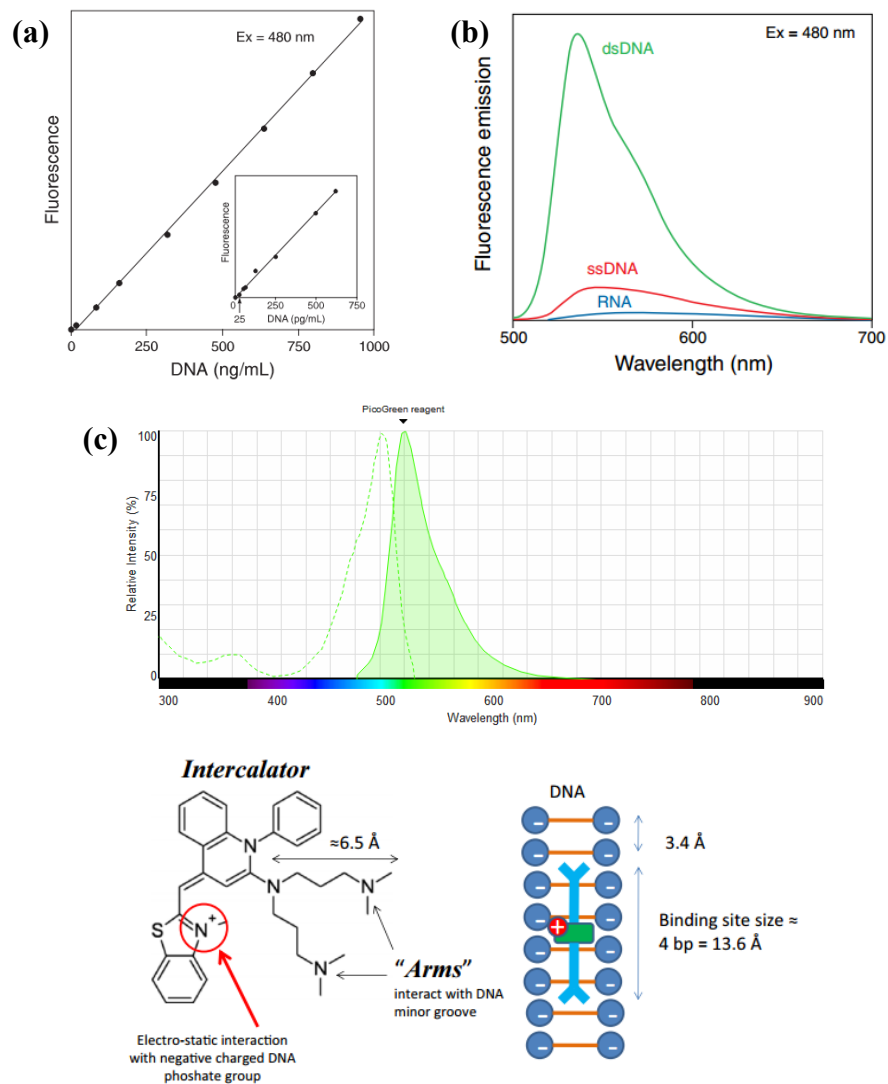


Figure 4.4 Properties of PicoGreen reagent: the emission fluorescence was measured at 520nm using a spectrofluorometer. (a) linearity and sensitivity of PicoGreen at low dsDNA concentration range (<1µg/ml); (b) fluorescence enhancement of PicoGreen upon binding dsDNA, ssDNA, and RNA; (c) PicoGreen fluorescence excitation spectra (dash line) and emission spectra (green area); (d) structural elements of the PicoGreen molecule and a model demonstrating the binding between PicoGreen and DNA [94].

The samples are provided by another research project: DNA as Prognostic Marker in ICU Patients Study, Clinical Trials (DYNAMICS, government identifier: NCT01355042). In that study, plasma samples and clinical data have been collected from septic and non-septic critically ill patients at nine study sites. For each of the patients, data on cfDNA levels and clinical outcomes are available.

4.2.1.3 Whole blood

Fresh whole blood was drawn from a healthy volunteer who had signed a consent document for the use of blood in the experiments. It was used right after the blood drawn to make sure the sample can effectively simulate whole blood from septic patients.

4.2.1.4 Agarose gel

Agarose gel is a three dimensional porous structure formed by agarose molecules. It is mainly used for DNA electrophoresis and other biological studies. It is in a liquid state at high temperature (85-95°C), and becomes a gel at lower temperature (35-42°C), [95]. This phase transition is utilized to melt the agarose solution and fill it into the microchannel before it rapidly solidifies and assumes the shape of the channel. Agarose used in this process is purchased from BioShop Canada Inc.

4.2.2 Sample preparation

To test the device, four samples are prepared:

1) DNA in buffer sample

DNA in buffer sample was prepared by diluting the λ -DNA with TE buffer to a certain concentration. Then PicoGreen reagent was added into the solution to fluorescently label DNA. This sample was used in proof-of-concept experiments to demonstrate DNA accumulation at the intersection using electric field.

2) DNA spiked plasma sample

In order to simulate clinical plasma samples, plasma from healthy donors was used to dilute commercial DNA solutions down to certain concentrations. Thus, this prepared sample contains all the proteins and other plasma constituents apart from the DNA. Since plasma from healthy donors contains very small amount of DNA, it would not significantly affect the DNA concentration. PicoGreen was added later into the DNA spiked plasma mixture.

3) Clinical plasma sample

This sample was prepared by directly adding PicoGreen reagent into clinical plasma samples from healthy donors and septic patients. It was used to validate the device and to demonstrate differentiation between clinical samples of healthy and septic patients.

4) DNA spiked whole blood sample

In order to simulate clinical whole blood samples which include blood cells and various proteins, λ -DNA was diluted into certain concentrations with whole blood from a healthy donor. Then PicoGreen was added into the mixture. It was used in preliminary experiments to test the feasibility of applying clinical whole blood to the device.

4.3 Sample Loading and Experimental Setup

4.3.1 Sample loading

Sample was loaded with a clean 1 ml syringe (BD Luer-Lok™ Tip, NJ, USA) and 20G needle (BD PrecisionGlide™, NJ, USA). It was injected into sample channel by sticking the needle in the sample inlet and pushing syringe slowly (Figure 4.5). Once sample fluid was seen at the outlet, the injection was stopped.

4.3.2 Experimental setup

The experiment was set up as in Figure 4.5. The device was placed on a compact fluorescent microscope (Model 500, Etaluma Inc., CA, USA) with a 10x lens. Silver wire electrodes were connected with a DC power supply (Keithley 2410, OH, USA). The accumulation channel was connected with anode (red), while the sample channel was connected with cathode (black). When a positive voltage was applied, a DC electric field

from accumulation channel to sample channel would be generated. During experiments, the device was covered with a black cloth which reduces light interference from outside.

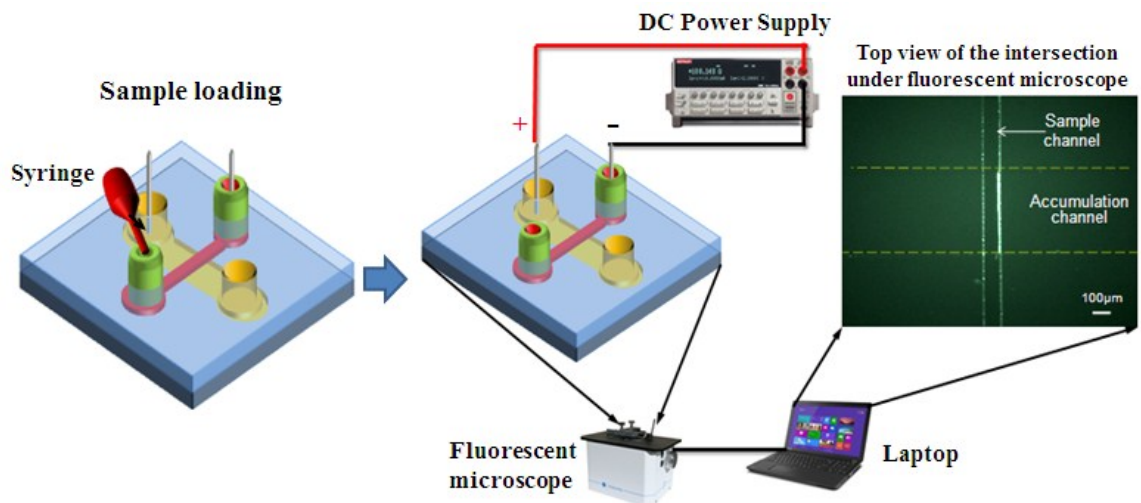


Figure 4.5 Sample loading and experimental setup: sample is represented in red.

4.4 Image Processing Methods

Fluorescent images obtained from the microscope contained the spatial distribution of the fluorescent intensity from the fluorophore that represents the DNA concentration at various locations in the device. In order to quantify the intensity and make a co-relation with the DNA concentration, two methods were applied to process the images.

4.4.1 Average gray scale measurement

Original fluorescent pictures taken on the microscope are RGB images as displayed in [Figure 4.6\(a\)](#). It shows a 4-minute DNA accumulation result with DNA in buffer sample in the device. Pictures were transferred from RGB to 8-digit gray scale format by ImageJ 1.48v, with gray scale values distributed between 0 and 255 ([Figure 4.6\(b\)](#)). For each pixel in the image, the brighter the fluorescence was, the higher the gray scale value. Then the intersection area was selected ([Figure 4.6\(b\)](#)), where the mean gray scale value was measured and calculated. This mean gray scale value was used as a parameter to represent the average fluorescent intensity of the intersection area.

4.4.2 Relative Gray scale measurement

Similar to the previous method, original photos were transferred into 8-digit gray scale images for calibration. Following that two regions – one at top of the intersection region ($M1$ in [Figure 4.7](#)) and the other at the top edge of the sample channel ($M2$ in [Figure 4.7](#)) were selected and the difference in the average intensity in these regions was used for quantification. This method compares the intensities of the region where the accumulation of DNA is the most intense with the region where the concentration of the DNA is that of the original sample solution and normalizes for variation in the external environmental factors such as illumination intensity, light leakage etc.

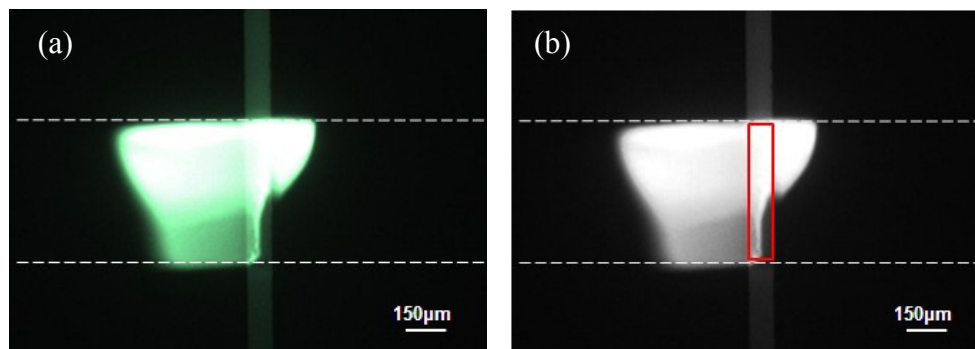


Figure 4.6 A 4-minute DNA accumulation result with DNA in buffer sample in the device: the dash lines are the outline of accumulation channel; (a) RGB fluorescent image; (b) 8-digit gray scale image. Mean gray scale value is measured and calculated in the area enclosed by red lines.

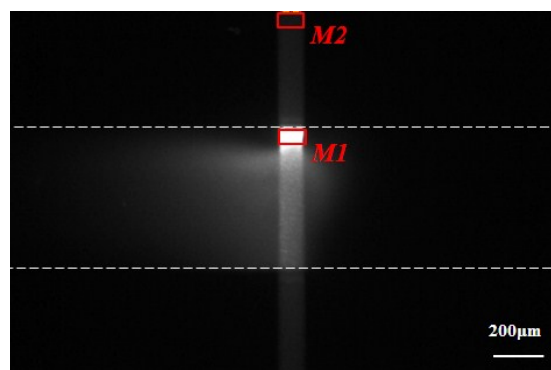


Figure 4.7 A 5-minute DNA accumulation result with clinical plasma sample in the device: the dash lines label the boundary of accumulation channel; *M1* and *M2* represent areas for gray scale value calculation.

4.5 Summary

In this chapter, the fabrication of device and the preparation of experiments are introduced. Silicon molds was constructed using photolithography, and soft-lithography

was used in PDMS channels casting. Agarose gel was filled in the accumulation channel with air aspiration method. Experiments were carried out following loading sample, applying DC electric field, and taking fluorescent pictures of the intersection. Finally, fluorescent images were processed quantitative data analysis.

Chapter 5.

DNA Accumulation and Characterization

In last chapter, the device fabrication, sample preparation, and experimental setup were introduced in detail. This chapter presents the DNA accumulation and fluorescent intensity measurement results using different samples mentioned in [Chapter 4.4.2](#). A demonstration of DNA accumulation in the proposed device was carried out first. Then the DNA concentration from complex samples was characterized. Next, the effect of applied voltage on DNA accumulation was analyzed. Finally, a device configuration that eliminated sample preparation was demonstrated.

5.1 Demonstration of DNA Accumulation

The purpose of this experiment was to prove that cfDNA in blood can be efficiently accumulated on the gel at the intersection region between the two channels in the device, which is a prerequisite step for subsequent quantification.

A λ -DNA spiked plasma sample was prepared using the DNA quantification kit introduced in [Chapter 4.2.1](#). The original 100 μ g/ml λ -DNA in the kit was diluted into 20 μ g/ml using the TE buffer. The concentration of 20 μ g/ml was verified by measuring

the prepared DNA solution with a spectrophotometer. Then the DNA concentration of 1 μ g/ml was prepared by mixing 25 μ l 20 μ g/ml DNA with 100 μ l blood plasma from a healthy donor, followed by adding 375 μ l 200-fold diluted PicoGreen reagent from the kit into the sample solution. The tube containing prepared sample was wrapped with aluminum foil to prevent photo bleaching of PicoGreen, and was left in room temperature for 10 minutes to make sure DNA and PicoGreen were thoroughly intercalated. The brightness of the light source (LED) was set as 29 in the software, which represented an illuminance of around 1.0×10^4 lux, measured with a digital lux meter (LX1332B, Vicimeter Technology CO., LTD., Shenzhen, China). Brightness was maintained the same throughout all the experiments.

The DNA spiked plasma was loaded in the sample channel using a 1ml syringe, which was removed once the sample channel was filled. No voltage was applied for the first 5 minutes after sample loading. Then 9V was applied for the following 5 minutes. Images of the fluorescent intensity at the intersection between the sample channel and the accumulation channel were taken every one min. The DNA accumulation results before and after applying the electric field could be compared by measuring the fluorescence change within the first 5 minutes (no electric field) and the last 5 minutes (electric field applied) respectively. The results are shown in [Figure 5.1](#).

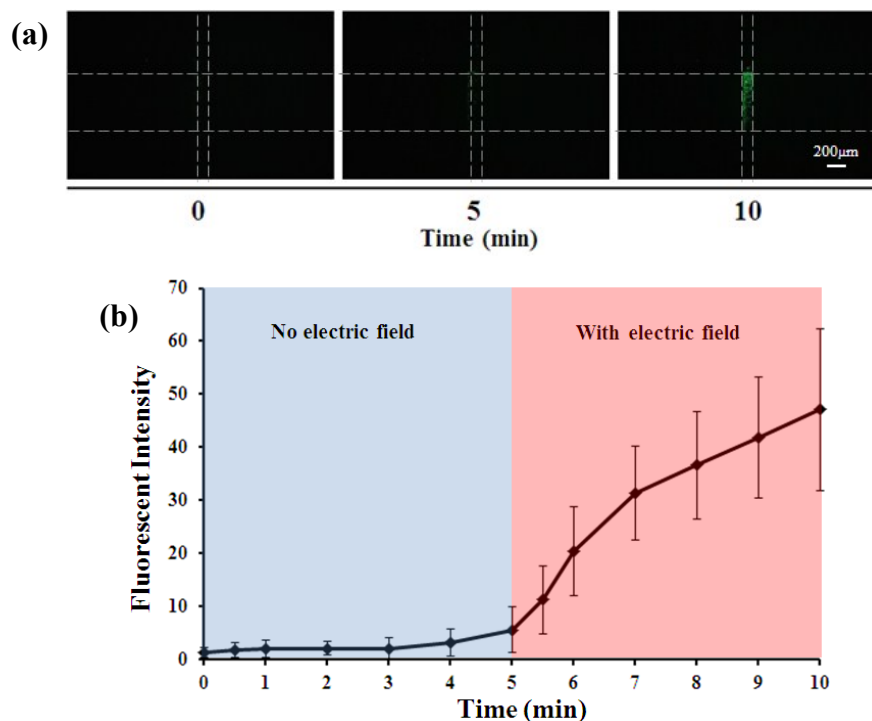


Figure 5.1 Experiment demonstrating DNA accumulation: (a) fluorescent images taken at time points of 0, 5, and 10min. The dash lines represent the outlines of the sample channel and the accumulation channel; (b) fluorescent intensity curve with no voltage applied (blue) and with 9V applied (red). Error bars represent standard deviation (SD).

Figure 5.1(a) shows the images of the fluorescent intensity upon sample loading (0min), at the beginning of applying the electric field (5min), and at the end of voltage application (10min). It can be seen that there was no obvious increase of fluorescence from 0min to 5min, while the contrast of fluorescence between 5min and 10min was large.

Figure 5.1(b) shows the change in intensity of the fluorescence at the intersection obtained using the relative gray scale measurement method (Chapter 4.4.1) over the duration of the experiment. When no electric field was applied (blue area), no increase in fluorescence intensity can be observed ($p=0.2281$, $\alpha=0.01$ for intensity between 0min and 5min). After applying a potential of 9V (red area), a rapid increase of the fluorescent intensity can be observed from 5min to 7min, which is followed by a slower and more linear increase from 7min to 10min.

Upon the application of the electric field, DNA at the intersection was immediately attracted to the gel by the electrophoretic (EP) force, which led to a rapid increase during the first minute. After the initial accumulation the region close to the gel is depleted of the DNA and rate of accumulation will depend on the rate of electrophoretic transport of DNA from the bulk solution leading to establishment of a steady flux.

This experiment demonstrates that DNA could be efficiently concentrated at the intersection in the presence of other biological materials (e.g. proteins) in 5 min by applying 9V on the device, which meets the design criteria set in Chapter 3.2.1. The next step is to distinguish various cfDNA concentrations using the device.

5.2 DNA Concentration from Complex Samples

The objective of the thesis is to distinguish blood samples of survivors ($\approx 1\mu\text{g/ml}$ cfDNA) from that of non-survivors ($>5\mu\text{g/ml}$ cfDNA) in severely septic patients. However, the storage of whole blood sample is difficult and patient samples are not stored in that form. Thus characterization of the device is conducted by using 4 types of samples, which is stable and can be good simulations of human blood sample.

5.2.1 Sample Type 1- DNA in Buffer

DNA mixed in buffer was used as a model sample in order to study the DNA accumulation process, and was used in proof-of-concept test on distinguishing between DNA concentrations of $1\mu\text{g/ml}$ and $5\mu\text{g/ml}$. This sample contains no proteins, cells or other contaminants and is a simplified system that would allow characterization.

The sample was prepared by diluting $50\mu\text{l}$ of $100\mu\text{g/ml}$ λ -DNA solution with $950\mu\text{l}$ TE buffer, producing 1ml of $5\mu\text{g/ml}$ DNA in buffer solution. Then $800\mu\text{l}$ of this sample ($5\mu\text{g/ml}$) was mixed with $4\mu\text{l}$ original PicoGreen reagent in the kit. Dilution of the sample concentration due to addition of the PicoGreen was ignored as the volume added was small. Similarly, $1\mu\text{g/ml}$ DNA in buffer sample was prepared by mixing $100\mu\text{l}$ $5\mu\text{g/ml}$ DNA sample (containing PicoGreen) with $400\mu\text{l}$ TE buffer.

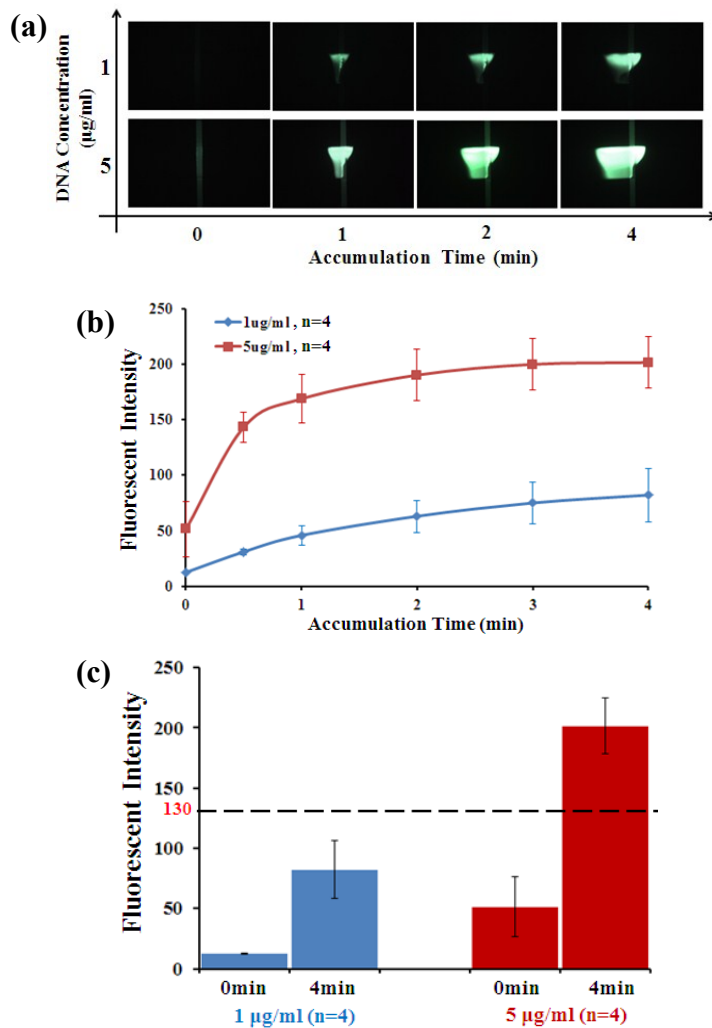


Figure 5.2 Experimental results using DNA in buffer sample: error bars represent standard deviation (SD). 9V was applied; (a) fluorescent images taken at time intervals of 0, 1, 2, and 4min demonstrating the DNA accumulation process at the intersection with 1µg/ml and 5µg/ml DNA concentration; (b) fluorescent intensity curves during DNA accumulation; (c) fluorescent intensity values at the beginning (0 min) and the end (4 min) of DNA accumulation.

The samples were loaded in the sample channel and 9V was applied on the device for 4 minutes. Images of the fluorescent intensity at the intersection were taken right before applying the electric field (0 min), and after applying electric field for 30s, 1min, 2min, 3min and 4min.

Figure 5.2(a) shows the images of the fluorescent intensity at different time points throughout the DNA accumulation at the intersection. It is clear that the fluorescent intensity of both samples (1 μ g/ml and 5 μ g/ml) increased with time. The area of DNA accumulation increased as well, which indicated a migration process of DNA towards the anode in the accumulation channel.

The average gray scale measurement method (**Chapter 4.4.1**) was employed to process fluorescent images collected. The fluorescent intensity curve acquired during various accumulation periods (**Figure 5.2(b)**) also showed a clear difference between 1 μ g/ml and 5 μ g/ml samples. The fluorescence curve of 1 μ g/ml sample was relatively linear and slow throughout the 4 minutes, while the fluorescent intensity of 5 μ g/ml sample increased rapidly and linearly within the first 30 second followed by a slower increase and a plateau after 3min. The reason for this trend was analyzed in **5.1**. The plateau was formed due to the saturation of the fluorescent signals at the intersection.

Figure 5.2(c) shows that during the accumulation process, the fluorescent intensity of 1 μ g/ml sample increased from average 12.4 to 82.0, while that of 5 μ g/ml sample increased from average 51.3 to 201.4. Before applying an electric field, no significant

difference between 1µg/ml and 5µg/ml sample could be observed ($P=0.0527$, $\alpha=0.01$). But after 4 minutes DNA accumulation, the average fluorescent intensities were significantly different ($P=3.7\times 10^{-4}$, $\alpha=0.01$). The dash line indicated a threshold value of 130 could be set to distinguish the two concentrations.

Based on data analysis, significant difference in the fluorescent intensity can be obtained even after 30 seconds ($P=3.3\times 10^{-4}$, $\alpha=0.01$). Therefore, the time required to identify if the sample had >5µg/ml DNA in simple DNA mixed in buffer samples can be as short as 30 seconds using a DC electric field; however, experiments using more complex samples were needed to verify the results.

5.2.2 Sample Type 2- DNA Spiked Plasma

DNA spiked plasma sample was prepared to simulate the blood plasma collected from ICU patients in hospital. This sample contains other biomolecules like proteins in the DNA accumulation process. Experiments using this sample were conducted to differentiate 1µg/ml and 5µg/ml DNA samples with the interference of proteins.

The original 100µg/ml DNA solution was first diluted into 50µg/ml with TE buffer. Then 10µl of 50µg/ml DNA was added into 50µl blood plasma from a healthy donor, followed by adding 60µl 200-fold diluted PicoGreen reagent from the kit, which yielded a final concentration of nearly 4.2µg/ml. Meanwhile, 2µl 50µg/ml DNA was mixed with 58µl blood plasma and 60µl 200-fold diluted PicoGreen reagent to get a

0.8 μ g/ml DNA in plasma sample. These two concentrations (4.2 μ g/ml & 0.8 μ g/ml) were used in the experiments to simulate the cfDNA concentrations of non-survivors and survivors in severe septic patients. All the experimental setup was the same as using DNA in buffer sample in 5.2.1. The results are displayed in Figure 5.3.

Images of the fluorescent intensity at various time points throughout the accumulation process were shown in Figure 5.3(a). The fluorescent signals of 4.2 μ g/ml and 0.8 μ g/ml samples both increased at the intersection. After the DNA accumulation in 4 minutes, the fluorescence of 4.2 μ g/ml sample was much stronger than that of the 0.8 μ g/ml sample.

Results in Figure 5.3(b) & (c) were achieved by processing the images using the relative gray scale measurement method (Chapter 4.4.2). Based on Figure 5.3(b), the fluorescent intensity of 0.8 μ g/ml DNA showed a linear increase which was similar as that of DNA in buffer sample. The fluorescent signals of 4.2 μ g/ml sample increased rapidly within the first minute followed by a smaller slope in the rest accumulation period. This trend is comparable with the fluorescence curve of 5 μ g/ml DNA in buffer sample, and the reason for the increasing pattern was analyzed at the end of 5.1.

In contrast with the result using DNA in buffer sample, when using the DNA spiked plasma sample, the two concentrations could not be distinguished within 30 seconds as shown in Figure 5.3(b).

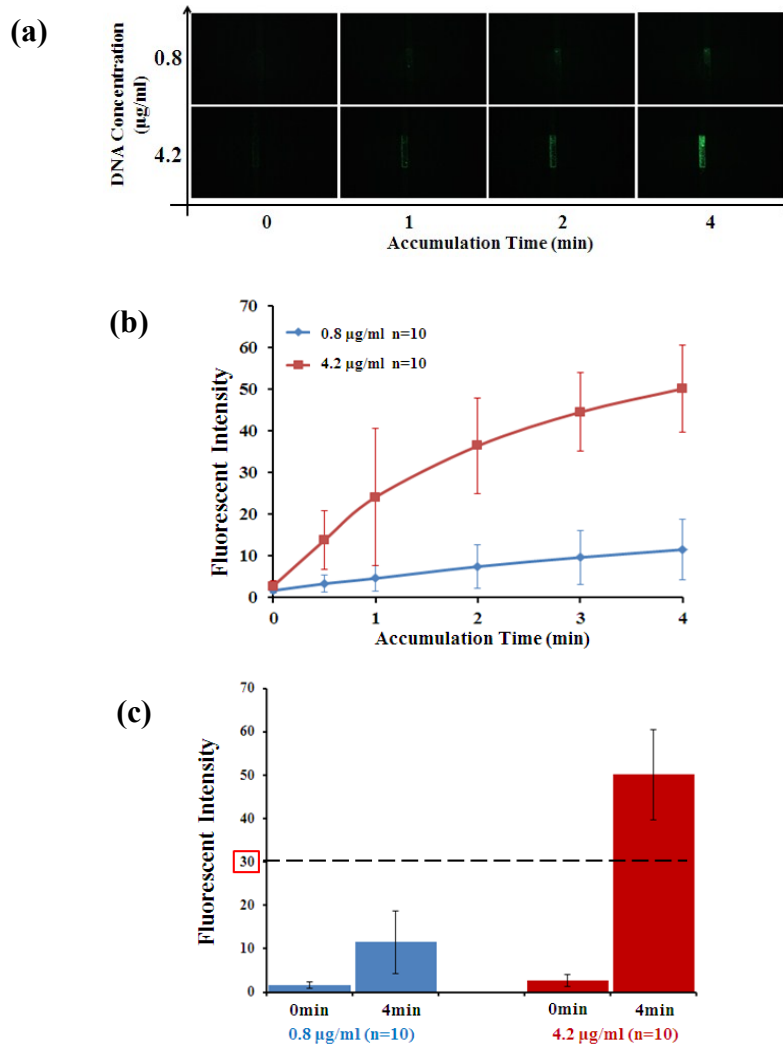


Figure 5.3 Experimental results using DNA spiked plasma sample: error bars represent standard deviation (SD). 9V was applied; (a) fluorescent images taken at time intervals of 0, 1, 2, and 4min demonstrating the DNA accumulation process at the intersection with 0.8µg/ml and 4.2µg/ml DNA concentration; (b) fluorescent intensity curves during DNA accumulation; (c) fluorescent intensity values at the beginning (0 min) and the end (4 min) of DNA accumulation.

In **Figure 5.3(c)**, the 0.8 μ g/ml sample reflects an increase in fluorescent intensity from average 1.7 to 11.5 during the 4 minutes electrokinetic accumulation, while the 4.2 μ g/ml sample demonstrates a faster increase from average 2.7 to 50.1. There was no significant difference ($P=0.0444$, $\alpha=0.01$) between 1 μ g/ml and 5 μ g/ml samples before applying the electric field (0min), but a highly significant difference ($P=4.5\times 10^{-8}$, $\alpha=0.01$) could be seen after applying 9V for 4 minutes on the device. A threshold value of 30 could be set to distinguish the samples.

Comparing the data between DNA in buffer samples and the DNA spiked plasma samples, at the end of DNA accumulation (4 min), the fluorescent intensity values of DNA in buffer samples are 82.0 ± 24.0 (1 μ g/ml) and 201.4 ± 23.0 (5 μ g/ml), while values of the DNA spiked plasma samples are 11.5 ± 7.2 (0.8 μ g/ml) and 50.1 ± 10.4 (4.2 μ g/ml). The values are clearly different between the two groups of samples even though the experimental setups are identical. There are two main aspects worth noting in the results, and they are as follows:

- 1) The variation of the fluorescent intensity of the DNA in buffer samples is larger than that of the DNA spiked plasma samples.

According to the data above, the relative uncertainties of DNA in buffer samples are $\approx 29.3\%$ (1 μ g/ml) and $\approx 11.4\%$ (5 μ g/ml), which is smaller than the relative

uncertainties of the DNA spiked plasma samples ($\approx 62.6\%$ for $1\mu\text{g/ml}$ and $\approx 20.8\%$ for $5\mu\text{g/ml}$).

2) The average values of the fluorescent intensity of the DNA in buffer samples are significantly higher than that of the DNA spiked plasma samples.

Significant differences are observed by comparing the fluorescent intensity values between the DNA spiked plasma sample and the DNA in buffer sample. This is seen despite using the same voltage, DNA concentrations, and DNA accumulation time period.

Possible reasons are as follows:

1) DNA binds with plasma proteins.

In the DNA in buffer sample, PicoGreen molecules can thoroughly bind with DNA molecules, thus the fluorescence is not affected. In DNA spiked plasma sample, due to the presence of various plasma proteins, DNA-proteins complexes can be formed. For example, it has been shown that strong bindings can happen between human serum albumin (HSA) and DNA G-C bases and the backbone PO_2 groups after mixing HSA and DNA solution [95]. These interactions between DNA and proteins can compete with DNA-PicoGreen binding, which potentially leads to a decreased fluorescence using the DNA spiked plasma sample.

DNA-protein complexes may also have a different electrophoretic mobility, and take a longer time to accumulate in the gel.

2) PicoGreen molecules interact with contaminants in plasma.

PicoGreen molecules may have interactions with proteins or other contaminants as well. Therefore, less dye is available for PicoGreen-DNA binding. For example, a characterization study has shown that although the linearity of PicoGreen can hardly be affected, fluorescent signal variations can be observed with presence of certain contaminants, including bovine serum albumin (BSA) [98]. It implies a similar change may probably occur in plasma samples.

3) The DNA-protein complex can be affected by an increased DEP force

The DNA-protein complex can be formed as explained in the first reason, and has a smaller charge-to-volume ratio than that of a single DNA molecule. Therefore, the dielectrophoretic (DEP) force which was dragging the DNA-protein complex away from the accumulation channel could weaken the dominant effect of the electrophoretic (EP) force on the motion of particles. Thus the net force driving DNA into the gel becomes smaller, which led to an impaired and less stable DNA accumulation process. The fluorescent intensity was directly affected.

Based on the discussion above, more PicoGreen reagent needs to be added into the plasma sample to meet a through binding between DNA and PicoGreen. But a higher PicoGreen concentration implies a higher fluorescent background which may affect the accuracy of intensity measurement. More experiments are needed to study the optimized amount of PicoGreen added in the sample.

5.2.3 Sample Type 3- Clinical Plasma

Previous samples prepared were simulations of the clinical sample, thus can only be used for preliminary test of the device. Clinical samples from severe septic patients were used to further test the validity of the device and experimental setup.

Clinical plasma sample comes from non-survivors of severe septic patients and healthy volunteers as a control. The plasma sample from healthy donors was also used to simulate the survivors of severe septic patients due to the similar concentration of these two groups. The source of the clinical sample was introduced in [Chapter 4.2.1.2](#). In this experiment, 3 samples from patients with different cfDNA concentrations were selected: 6µg/ml, 10µg/ml, and 20µg/ml. These concentrations were measured with a conventional method: QIAamp DNA Blood Mini Kit (Qiagen, Valencia, CA, USA) was used to isolate cfDNA from plasma. Then the purified DNA was measured using a spectrophotometer (Beckman DU 7400; Beckman Coulter Inc., Brea, CA, USA) at 260nm UV absorbance [\[5\]](#). Plasma samples from 3 healthy donors were also used in the experiment but were not pre-measured, thus the concentrations were unknown. Before loading the sample into the device, 10-fold diluted PicoGreen reagent from the kit was mixed with the clinical plasma in a 10:1 volume ratio (plasma sample: PicoGreen solution).

All the experimental setup was the same as using DNA spiked plasma sample in [5.2.2](#), and the results are displayed in [Figure 5.4](#).

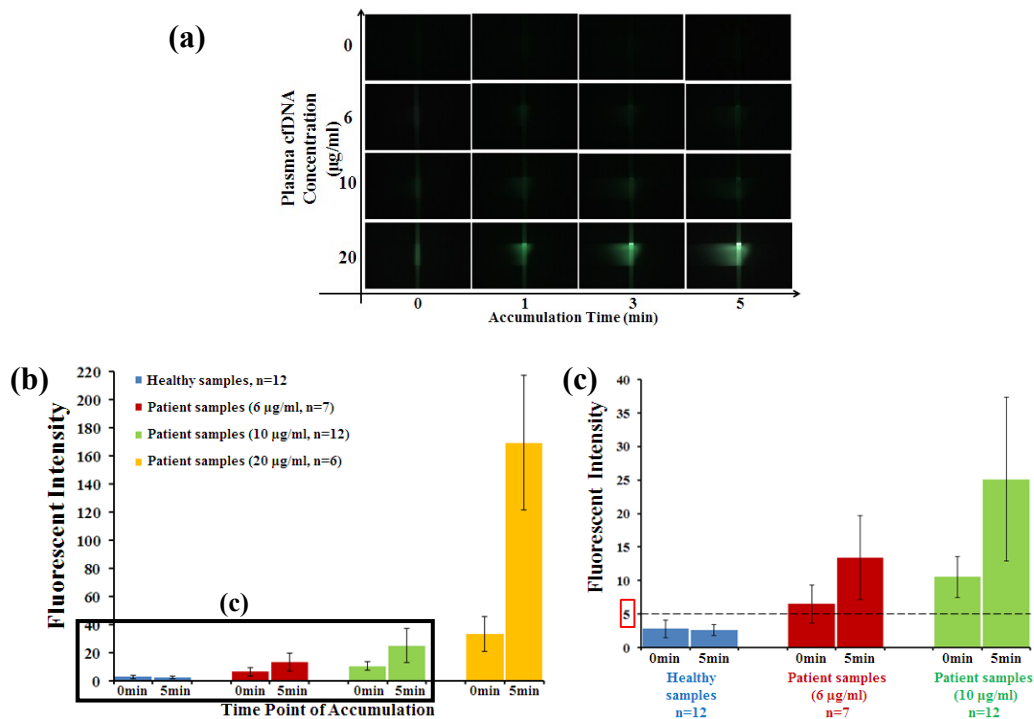


Figure 5.4 Experimental results using the clinical plasma sample: error bars represent standard deviation (SD). 9V was applied; (a) fluorescent images taken at time intervals of 0, 1, 3, and 5min demonstrating the DNA accumulation process at the intersection with samples from healthy donors (healthy samples, 0µg/ml) and samples from severe septic patients with various concentration (patient samples, 6µg/ml, 10µg/ml and 4.2µg/ml); (b) fluorescent intensity at the beginning (0 min) and the end (4 min) of DNA accumulation; (c) a zoom-in-view of the data in (b).

Figure 5.4(a) shows images of the fluorescent intensity from healthy samples (0µg/ml) and patient samples (6µg/ml, 10µg/ml and 20µg/ml) at different time points during DNA accumulation. The increase of fluorescent signals at the intersection could barely be detected for samples from healthy donors, while it was noticeable and similar

for 6µg/ml and 10µg/ml samples from patients. There was a significant increase of fluorescent signals for 20µg/ml sample from patients.

Figure 5.4(b) and Figure 5.4(c) were obtained after image processing with the relative gray scale measurement method. It could be seen that after 5 minutes DNA accumulation with 9V applied across the channels, the average fluorescent intensity of the healthy samples slightly decreased from 2.8 to 2.7, while that of patient samples increased for all the concentrations (6µg/ml: from 6.5 to 13.4; 10µg/ml: from 10.6 to 25.1; and 20µg/ml: from 33.4 to 169.3). Three main conclusions from the results are:

- 1) The patient samples with relatively high cfDNA concentrations (10µg/ml and 20µg/ml) were significantly different from the healthy donor samples, even before applying electric field ($p=7.9\times 10^{-7}$ between healthy sample and 10µg/ml sample; $p=0.0019$ between healthy sample and 20µg/ml sample, $\alpha=0.01$). After applying the electric field for 5 minutes, the distinctions remained highly significant ($p=5.0\times 10^{-5}$ between healthy sample and 10µg/ml sample; $p=3.6\times 10^{-4}$ between healthy sample and 20µg/ml sample, $\alpha=0.01$).
- 2) There was no significant difference between the patient sample with relatively low cfDNA concentration (6µg/ml) and the samples from healthy donors before applying electric field ($P=0.0126$, $\alpha=0.01$). But at the end of DNA accumulation, a highly significant difference could be detected between them ($P=0.004$, $\alpha=0.01$).

It revealed a more reliable distinction between the two samples after applying the electric field.

- 3) The fluorescent intensities between patient samples of 6 μ g/ml and 10 μ g/ml were not statistically different both in the beginning ($P=0.0110$, $\alpha=0.01$) and at the end ($P=0.0134$, $\alpha=0.01$) of DNA accumulation; however, the distinction between 10 μ g/ml and 20 μ g/ml samples was significant both before ($P=0.0062$, $\alpha=0.01$) and after ($P=5.9\times 10^{-4}$, $\alpha=0.01$) applying the electric field. The gap of fluorescent intensity between the two samples was obviously expanded by DNA accumulation, which reflected a much smaller p value.

The results have showed that healthy donor samples and patient samples with high levels of cfDNA could be differentiated using the device. However, samples with relatively small concentration gap (between 6 μ g/ml and 10 μ g/ml) could not be separated using the current cfDNA quantification setup. Therefore a higher resolution on cfDNA quantification is required.

The fluorescent intensity of the 6 μ g/ml clinical plasma sample is much lower (13.4 \pm 6.3), compared with the 5 μ g/ml DNA in buffer sample (201.4 \pm 23.0) and the 4.2 μ g/ml DNA spiked plasma sample (50.1 \pm 10.4). The relative uncertainty of the 6 μ g/ml clinical plasma (\approx 47.0%) is larger as well. This further shows that the interference of proteins and other contaminants on the cfDNA accumulation and quantification.

Besides the reasons illustrated in 5.2.2, there are 2 other factors may contribute to the low value and large variation of the fluorescent intensity with clinical plasma samples:

1) The individual variations of the clinical plasma samples

The clinical plasma samples used in this experiment were collected from different patients and healthy donors. Therefore, the samples may not be homogeneous and will have individual variations. The amount of protein and other contaminants in plasma could possibly change with patients which could indirectly affect the DNA accumulation process.

2) The interference of histone in the patient plasma samples

Increased histone levels have been found in samples from severe septic patients, due to possible apoptotic or necrotic cells [98]. Histone is able to keep cfDNA tightly coiled, thus the binding between DNA and PicoGreen molecules can be significantly interfered. Meanwhile, there are other non-histone proteins involved in sepsis process, which can potentially bind with DNA molecules in plasma from septic patients [98]. These mechanisms can lead to less DNA-PicoGreen binding, which further lead to a decreased fluorescent intensity.

5.2.4 Sample Type 4- DNA Spiked Whole Blood

The ultimate goal of this device is to complete cfDNA quantification directly in whole blood sample, which can further simplify the sample preparation procedure and realize a true point-of-care testing. Before moving to the clinical whole blood sample, preliminary experiments were conducted using DNA spiked whole blood sample.

During sample preparation, 20 μ l of 20 μ g/ml DNA was mixed with 20 μ l whole blood from a healthy donor and 40 μ l 10-fold diluted PicoGreen reagent, producing 5 μ g/ml DNA spiked whole blood sample. Similarly, 1 μ g/ml DNA spiked whole blood sample was prepared by diluting 3 μ l 20 μ g/ml DNA with 27 μ l whole blood and 30 μ l 10-fold diluted PicoGreen reagent. A control sample was prepared by mixing PicoGreen and whole blood in 1:1 volume ratio directly, in which no extraneous DNA was added. The results were shown in [Figure 5.5](#) with the same experimental setup as before.

[Figure 5.5\(a\)](#) shows images of the fluorescent intensity at various time points during DNA accumulation. It can be seen that the fluorescent intensity of the 0 μ g/ml sample cannot be visualized, while the fluorescent signals of the 1 μ g/ml and 5 μ g/ml samples increase clearly. Also, the fluorescence of the 5 μ g/ml sample is much stronger than that of the 1 μ g/ml sample.

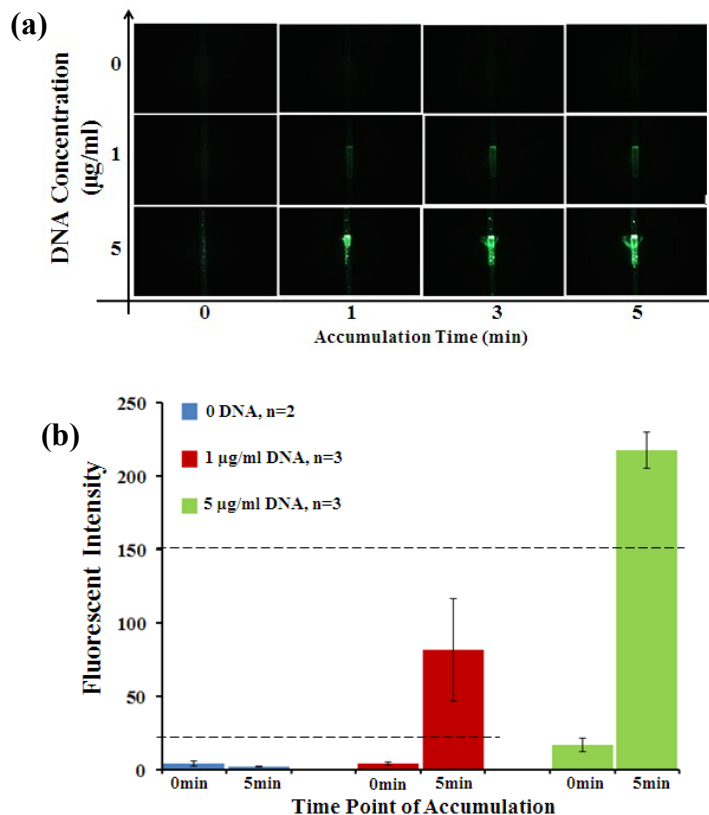


Figure 5.5 Experimental results using DNA spiked whole blood sample: error bars represent SD. 9V was applied. The concentration of 0µg/ml represents whole blood with no extraneous DNA added. (a) fluorescent images taken at time intervals of 0, 1, 3, and 5min demonstrating the DNA accumulation process at the intersection with samples of no DNA added, 1µg/ml and 5µg/ml DNA added; (b) fluorescent intensity at the beginning (0 min) and the end (5 min) of DNA accumulation.

After image processing with the relative gray scale value measurement method, fluorescent intensities at the start and the end of accumulation is presented in [Figure 5.5\(b\)](#). It shows that after DNA accumulation in 5 minutes applying 9V on the device, the

distinction between the 3 concentrations becomes larger compared to that before applying the electric field: the contrast of the fluorescent intensity between the 0 μ g/ml sample and the 1 μ g/ml sample increases substantially after DNA accumulation ($p=0.058$, $\alpha=0.01$) compared with before applying the electric field ($p=0.9711$, $\alpha=0.01$); the difference between the 5 μ g/ml sample and the 0 μ g/ml sample is not significant before DNA accumulation ($p=0.0278$, $\alpha=0.01$). However, the difference becomes significant ($p=0.0010$, $\alpha=0.01$) after accumulation.

It can be seen that the p values are relatively large due to the small number of experiments conducted (n), especially for the 0 μ g/ml sample ($n=2$). However, the data has provided preliminary proof that the whole blood of healthy donors, which has a similar cfDNA concentration as survivors, can be directly distinguished from the whole blood of non-survivors in severe sepsis patients.

5.3 Effect of Applied Voltage on DNA Accumulation

Voltage is the most direct and critical factor that affects DNA accumulation in the device. This experiment was used to characterize the effect of voltage on DNA accumulation.

The voltages applied between the sample channel and accumulation channel determines the electric field strength and its distribution in the device, which directly

affects the motion of DNA molecules. Based on the analysis in [Chapter 3.3](#), the dominant force for DNA molecules at the intersection is electrophoretic (EP) force. The electric field strength within the channel can be increased by increasing the voltage, which leads to larger EP forces on DNA. Therefore DNA molecules can be accumulated faster at the intersection and less time is required for DNA quantification.

DNA spiked plasma sample was used in the characterization. The DNA concentration of the sample was around 1.6 μ g/ml, which was prepared by diluting 20 μ l 8.3 μ g/ml DNA solution with 80 μ l blood plasma from a healthy donor and 5 μ l 10-fold diluted PicoGreen reagent. During the experiment, 3 different voltages (3V, 9V, and 15V) were applied while other settings were kept the same as in [5.5.2](#). The results were shown in [Figure 5.6](#).

[Figure 5.6\(a\)](#) shows the images of the fluorescent intensity at the end of DNA accumulation (5 min) with different voltages. It shows that a clear difference of fluorescence at the intersection can be seen between 3V and 9V, while the fluorescence intensity between 9V and 15V images is difficult to differentiate.

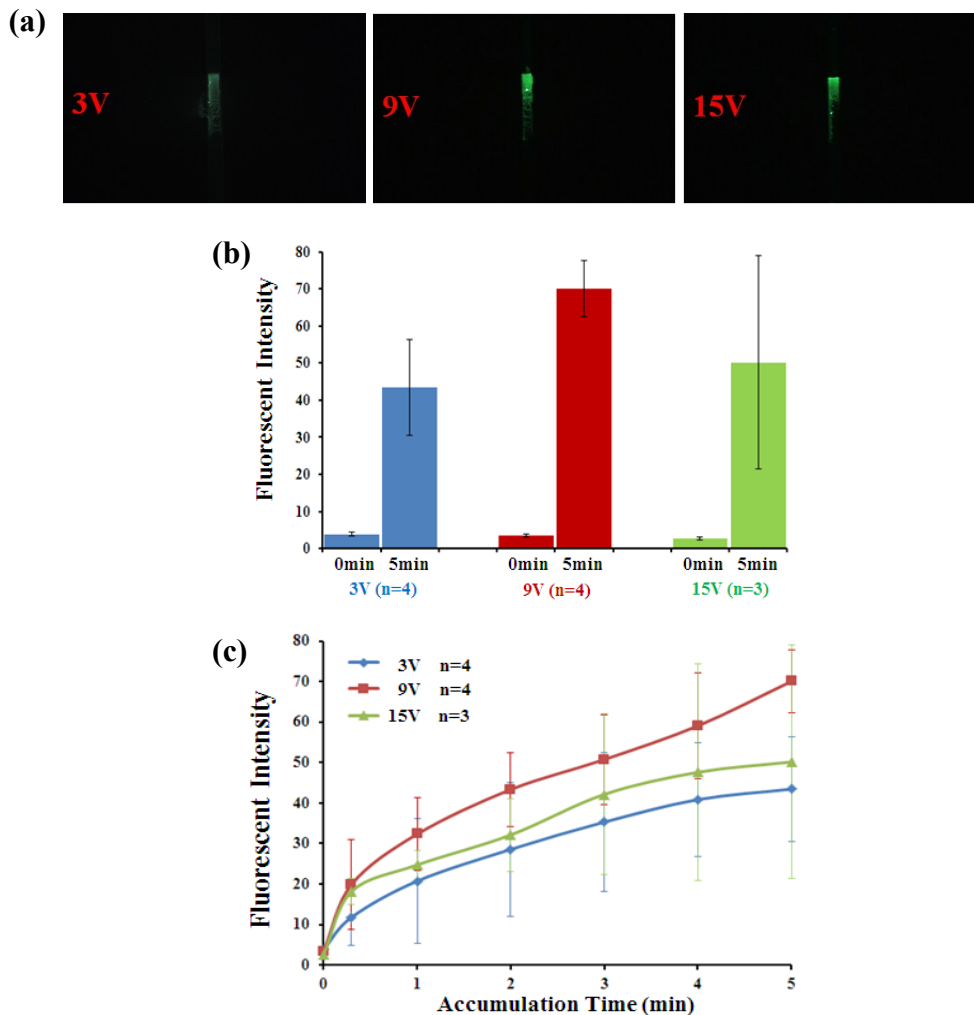


Figure 5.6 Experimental results using 1.6 μ g/ml DNA spiked plasma sample with 3V, 9V, and 15V applied on the device: error bars represent SD. (a) fluorescent images at the intersection after applying various voltages for 5 minutes; (b) fluorescent intensity values at the beginning (0 min) and the end (5 min) of DNA accumulation; (c) fluorescent intensity curves during DNA accumulation.

Figure 5.6(b) & (c) were graphed after processing the fluorescent images with the relative gray scale measurement method. The fluorescence curves acquired using the 3

voltages share a similar pattern as described and analyzed in 5.1. With an accumulation period of 5 minutes, a slight difference of the fluorescent intensity can only be observed between 3V and 9V ($p=0.0172$, $\alpha=0.01$); whereas the difference cannot be seen when applying 15V ($p=0.7355$, $\alpha=0.01$ between 3V and 15V; $p=0.354$, $\alpha=0.01$ between 9V and 15V). Also, the standard deviation of the data yielded using 15V is much larger than that of 3V and 9V, so much so that it covers the entire data range of 3V and 9V curves. Similar results were observed using 5 μ g/ml DNA spiked plasma sample (data not shown).

According to the results above, the fluorescent intensity is the highest when applying 9V throughout the accumulation process. However, based on the COMSOL simulation and the force calculation (Appendix D), the EP force increases nearly 3 fold if the voltage is changed from 3V to 9V, and around 1.7 fold from 9V to 15V. Therefore in theory, within a fixed accumulation time, the fluorescent intensity of using 15V should be the highest.

There are 2 possible reasons for the unexpected results:

1) Larger variations in current with the increase of the voltage applied.

When an electric potential is applied, the current drops from its initial high value before stabilizing towards the end of the experiment (5 min). The exact current values vary between the devices. The variations and the final values of the current with various voltages are shown in Table 5.1.

Voltage applied	Initial current (μA)	Final current (μA)	Current drop
3V	4~5	3~4	$\approx 1\mu\text{A}$
9V	12~15	8~10	$\approx 5\mu\text{A}$
15V	18~29	8~19	$>10\mu\text{A}$

Table 5.1 The electric current variation in the device with different voltages applied. The initial current implies the current upon applying the electric field; the final current represents the current at the end of DNA accumulation; the current drop indicates the decreased value between the initial current and final current. The total time for electric field application is 5 minutes.

It can be seen that the drop in current between the initial and the final time points is larger at higher voltages. The variation of the initial current and the final current rise with the increased voltage as well. The results indicates that the electric system in the channels was getting less stable when a higher voltage was applied, which lead to a larger standard deviation value. The worsened stability of the electric system could be resulted from the bubble generation at the surface of electrodes, which partly impaired the direct contact between the sample solution and the silver electrodes.

2) The heat generated in the channels rises with the increase of the voltage applied.

Based on Eq. 2.3 in Chapter 2.6.2, the heat generated in the channel can increase around 9 fold when the voltage changes from 3V to 9V, and nearly 25 fold from 3V to

15V. The increase of the temperature can affect the DNA accumulation process, and also accelerate the photodegradation of the fluorescent dye [99].

The increased heat can also affect the agarose gel at the intersection. In a regular agarose gel electrophoresis, the applied voltage is usually below 10V/cm, in which the distance is that between the two electrodes [100]. The main reason for this voltage restriction is to prevent the gel from being affected. In this experiment, when 15V was applied between the two electrodes located 4mm from each other, a much higher electric field was reached. Therefore, the gel at the intersection was probably destroyed partially by the heat generated, and the DNA capture and accumulation process could be substantially affected.

Based on the results in this experiment, a low voltage is preferred as it provides a more stable DNA accumulation environment than using a high voltage. Also, a lower voltage generates less heat. The device can be further modified to decrease the distance between the two electrodes so that a lower voltage can be used while the electric field intensity is not changed.

5.4 Immobilization of Reagents and Elimination of Sample Preparation

Although the sample preparation process has been significantly simplified by using the device, current experiments still require pre-mixing of the fluorescent dye

reagents and the sample liquid, which leads to a dilution effect of the original cfDNA concentrations in samples. Therefore a zero sample preparation is necessary to fulfill a one-step sample loading and measuring concept. To realize this goal, PicoGreen dye must be integrated with the device in advance.

In this experiment, 50-fold diluted PicoGreen reagent from the kit was injected into the channels before gel filling and sample loading. Both the sample channel and accumulation channel were fully exposed to the PicoGreen solution. The device was then wrapped with aluminum foil with a small opening to let the liquid evaporate. Leaving the device in a dark and ventilated environment for overnight, the buffer solution in PicoGreen reagent was fully evaporated, while the majority of the PicoGreen molecules were dried and attached to the channel walls. These molecules could later be re-suspended upon loading of sample liquids, and intercalated with cfDNA molecules in the samples. DNA spiked plasma sample was prepared by diluting λ -DNA into 5 μ g/ml with blood plasma from a healthy donor without adding dyes or other reagents. All the experimental setup was the same as section 5.2.2. Figure 5.7 showed the different results using a PicoGreen-integrated device and a regular device which has no PicoGreen deposited in advance.

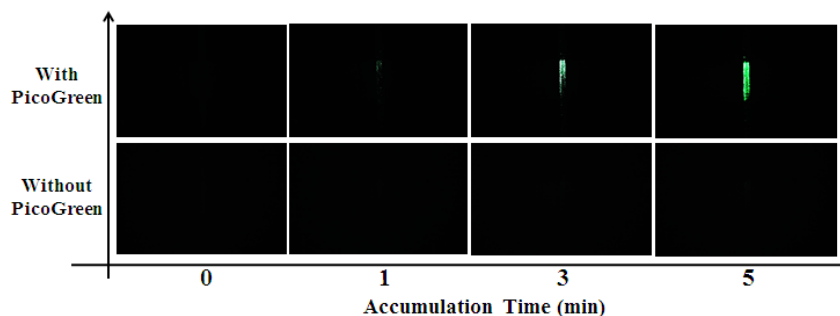


Figure 5.7 Fluorescent images taken at time intervals of 0, 1, 3, and 5min with PicoGreen-integrated device (with PicoGreen) and regular device (without PicoGreen); 9V was applied. The sample was 5µg/ml DNA spiked plasma with no PicoGreen added in the solution.

It was clear that with PicoGreen molecules pre-deposited in the channels, fluorescence could be detected and the accumulation of cfDNA was observed. In comparison, with no PicoGreen integrated with the device, no fluorescence was observed during the whole process since there was no binding of DNA and the dye.

This experiment demonstrated the possibility of dye integration with the device, which further simplifies the sample preparation steps. But the stability and cost increase of this method remains to be investigated. To make sure enough amount of PicoGreen is deposited in the sample channel for DNA-PicoGreen binding, a highly concentrated PicoGreen reagent need to be injected into the device for evaporation. Compared with direct mixing with sample liquid before loading into the device, this method requires higher concentration (>10 times concentrated) and larger volume (>20 times) of PicoGreen, which is a relatively expensive dye. More importantly, if the PicoGreen

molecules are not evenly distributed on the channel walls, the binding of cfDNA and PicoGreen may not be the same every time. Actually, fluorescent pictures yielded from two PicoGreen-integrated devices are noticeably different even though the sample and device processing approach are identical. More experiments will be carried out to test the uniformity of the PicoGreen-integrated device, and to evaluate the potential effect on DNA quantification.

5.5 Summary

In this chapter, the DNA accumulation was demonstrated. The experimental results with 4 types of samples (DNA in buffer, DNA spiked plasma, clinical plasma, and DNA spiked whole blood) were illustrated and discussed. The effect of voltage applied on the DNA accumulation was characterized. The experiment on eliminating sample preparation was conducted.

The results show that the samples from healthy donors are able to be distinguished from that of severely septic patients in 5 minutes. However, better resolution is required for quantification using samples with various cfDNA concentrations. The DNA accumulation process can be heavily interfered by contaminants (e.g. proteins, cells) in the blood sample, which leads to a decrease on the fluorescent intensity and an increase on the data variation. There is a clear increase of fluorescent signals after DNA

accumulation when the voltage increases from 3V to 9V. However, no fluorescent change can be seen when applying 15V, compared with using 3V and 9V. Therefore 9V is an optimized setup currently.

Chapter 6.

Contributions and Future Work

6.1 Contributions

The primary contribution of this thesis is realization of a simplified rapid DNA quantification method directly in blood plasma, and its potential to be used in whole blood samples. The device developed is low-cost, consumes small amounts of power, simple in fabrication, and requires a small sample. In addition, the device can be potentially applied to diagnosis of other conditions, such as cancer. Other bio-samples such as urine samples can also be prepared using this method, which makes the device a more versatile tool in assisting clinical diagnostics.

6.1.1 A Direct DNA Quantification Method

Compared with the conventional DNA quantification methods introduced in [Chapter 2](#), the approach developed in this thesis has the potential for DNA quantification from whole blood sample or other complicated samples directly. As long as the cfDNA in the sample can be specifically labelled with a fluorescent probe, it can be electrically collected and characterized. With the integration of the dye and the device shown in

Chapter 5.4, the sample can be loaded into the channel for detection without any pre-treatment. This is the first automated direct quantification method using human samples.

6.1.2 A Low Cost Device

By using microfluidic technologies, the cost for fabrication and operation of the device can be very low at the following aspects:

1) Fabrication

As introduced in **Chapter 4**, the device mold was fabricated using photolithography, soft-lithography, and plasma bonding, which can be easily developed into mass production with very low cost per unit. The material for casting the channels (PDMS) is relatively cheap, so the cost is still low even though it is a disposable device. The relatively expensive materials, such as electrodes, can be used repetitively. Besides, the device size can be as small as a dime, which further decreases the fabrication cost.

2) Sample and reagent consumption

Due to the use of microscale channels, the sample volume (including fluorescent reagent) required for quantification and the agarose gel necessary for prefilling are both less than 1 μ l. Even considering the waste may occur during the experimental process, the consumption of the sample and reagents is only several microliters, which can be regarded as “droplet test”. Lower cost is also contributed by the reagent-free method employed. Unlike conventional quantification methods, which involve various reagents

for DNA purification and PCR process, the method in this thesis requires only the sample, a fluorescent reagent, and agarose gel. It is a substantial simplification of the quantification reagents needed.

3) Power supply

The electrical potential used in these experiments is 9V, which can actually be further decreased by modifying the device in future. These voltages can be supplied by portable power sources like batteries, which favorable for this technology to be developed into a portable device.

4) Quantification time

Current duration needed for quantification is 5min. It can be 10 min at most including the time for gel prefilling and sample loading. The most important improvement is saving the time for sample preparation because direct quantification can be realized using the device in this thesis.

6.1.3 A Variety of Potential Applications

The rapid direct cfDNA quantification method developed in this thesis is specifically applied for severe sepsis outcome prediction, while this device can be potentially used in some other cases. For instance, detecting cfDNA in plasma or serum could serve as a “liquid biopsy” [20], which can be monitored continuously with a minimum-invasive test using the device. As demonstrated by various studies, increased

level of cfDNA reflects many physiological and pathological processes, including some types of tumors, benign lesions, inflammatory diseases and tissue trauma [101]. Therefore, rapid detection of the cfDNA level in the blood sample can be used as a health screening tool: a healthy subject should maintain a low cfDNA level in the circulating system. This quantification method can also be used to exam the efficacy of therapy on patients. By repetitively real-time detecting the cfDNA concentrations in blood, it is easy to see if the cfDNA level is brought back to normal.

6.2 Future Work

Although the preliminary experiments have shown the value and potential of the device, more work is needed including:

- 1) Experiments using clinical whole blood samples. In this thesis, a DNA spiked whole blood sample was used to simulate the clinical whole blood sample, which can only be served as a proof-of-concept. Therefore, more data needs to be collected using clinical whole blood samples from non-survivors and survivors in severe septic patients. Meanwhile, patients' blood samples with various cfDNA concentrations remain to be tested with the device for the quantification objective.

2) Calibration and standardization of the device. A fluorescence-concentration standard curve needs to be carried out. Key parameters, such as quantification dynamic range, need to be confirmed.

3) Development of the device into a fully functionalized system. Current experimental setup ([Chapter 4.3.2](#)) involves a DC power supply, a fluorescent microscope, and a laptop, which can be potentially integrated with the microfluidic device, and be developed into a compact system. For example, the DC power supply can be replaced by ordinary batteries. Also, the fluorescent microscope can be simplified with a LED light source, optical filters and a light detector.

4) Extension on the application of the device. Due to the potential usage of cfDNA quantification in other topics ([6.1.3](#)), this device is able to be applied to other purposes besides severe sepsis prognosis. In future, the device may serve as a health screening tool as it is a fast and low-cost test. If the result shows an abnormal level of cfDNA in blood, further examination may be necessary because the increase of cfDNA concentration implies health issues.

6.3 Summary

In conclusion, the device presented in this thesis realizes direct cfDNA quantification from human plasma samples, and shows potential of quantification in

whole blood. The device is economical in many aspects including fabrication, sample consumption and power supply. With increased applications of cfDNA in healthcare areas, the device can possibly be utilized in other purposes like health screening.

In future, more experiments need to be done using clinical whole blood samples. Also, the device remains to be calibrated and standardized. The ultimate goal is to develop the device into a reliable, stable and compact appliance for bedside cfDNA monitoring.

Reference:

- [1] Bone RC, Balk RA, Cerra FB, Dellinger RP, Fein AM, Knaus WA, Schein RM, and Sibbald WJ, “Definitions for Sepsis and Organ Failure and Guidelines for the Use of Innovative Therapies in Sepsis”, *Chest.*, Vol.101, No.6, pp.1644-55, 1992.
- [2] Liudmila Husak, Annette Marcuzzi, Jeremy Herring, Eugene Wen, Ling Yin, Dragos Daniel Capan, and Geta Cernat, “National Analysis of Sepsis Hospitalizations and Factors Contributing to Sepsis In-Hospital Mortality in Canada”, *Healthcare Quarterly*, Vol.13, pp.35-41, 2010.
- [3] Strand K, and Flaatten H, “Severity scoring in the ICU: a review”, *Acta Anaesthesiol Scand.* Vol.52, No.4, pp.467-78, 2008.
- [4] Terence Chan, and Frank Gu, “Early Diagnosis of Sepsis Using Serum Biomarkers”, *Expert Rev Mol Diagn.*, Vol.11, No.5, pp.487-496, 2011.
- [5] Dwivedi DJ, Toltl LJ, Swystun LL, Pogue J, Liaw KL, Weitz JI, Cook DJ, Fox-Robichaud AE, “Prognostic utility and characterization of cell-free DNA in patients with severe sepsis”, *Crit Care*, Vol.16, No.4, pp. R151, 2012.
- [6] Michael Fleischhacker, Bernd Schmidt, Sabine Weickmann, Debora M.I. Fersching, Gloria S. Leszinski, Barbara Siegele, Oliver J. Stötzer, Dorothea Nagel, and Stefan Holdenrieder, “Methods for isolation of cell-free plasma DNA strongly affect DNA yield”, *Clinica Chimica Acta*, Vol.412, pp.2085–2088, 2011.
- [7] Luke A. Shokere, Marcia J. Holden, and G. Ronald Jenkins, “Comparison of fluorometric and spectrophotometric DNA quantification for real-time quantitative PCR of degraded DNA”, *Food Control*, Vol.20, pp.391–401, 2009.

- [8] Bone RC, Balk RA, Cerra FB, Dellinger RP, Fein AM, Knaus WA, Schein RM, and Sibbald WJ, “Definitions for Sepsis and Organ Failure and Guidelines for the Use of Innovative Therapies in Sepsis”, *Chest.*, Vol.101, No.6, pp.1644-55, 1992.
- [9] Canadian Institute for Health Information, In Focus: A National Look at Sepsis (Ottawa, Ont.: CIHI, 2009).
- [10] Liudmila Husak, Annette Marcuzzi, Jeremy Herring, Eugene Wen, Ling Yin, Dragos Daniel Capan, and Geta Cernat, “National Analysis of Sepsis Hospitalizations and Factors Contributing to Sepsis In-Hospital Mortality in Canada”, *Healthcare Quarterly*, Vol.13, pp.35-41, 2010.
- [11] Strand K, and Flaatten H, “Severity scoring in the ICU: a review”, *Acta Anaesthesiol Scand.* Vol.52, No.4, pp.467-78, 2008.
- [12] Pettilä V, Pettilä M, Sarna S, Voutilainen P, and Takkunen O, “Comparison of multiple organ dysfunction scores in the prediction of hospital mortality in the critically ill”, *Crit Care Med.*, Vol.30, No.8, pp.1705-11, 2002.
- [13] Patel PA1, and Grant BJ, “Application of mortality prediction systems to individual intensive care units”, *Intensive Care Med.*, Vol.25, No.9, pp.977-82, 1999.
- [14] Jean-Louis Vincent and Rui Moreno, “Clinical review: Scoring systems in the critically ill”, *Vincent and Moreno Critical Care*, Vol.14, pp.207, 2010.
- [15] Ventetuolo CE, and Levy MM, “Biomarkers: diagnosis and risk assessment in sepsis”, *Clin Chest Med.*, Vol.29, No.4, pp.591-603, 2008.
- [16] Terence Chan, and Frank Gu, “Early Diagnosis of Sepsis Using Serum Biomarkers”, *Expert Rev Mol Diagn.*, Vol.11, No.5, pp.487-496, 2011.

- [17] Pierrakos C, and Vincent JL, “Sepsis biomarkers: a review”, *Crit Care.*, Vol.14, No.1, pp.R15, 2010.
- [18] Heidi Schwarzenbach, Dave S. B. Hoon, and Klaus Pantel, “Cell-free nucleic acids as biomarkers in cancer patients”, *Nature Reviews Cancer*, Vol.11, pp.426-437, 2011.
- [19] Jung K, Fleischhacker M, and Rabien A, “Cell-free DNA in the blood as a solid tumor biomarker--a critical appraisal of the literature”, *Clin Chim Acta.* Vol.411, pp.1611-24, 2010.
- [20] Beiter T, Fragasso A, Hudemann J, Schild M, Steinacker J, Mooren FC, and Niess AM, “Neutrophils release extracellular DNA traps in response to exercise”, *J Appl Physiol (1985)*. Vol.117, No.3, pp.325-33, 2014.
- [21] E.S. Taglauer, L. Wilkins-Haug, and D.W. Bianchi, “Review: Cell-free fetal DNA in the maternal circulation as an indication of placental health and disease”, *Placenta 35, Supplement A, Trophoblast Research*, Vol. 28, pp.S64-S68, 2014.
- [22] Rhodes A, Wort SJ, Thomas H, Collinson P, and Bennett ED, “Plasma DNA concentration as a predictor of mortality and sepsis in critically ill patients”, *Crit Care.* Vol.10, No.2, pp.R60, 2006.
- [23] Boom R, Sol CJ, Salimans MM, Jansen CL, Wertheim-van Dillen PM, and van der Noordaa J, “Rapid and simple method for purification of nucleic acids”, *J Clin Microbiol.* Vol. 28, No.3, pp.495-503, 1990.
- [24] Weimin Sun, “Chapter 4 - Nucleic Extraction and Amplification,” in *Molecular Diagnostics—Techniques and Applications for the Clinical Laboratory*, San Diego: Academic Press, pp. Pages 35–47, 2010.

- [25] Loparev VN, Cartas MA, Monken CE, Velpandi A, and Srinivasan A, “An efficient and simple method of DNA extraction from whole blood and cell lines to identify infectious agents”, *J Virol Methods*. Vol.34, No.1, pp.105-12, 1991.
- [26] Sarah Breitbach, Suzan Tug, Susanne Helmig, Daniela Zahn, Thomas Kubiak, Matthias Michal, Tommaso Gori, Tobias Ehlert, Thomas Beiter, and Perikles Simon, “Direct Quantification of Cell-Free, Circulating DNA from Unpurified Plasma”, *PLoS ONE*, Vol. 9, No.3, pp. e87838, 2014.
- [27] Fleischhacker M, Schmidt B, Weickmann S, Fersching DM, Leszinski GS, Siegele B, Stötzer OJ, and Nagel D, Holdenrieder S, “Methods for isolation of cell-free plasma DNA strongly affect DNA yield”, *Clinica Chimica Acta*, Vol.412, pp.2085–2088, 2011.
- [28] Somanath Bhat , Natalie Curach , Thomas Mostyn, Gursharan Singh Bains , Kate R. Griffiths, and Kerry R. Emslie, “Comparison of Methods for Accurate Quantification of DNA Mass Concentration with Traceability to the International System of Units”, *Anal. Chem.*, Vol.82, No.17, pp.7185–7192, 2010.
- [29] K. Nielsen, H.S. Mogensen, B. Eriksen, J. Hedman, W. Parson, and N. Morling, “Comparison of six DNA quantification methods”, *International Congress Series 1288*, pp.759 – 761, 2006.
- [30] Bruce Venning, “Electrophoresis Band Quantification - an Art or a Science”, *Biostep GmbH*. [Online] www.biostep.de/DocumentDownloadServlet?docid=17
- [31] Life Technologies®, “Low DNA Mass Ladder”, *datasheet*.
[Online] <http://www.lifetechnologies.com/order/catalog/product/10068013>
- [32] Sigma Aldrich®, “qPCR Technical Guide”, *technical note*.

[Online] http://www.sigmaaldrich.com/content/dam/sigma-aldrich/docs/Sigma/General_Information/qpcr_technical_guide.pdf

- [33] Sarah Webb, “Getting over qPCR’s technical hurdles”, *BioTechniques*, Vol. 55, No. 4, pp. 165–168, 2013.
- [34] Umetani N, Kim J, Hiramatsu S, Reber HA, Hines OJ, Bilchik AJ, and Hoon DS, “Increased integrity of free circulating DNA in sera of patients with colorectal or periampullary cancer: direct quantitative PCR for ALU repeats”, *Clin Chem.*, Vol. 52, No.6, pp.1062-9, 2006.
- [35] Naoyuki Umetani, Armando E. Giuliano, Suzanne H. Hiramatsu, Farin Amersi, Taku Nakagawa, Silvana Martino, and Dave S.B. Hoon, “Prediction of Breast Tumor Progression by Integrity of Free Circulating DNA in Serum”, *J Clin Oncol.*, Vol.24, pp.4270-4276, 2006.
- [36] Chiu RW, Poon LL, Lau TK, Leung TN, Wong EM, and Lo YM, “Effects of blood-processing protocols on fetal and total DNA quantification in maternal plasma”, *Clin Chem.*, Vol.47, No.9, pp.1607-13, 2001.
- [37] Yi Chen, Zhenpeng Guo, Xiaoyu Wang, and Changgui Qiu, “Sample preparation”, *Journal of Chromatography A*, Vol.1184, pp.191–219, 2008.
- [38] Jungkyu Kim, Michael Johnson, Parker Hill and Bruce K. Gale, “Microfluidic sample preparation: cell lysis and nucleic acid purification”, *Integr. Biol.*, Vol.1, pp.574–586, 2009.
- [39] George M. Whitesides, “The origins and the future of microfluidics”, *Nature*, Vol.442, pp.368-373, 2006.
- [40] Gareth Jenkins, Colin D. Mansfield, “Microfluidic Diagnostics”, *Humana Press*, 2013.

- [41] Thomas H. Schulte*, Ron L. Bardell, and Bernhard H. Weigl, “Microfluidic technologies in clinical diagnostics”, *Clinica Chimica Acta*, Vol.321, pp.1-10, 2002.
- [42] Jayamohan H1, Sant HJ, and Gale BK, “Applications of microfluidics for molecular diagnostics”, *Methods Mol Biol.*, Vol.949, pp.305-34, 2013.
- [43] Joel Voldman, “Dielectrophoretic Traps for Cell Manipulation”, *BioMEMS and Biomedical Nanotechnology*, pp.159-186, 2007.
- [44] Christopher J. Easley, James M. Karlinsey, Joan M. Bienvenue, Lindsay A. Legendre, Michael G. Roper, Sanford H. Feldman, Molly A. Hughes, Erik L. Hewlett, Tod J. Merkel, Jerome P. Ferrance, and James P. Landers, “A fully integrated microfluidic genetic analysis system with sample-in–answer-out capability”, *PNAS*, Vol.103, pp. 19272–19277, 2006.
- [45] Kim H. Wong and Kenneth L. Campbell, “Factors That Affect Use of Intercalating Dyes Such as PicoGreen, SYBR Green I, Syto-13 and Syto-82 in DNA Assays”, *Biology of Reproduction*, Vol.85, pp.725, 2011.
- [46] Jian Wen, Lindsay A. Legendre, Joan M. Bienvenue, and James P. Landers, “Purification of Nucleic Acids in Microfluidic Devices”, *Anal. Chem.*, Vol.80, pp.6472–6479, 2008.
- [47] Jungkyu Kim, Michael Johnson, Parker Hill, and Bruce K. Gale, “Microfluidic sample preparation: cell lysis and nucleic acid purification”, *Integr. Biol.*, Vol.1, pp.574–586, 2009.
- [48] Nathaniel C. Cady, Scott Stelick, and Carl A. Batt, “Nucleic acid purification using microfabricated silicon structures”. *Biosensors and Bioelectronics*, Vol.19, pp.59-66, 2003.

- [49] Michael C. Breadmore, Kelley A. Wolfe, Imee G. Arcibal, Wayne K. Leung, Dana Dickson, Braden C. Giordano, Mary E. Power, Jerome P. Ferrance, Sanford H. Feldman, Pamela M. Norris, and James P. Landers, “Microchip-Based Purification of DNA from Biological Samples”, *Anal. Chem.*, Vol.75, pp.1880-1886, 2003.
- [50] Thomas Rohr, Emily F. Hilder, John J. Donovan, Frantisek Svec, and Jean M. J. Fre'chet, “Photografting and the Control of Surface Chemistry in Three-Dimensional Porous Polymer Monoliths”, *Macromolecules*, Vol.36, pp.1677-1684, 2003.
- [51] Kin Fong Lei, Han Cheng, Kit Ying Choy, and Larry M.C. Chow, “Electrokinetic DNA concentration in microsystems”, *Sensors and Actuators*, Vol.156, pp.381–387, 2009.
- [52] Pak Kin Wong, Che-Yang Chen, Tza-Huei Wang, and Chih-Ming Ho, “Electrokinetic Bioprocessor for Concentrating Cells and Molecules”, *Anal. Chem.*, Vol.76, pp.6908-6914, 2004.
- [53] M. R. Bown, and C. D. Meinhart, “AC electroosmotic flow in a DNA concentrator”, *Microfluid Nanofluid*, Vol.2, pp.513–523, 2006.
- [54] Jung-Rong Du, and Hsien-Hung Wei, “Focusing and trapping of DNA molecules by head-on ac electrokinetic streaming through join asymmetric polarization”, *BIOMICROFLUIDICS*, Vol.4, pp.034108, 2010.
- [55] N. G. Green, A. Ramos, A. Gonza'lez, H. Morgan, and A. Castellanos, “Fluid flow induced by nonuniform ac electric fields in electrolytes on microelectrodes. I. Experimental measurements”, *Phys Rev E.*, Vol.61, pp.4011-8, 2000.
- [56] N. G. Green, A. Ramos, A. Gonza'lez, H. Morgan, and A. Castellanos, “Fluid flow induced by nonuniform ac electric fields in electrolytes on microelectrodes. III.

Observation of streamlines and numerical simulation”, *Phys Rev E.*, Vol.66, pp.026305, 2002.

- [57] Ryuji Yokokawa, Yoshihiro Manta, Moriaki Namura, Yusuke Takizawa, Nam Cao Hoai Led, and Susumu Sugiyama, “Individual evaluation of DEP, EP and AC-EOF effects on DNA molecules in a DNA concentrator”, *Sensors and Actuators B*, Vol.143, pp.769–775, 2010.
- [58] Dazhi Wang, Marin Sigurdson, and Carl D. Meinhart, “Experimental analysis of particle and fluid motion in ac electrokinetics”, *Experiments in Fluids*, Vol.38, pp.1–10, 2005.
- [59] Dinesh Kalyanasundaram, Shinnosuke Inoue, Jong-Hoon Kim, Hyun-Boo Lee, Zenko Kawabata, Woon-Hong Yeo, Gerard A. Cangelosi, Kieseok Oh, Dayong Gao, Kyong-Hoon Lee, and Jae-Hyun Chung, “Electric field-induced concentration and capture of DNA onto microtips”, *Microfluid Nanofluid*, Vol.13, pp.217–225, 2012.
- [60] D. Kalyanasundaram, J.-H. Kim, W.-H. Yeo, K. Oh, K.-H. Lee, M.-H. Kim, S.-M. Ryew, S.-G. Ahn, D. Gao, G. A. Cangelosi, J.-H. Chung, “Rapid extraction and preservation of genomic DNA from human samples”, *Anal Bioanal Chem*, Vol.405, pp.1977–1983, 2013.
- [61] Faisal A. Shaikh and Victor M. Ugaz, “Collection, focusing, and metering of DNA in microchannels using addressable electrode arrays for portable low-power bioanalysis”, *PNAS*, Vol.103, pp.4825– 4830, 2006.
- [62] Ho Suk Lee, Wai Keung Chu, Kun Zhang, and Xiaohua Huang, “Microfluidic devices with permeable polymer barriers for capture and transport of biomolecules and cells”, *Lab Chip*, Vol.13, pp.3389-3397, 2013.

- [63] Rahul Dhopeswarkar, Li Sun, and Richard M. Crooks, “Electrokinetic concentration enrichment within a microfluidic device using a hydrogel microplug”, *Lab Chip*, Vol.5, pp.1148–1154, 2005.
- [64] Takahito Nakagawaa, Tsuyoshi Tanakaa, Daisuke Niwab, Tetsuya Osakab, Haruko Takeyamaa, Tadashi Matsunaga, “Fabrication of amino silane-coated microchip for DNA extraction from whole blood”, *Journal of Biotechnology*, Vol.116, pp.105–111, 2005.
- [65] Weidong Cao, Christopher J. Easley, Jerome P. Ferrance, and James P. Landers, “Chitosan as a Polymer for pH-Induced DNA Capture in a Totally Aqueous System”, *Anal. Chem.*, Vol.78, pp.7222-7228, 2006.
- [66] Jungkyu Kim and Bruce K. Gale, “Quantitative and qualitative analysis of a microfluidic DNA extraction system using a nanoporous AlO_x membrane”, *Lab Chip*, Vol.8, pp.1516–1523, 2008.
- [67] Hiroyuki Ota, Tae-Kyu Lim, Tsuyoshi Tanaka, Tomoko Yoshino, Manabu Harada, and Tadashi Matsunaga, “Automated DNA extraction from genetically modified maize using aminosilane-modified bacterial magnetic particles”, *Journal of Biotechnology*, Vol.125, pp.361–368, 2006.
- [68] Marc Karlel, Junichi Miwa, Gunter Roth, Roland Zengerle, and Felix von Stetten, “A Novel Microfluidic Platform for Continuous DNA Extraction and Purification using Laminar Flow Magnetophoresis”, *IEEE 22nd International Conference on Micro Electro Mechanical Systems*, pp.276 – 279, 2009.
- [69] Małgorzata A. Witek, Shawn D. Llopis, Abigail Wheatley, Robin L. McCarley, and Steven A. Soper, “Purification and preconcentration of genomic DNA from whole

- cell lysates using photoactivated polycarbonate (PPC) microfluidic chips”, *Nucleic Acids Research*, Vol. 34, pp.e74, 2006.
- [70] Kathryn A. Melzak, Chris S. Sherwood, Robin F.B. Turner, and Charles A. Haynes, “Driving Forces for DNA Adsorption to Silica in Perchlorate Solutions”, *Journal of Colloid and Interface Science*, Vol.181, pp.635–644, 1996.
- [71] J. T. Trevors, “DNA in soil: adsorption, genetic transformation, molecular evolution and genetic microchip”, *Antonie van Leeuwenhoek*, Vol.70, pp.1-10, 1996.
- [72] Joel Voldman, “Dielectrophoretic Traps for Cell Manipulation”, *BioMEMS and Biomedical Nanotechnology*, pp.159-186, 2007.
- [73] George M. Whitesides, “The origins and the future of microfluidics”, *NATURE*, Vol.442, pp. 368-373, 2006.
- [74] Jean-Louis Viovy, “Electrophoresis of DNA and other polyelectrolytes: Physical mechanisms”, *Rev. Mod. Phys.*, Vol.72, pp.813-872, 2000.
- [75] Cohen, Adam E. "Trapping and manipulating single molecules in solution." *PhD diss.*, Stanford University, 2006.
- [76] Kevin D. Dorfman, “DNA electrophoresis in microfabricated devices”, *Rev. Mod. Phys.*, Vol.82, pp.2903, 2010.
- [77] Blanca H. Lapizco-Encinas, Sandra Ozuna-Chacón, and Marco Rito-Palomares, “Protein manipulation with insulator-based dielectrophoresis and direct current electric fields”, *Journal of Chromatography A*, Vol.1206, pp.45-51, 2008.
- [78] Noah G. Weiss, Paul V. Jones, Prasun Mahanti, Kang P. Chen, Thomas J. Taylor, and Mark A. Hayes, “Dielectrophoretic mobility determination in DC insulator-based dielectrophoresis”, *Electrophoresis*, Vol.32, pp.2292–2297, 2011.

- [79] John Doe, Richard Miles, Richard Roe, and Claus Santa, “Electroosmotic Flow (DC)”, *Encyclopedia of Microfluidics and Nanofluidics*, pp.560-567, 2008.
- [80] Walter Schrott, Zdeněk Slouka, Petr Červenka, Jiří Šton, Marek Nebyla, Michal Příbyl, and Dalimil Šnita, “Study on surface properties of PDMS microfluidic chip treated with albumin”, *Biomicrofluidics*, Vol.3, 044101, 2009.
- [81] M. Wolf, R. Gulich, P. Lunkenheimer, A. Loidl, “Broadband Dielectric Spectroscopy on Human Blood”, *Biochim. Biophys. Acta.*, pp.727, 2011.
- [82] J. L. Aragonés, L. G. MacDowell, and C. Vega, “Dielectric Constant of Ices and Water: A Lesson about Water Interactions”, *J. Phys. Chem. A*, Vol.115, pp.5745–5758. 2011.
- [83] Liming Yu, Francis E H Tay, Guolin Xu, Bangtao Chen, Marioara Avram and Ciprian Iliescu, “Adhesive bonding with SU-8 at wafer level for microfluidic devices”, *Journal of Physics: Conference Series*, Vol. 34, pp. 776–781, 2006.
- [84] MicroChem Corp., “SU-8 2000 Permanent Epoxy Negative Photoresist”, *product datasheet*.
- [Online] <http://www.microchem.com/pdf/SU-82000DataSheet2025thru2075Ver4.pdf>
- [85] J. Cooper McDonald, David C. Duffy, Janelle R. Anderson, Daniel T. Chiu, Hongkai Wu, Olivier J. A. Schueller, and George M. Whitesides, “Fabrication of microfluidic systems in poly(dimethylsiloxane)”, *Electrophoresis*, Vol. 21, pp. 27-40, 2000.
- [86] J C Lötters, W Olthuis, P H Veltink and P Bergveld, “The mechanical properties of the rubber elastic polymer polydimethylsiloxane for sensor applications”, *Journal of Micromechanics and Microengineering*, Vol. 7, pp. 145–147, 1997.

- [87] “Information about Dow Corning® Brand Silicone Encapsulants”, product datasheet.
[Online] <http://bdml.stanford.edu/twiki/pub/Rise/PDMSProceSS/PDMSdatasheet.pdf>
- [88] A. Colas, R. Malczewski, and K. Ulman, “Silicone Tubing for Pharmaceutical Processing”, Dow Corning, Life Sciences.
[Online] <http://www.dowcorning.com/content/publishedlit/52-1067-01.pdf>
- [89] H. Hillborg, J.F. Ankner, U.W. Gedde, G.D. Smith, H.K. Yasuda, and K. Wikstrom, “Crosslinked polydimethylsiloxane exposed to oxygen plasma studied by neutron reflectometry and other surface specific techniques”, *Polymer*, Vol.41, pp.6851–6863, 2000.
- [90] “Quant-iT™ PicoGreen ® dsDNA Reagent and Kits”, *product datasheet*, Invitrogen.
[Online] <http://tools.lifetechnologies.com/content/sfs/manuals/mp07581.pdf>
- [91] “λDNA/ Hind III Fragments”, *product datasheet*, Invitrogen.
[Online] <https://tools.lifetechnologies.com/content/sfs/manuals/15612013.pdf>
- [92] Jung K, Fleischhacker M, and Rabien A, “Cell-free DNA in the blood as a solid tumor biomarker--a critical appraisal of the literature”, *Clin Chim Acta*. Vol.411, pp.1611-24, 2010.
- [93] Victoria L. Singer, Laurie J. Jones, Stephen T. Yue, and Richard P. Haugland, “Characterization of PicoGreen Reagent and Development of a Fluorescence-Based Solution Assay for Double-Stranded DNA Quantitation”, *ANALYTICAL BIOCHEMISTRY*, Vol.249, pp.228–238, 1997.
- [94] A. I. Dragan, J. R. Casas-Finet, E. S. Bishop, R. J. Strouse, M. A. Schenerman, and C. D. Geddes, “Characterization of PicoGreen Interaction with dsDNA and the

- Origin of Its Fluorescence Enhancement upon Binding”, *Biophysical Journal*, Vol.99, pp.3010–3019, 2010.
- [95] Philip Serwer, “Agarose gels: Properties and use for electrophoresis”, *Electrophoresis*, Vol.4, pp.375-382, 1983.
- [96] H. MALONGA, J.F. NEAULT, H. ARAKAWA, and H.A. TAJMIR-RIahi, “DNA Interaction with Human Serum Albumin Studied by Affinity Capillary Electrophoresis and FTIR Spectroscopy”, *DNA AND CELL BIOLOGY*, Vol. 25, pp. 63-68, 2006.
- [97] Victoria L. Singer, Laurie J. Jones, Stephen T. Yue, and Richard P. Haugland, “Characterization of PicoGreen Reagent and Development of a Fluorescence-Based Solution Assay for Double-Stranded DNA Quantitation”, *ANALYTICAL BIOCHEMISTRY*, Vol.249, pp.228–238, 1997.
- [98] Jun Xu, Xiaomei Zhang, Rosana Pelayo, Marc Monestier, Concetta T. Ammollo, Fabrizio Semeraro, Fletcher B. Taylor, Naomi Esmon, Florea Lupu, and Charles T. Esmon, “Extracellular histones are major mediators of death in sepsis”, *Nat Med.*, Vol.15, pp.1318–1321, 2009.
- [99] Kim H. Wong and Kenneth L. Campbell, “Factors That Affect Use of Intercalating Dyes Such as PicoGreen, SYBR Green I, Syto-13 and Syto-82 in DNA Assays”, *Biology of Reproduction*, Vol.85, pp.725, 2011.
- [100] D Rickwood and B D Hames, “Gel Electrophoresis of Nucleic Acids A Practical Approach (Second Edition)”, *Oxford University Press*, Oxford, 1990.
- [101] Esposito A, Bardelli A, Criscitiello C, Colombo N, Gelao L, Fumagalli L, Minchella I, Locatelli M1, Goldhirsch A, Curigliano G, “Monitoring tumor-

derived cell-free DNA in patients with solid tumors: Clinical perspectives and research opportunities”, *Cancer Treat Rev.*, Vol.40, No.5, pp.648-55, 2014.

Appendix A:

Model Setup in COMSOL Simulation

1. Model Initialization:

- Select *3D* model, *Electrostatics AC/DC Module* and *Stationary Studies*.

2. Geometry

- At Geometry 1, set dimension unit as micrometer “ μm ”.
- Sample channel: Set a solid *block* with dimensions of 5000 (Width) \times 100 (Depth) \times 60 (Height) with the corner at the position $x=-2500$, $y=-50$, $z=0$. The *axis* is $(x,y,z)=(0,0,1)$.
- Accumulation channel: Set a solid *block* with dimensions of 500 (W) \times 5000 (D) \times 160 (H) with the corner at the position $x=-250$, $y=-2550$, $z=-160$. The *axis* is $(x,y,z)=(0,0,1)$.
- Sample reservoir: Set a solid *cylinder* with dimensions of 750 (Radius) \times 220 (Height) with the corner at the position $x=-2000$, $y=0$, $z=-160$. The *axis* is $(x,y,z)=(0,0,1)$.
- Electrode (sample channel): Set a solid *cylinder* with dimensions of 100 (Radius) \times 500 (Height) with the corner at the position $x=2000$, $y=0$, $z=30$. The *axis* is $(x,y,z)=(0,0,1)$.

- Electrode (accumulation channel): Set a solid *cylinder* with dimensions of 100(Radius) \times 500(Height) with the corner at the position $x=0, y=2000, z=-100$. The *axis* is $(x,y,z)=(0,0,1)$.
- Click *Build All*. The built geometry is as shown in **Figure A1**.

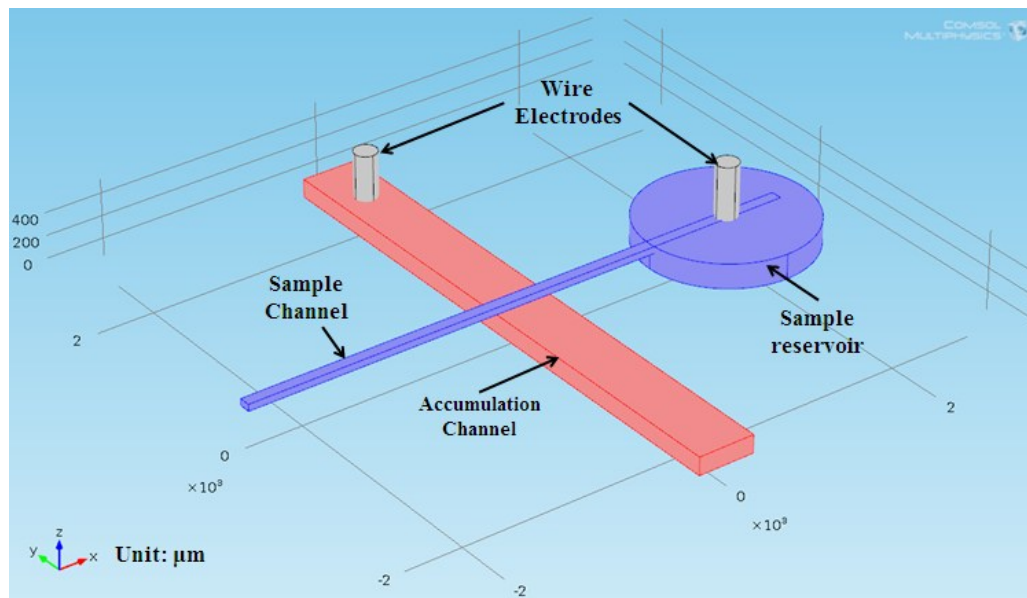


Figure A1: model geometry.

3. Materials:

- Define the sample channel and sample reservoir as “*water, liquid*” from the material library. Set “relative permittivity” as 70 and “electrical conductivity” as 0.01S/m (parameters for blood plasma).

- Define the accumulation channel as “*water, liquid*” from the material library. Set “relative permittivity” as 78.
- Define the two electrodes as *silver (Ag)* from the material library.

4. Electrostatics Module Setup

- Set *Charge Conservation* for all domains.
- Set *Zero Charge* boundary condition for the domains except for the two electrodes.
- Set *Initial Value* as 0 electric potential for the all domains ($V = 0$).
- Set *Electric Potential* boundary condition as 9V for the electrode in accumulation channel ($V = 9V$).
- Set *Ground* boundary condition for the electrode in sample channel ($V = 0V$).

5. Meshing

- Set *Free Tetrahedral* mesh type for all domains.
- Set Size as *Fluid dynamics, Normal*.
- Set Size 1 for two electrodes as *General physics, Extra fine*.
- Set Size 2 for sample inlet reservoir as *Fluid dynamics, Extra fine*.
- Set Size 3 for accumulation channel as *Fluid dynamics, Extra fine*.
- Set Size 3 for sample channel as *Fluid dynamics, Extremely fine*.
- Click *Build All*.

6. Study

- At Stationary Solver 1, add *Adaptive Mesh Refinement*. Keep the settings as default.
- Select *Compute* to solve the model.

Note: after setting up *Adaptive Mesh Refinement* and solving the model, a *Mesh 2* node will appear under the *Mesh* section. By clicking the node, a refined meshing result can be seen.

7. Post-processing

7.1 Three-dimensional (3D) Plot

- At Electric potential 1 (Data set: Solution 2), add *Contour 1*. Set Expression as “ $es.normE$ ”, unit as “ kV/m ”. Set Number of levels as 400. Keep other settings as default. Click Plot.
- At Electric potential 1 (Data set: Solution 2), add *Arrow Volume 1*. Set Expression as “ $es.Ex$ ” for x component, “ $es.Ey$ ” for y component, “ $es.Ez$ ” for z component. Set Arrow Positioning as $range(-300,5,400)$ for x-grid points, $range(-50,5,50)$ for y-grid points, 1 for z-grid points. Keep other settings as default. Click Plot.
- At Electric potential 1 (Data set: Solution 2), add *Arrow Volume 2*. Set Expression as “ $-d((es.Ex^2 + es.Ey^2 + es.Ez^2), x)$ ” for x component, “ $-d((es.Ex^2 + es.Ey^2 + es.Ez^2), y)$ ” for y component, “ $-d((es.Ex^2 + es.Ey^2 + es.Ez^2), z)$ ” for z component. Set Arrow Positioning as $range(-300,5,400)$ for x-grid points, $range(-50,5,50)$ for y-grid points, 1 for z-grid points. Keep other settings as default. Click Plot.

- At Electric potential 1 (Data set: Solution 2), add *Slice 1*. Set Expression as “*es.normE*”, unit as “*kV/m*”. Set Plane as *xy-planes*, z-coordinates as *1*. Keep other settings as default. Click Plot.

7.2 One-dimensional (1D) Plot

- At Data Sets, add *Cut Plane 1*. Set Data set as *Solution 2*, Plane as *xy-planes*, and z-coordinates as *1*.
- At Data Sets, add *Cut Plane 2*. Set Data set as *Solution 2*, Plane as *yz-planes*, and x-coordinates as *250*.
- At Data Sets, add *Cut Line 2D 1*. Set Data set as *Cut Plane 1*, Point 1 as $x=-300, y=0$, Point 2 as $x=400, y=0$.
- At Data Sets, add *Cut Line 2D 2*. Set Data set as *Cut Plane 1*, Point 1 as $x=250, y=50$, Point 2 as $x=250, y=-50$.
- At Data Sets, add *Cut Line 2D 3*. Set Data set as *Cut Plane 2*, Point 1 as $x=0, y=60$, Point 2 as $x=0, y=-160$.
- At Results, add *1D Plot Group*. Set Data set as *Solution 2*.
- At 1D Plot Group, add *Line graph 1*. Set Data set as *Cut Line 2D 1*. Click Plot.
- At 1D Plot Group, add *Line graph 2*. Set Data set as *Cut Line 2D 2*. Click Plot.
- At 1D Plot Group, add *Line graph 3*. Set Data set as *Cut Line 2D 3*. Click Plot.

8. Data Export

- At Export, add *Plot 1*. Set Plot group as *Electric Potential 1*, Plot *Arrow Volume 1*. Set the destination file. Click Export.
- At *Plot 1*. Set Plot group as *ID Plot Group 3*, Plot *Line Graph 1*. Set the destination file. Click Export.

Appendix B:

Mesh Dependence Test in COMSOL Simulation

One of the fundamental requirements for a numerical model is that the simulated results are not affected by the meshing resolution and methods. Thus in this appendix, 7 different mesh sizes were tested to ensure the simulated electric field intensity at the same location in the model is not changed because of meshing resolution.

In this model based on [Appendix A](#), there are 2 principal parameters controlling the meshing results. One is the *Element Size* (e.g. Extremely Fine, Extra Fine, Finer, Fine, Normal, and so on) of the mesh in various domains. It directly controls the size parameters of meshes, such as maximum/ minimum element size and curvature resolution. By adjusting one or more parameters specifically, the meshing results can be customized to meet certain needs. The other one is the *Adaptive Mesh Refinement*, which is used to minimize the $L2$ norm error estimate by refining or coarsening the meshes built previously based on the *Element Size* parameters. The *Adaptive Mesh Refinement* will substantially increase the accuracy of the solution in the whole model. Meshing results after setting up the two parameters are shown in [Figure B1](#).

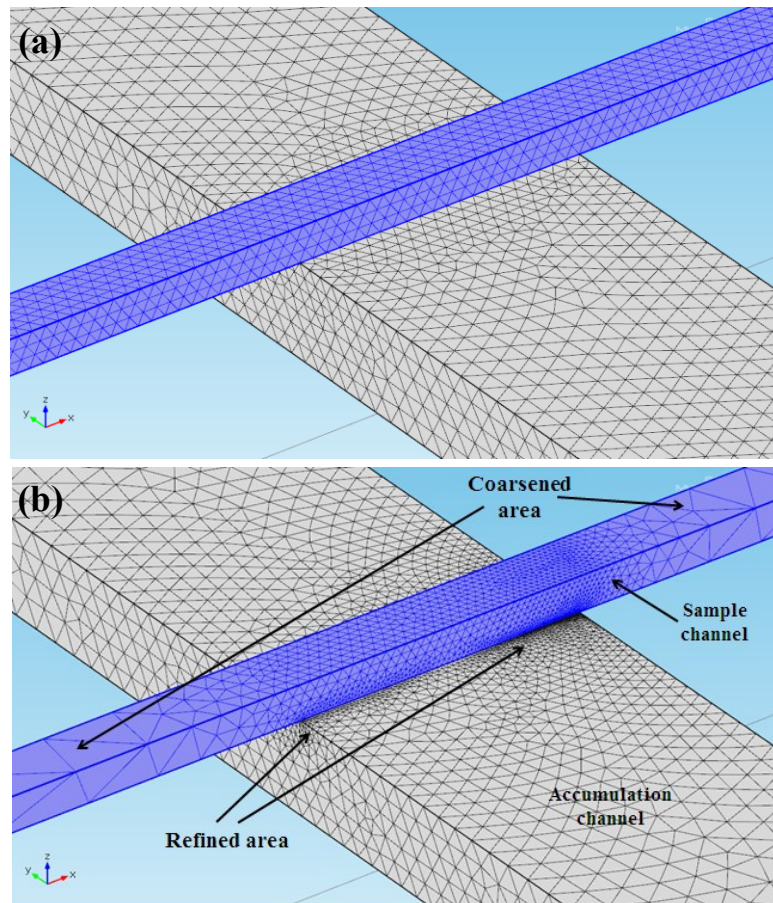


Figure B1: Meshing results (a) after setting up *Mesh Size* and (b) after setting up *Adaptive Mesh Refinement*. The meshes have been adaptively refined or coarsened to minimize the error estimation, which further increase the accuracy of the solution.

Various elements numbers and qualities will be achieved by adjusting the specific settings in the two parameters mentioned above. **Figure B2** demonstrates the change of simulated electric field intensities with different meshing resolutions, which is represented by the total element numbers.

As shown in **Figure B2**, the simulated electric field intensities are independent with the element numbers except for the first point (red), which means as long as the total element number is over 5.1×10^5 , the simulated result is reliable.

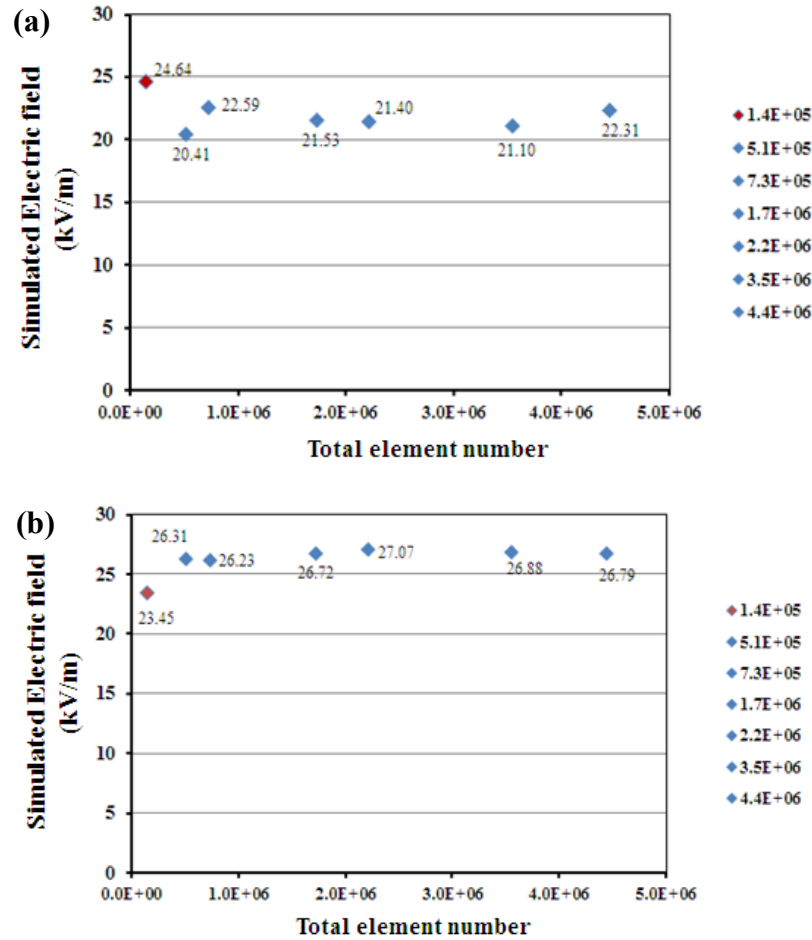


Figure B2: simulated electric field strength vs. total element number (a) at the center of sample channel ($d=50$) and (b) close to the channel wall ($d=5$) at 9V. The definition of d is illustrated in **Figure 3.7** in chapter 3. The two locations are at the edge of the intersection.

In summary, based on the analysis above, a minimum element number of 5.1×10^5 must be set to guarantee the independence of the simulated result with regards to the meshing resolution. To get a smooth curve which reflects the electric field distribution, an element number as high as possible is needed; however, with more elements, the calculation time will be longer.

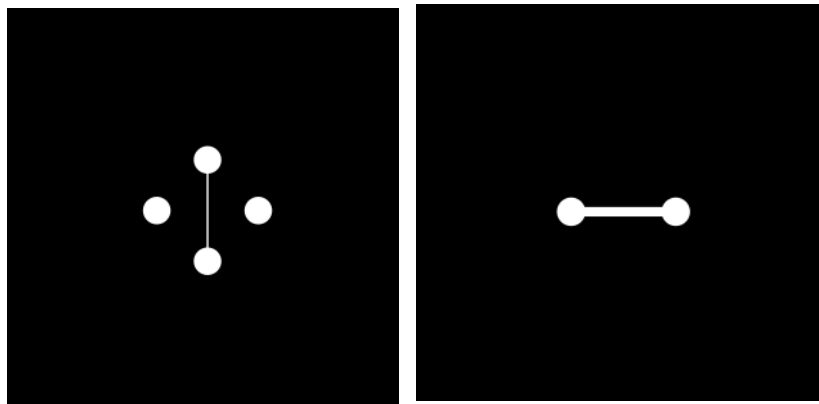
Appendix C:

Device Fabrication

The device were fabricated and assembled following these steps:

9. Mask Preparation

1.1 Design channel features and dimensions using *AutoCAD* as shown below.



Masks for molds fabrication

1.2 Send the file for mask printing.

10. Channel Mold Fabrication in Clean Room

2.1 Immerse a silicon wafer in Acetone (1min), Methanol (1min), and DI water (5min) in order.

2.2 Place the wafer on hot plate of 150°C for 2 minutes.

2.3 Expose the wafer to oxygen plasma at 50 Watts for 30 seconds.

- 2.4 Place the wafer at the center of the spinner chuck.
- 2.5 Spin for sample channel mold (~60 μm): pour about 3ml SU-8 2075 photoresist at the center of the wafer; start spinning at 500 rpm for 5-10 sec with acceleration of 100 rpm/sec; increase the speed up to 4000 rpm with an acceleration of 500 rpm/s, and continue for 30 sec at the final speed.
- 2.6 Spin for accumulation channel mold (~160 μm): pour about 3ml SU-8 100 photoresist at the center of the wafer; start spinning at 500 rpm for 5-10 sec with acceleration of 100 rpm/sec; increase the speed up to 3000 rpm with an acceleration of 500 rpm/s, and continue for 30 sec at the final speed.
- 2.7 Move the wafer from spinner to a hot plate for soft bake.
- 2.8 Soft bake for sample channel mold: keep the wafer on a hot plate at 65°C for 1min and 95°C for 8min. If wrinkles on the photoresist appear during soft bake, remove the wafer from the hot plate, and put it back after the wrinkles gone.
- 2.9 Soft bake for accumulation channel mold: keep the wafer on a hot plate at 65°C for 10min and 95°C for 30min. If wrinkles on the photoresist appear during soft bake, remove the wafer from the hot plate, and put it back after the wrinkles gone.
- 2.10 Mount the mask on the mask aligner.
- 2.11 Align the mask and the wafer, and attach them when alignment is done.
- 2.12 Exposure for sample channel mold: expose the wafer to UV light through the mask for total exposure energy of 160mJ/cm².

- 2.13 Exposure for accumulation channel mold: expose the wafer to UV light through the mask for total exposure energy $648\text{mJ}/\text{cm}^2$.
- 2.14 Move the wafer from mask aligner to a hot plate for post bake.
- 2.15 Post bake for sample channel mold: keep the wafer on a hot plate at 65°C for 1min and 95°C for 7min.
- 2.16 Post bake for accumulation channel mold: keep the wafer on a hot plate at 65°C for 1min and 95°C for 10min.
- 2.17 Immerse the wafer into SU-8 developer solution and occasionally stir until the features are clear.
- 2.18 Rinse the wafer with Isopropyl Alcohol (IPA).
- 2.19 Re-immerses the wafer back in developer solution if white residual appears.
- 2.20 Rinse with DI water, and dry with nitrogen.
- 2.21 Hard bake the wafer on hot place at 150°C for 30min.

11. PDMS Channels Replica and Assembly

- 3.1 Place the wafer for sample channel and the wafer for accumulation channel into two petri dishes respectively.
- 3.2 Mix 10:1 (base: curing agent) PDMS in a beaker by thoroughly string.
- 3.3 Cut two silicone tubing segments ($\sim 1\text{cm}$), and place them on the wafer for sample channel (inlet and outlet respectively).

- 3.4 Pour around 15ml PDMS into each petri dish.
- 3.5 Leave the petri dishes for overnight at room temperature. If PDMS is not thoroughly cured overnight, put the petri dish into oven at 70°C for 30min.
- 3.6 Peel PDMS substrates off the mold, and cut it into appropriate pieces.
- 3.7 Use a 1.2mm puncher to clean the silicone tubing and punch holes for the accumulation channel.
- 3.8 Put the PDMS channels into the air plasma machine, and expose to 18W air plasma for 2min.
- 3.9 Attach a sample channel and an accumulation channel together after alignment.

12. Gel Filling and Electrodes Placement

- 4.1 Weigh 0.02g agarose powder using a scale, and put in a glass beaker.
- 4.2 Drop 2ml 1×TAE buffer into the beaker using a pipette.
- 4.3 Seal the beaker with transparent wraps.
- 4.4 Put the beaker into a microwave, heating for 30s. If the powder is not thoroughly melted, keep heating till the solution become crystal clear.
- 4.5 Use a 1ml syringe with 22G needle to drop two droplets of the heated gel solution at the inlet of the accumulation channel.
- 4.6 Use the same syringe to conduct air aspiration slowly and stably at the outlet of the accumulation channel.

4.7 Hold the syringe at the outlet once the gel is filled in the accumulation channel.

Avoid over aspiration in case of air bubbles get into the accumulation channel.

4.8 Remove the syringe after the solution is gelled.

4.9 Place two silver wire electrodes at the inlet of accumulation channel and the outlet of sample channel respectively.

Appendix D:

Force Calculation

Based on COMSOL simulation and governing equations of the EP force and the DEP force, which are two principal forces in DNA accumulation process, the ratios of EP velocity and DEP velocity (*v ratio*) for DNA and blood cells were calculated with approximation. The results are shown in [Table D1](#) and [Table D2](#).

The equations applied to calculation are illustrated from [Eq. D1](#) to [Eq. D3](#).

$$F_{ep} = qE \quad \text{Eq. D1}$$

$$F_{dep} = 2\pi\epsilon_m r^3 \frac{\sigma_p - \sigma_m}{\sigma_p + 2\sigma_m} \nabla E^2 \quad \text{Eq. D2}$$

$$v_{ratio} = \frac{v_{ep}}{v_{dep}} = -\frac{qE}{\pi r^3 \epsilon_m \nabla E^2} = -\frac{6\zeta_c E}{r^2 \nabla E^2} \quad \text{Eq. D3}$$

where q is the particle charge, σ_p and σ_m are conductivity of the particle and the medium respectively, ϵ_m is the permittivity of the medium, r is the radius of the particle, E represents the strength of external electric field, and ∇E^2 stands for the gradient of electric field squared, ζ_c is the zeta potential of a cell. v_{ep} is the EP velocity, and v_{dep} is the DEP velocity.

For DNA molecules:

3V									
Location	DNA size	$E(V/m)$	$\nabla(E^2)$	$q(C)$	$\epsilon m (F/m)$	$r^3(m^3)$	$F_{ep} (N)$	$F_{dep} (N)$	$v \text{ ratio}$
y=0	DNA l=400bp	5897	1.77E+13	-1.28E-16	6.20E-10	1.05E-25	-7.55E-13	-3.62E-21	2.08E+08
	DNA l=23kbp	5897	1.77E+13	-7.36E-15	6.20E-10	1.00E-18	-4.34E-11	-3.45E-14	1.26E+03
y=45	DNA l=400bp	7389	4.22E+13	-1.28E-16	6.20E-10	1.05E-25	-9.46E-13	-8.63E-21	1.10E+08
	DNA l=23kbp	7389	4.22E+13	-7.36E-15	6.20E-10	1.00E-18	-5.44E-11	-8.22E-14	6.62E+02

9V									
Location	DNA size	$E(V/m)$	$\nabla(E^2)$	$q(C)$	$\epsilon m (F/m)$	$r^3(m^3)$	$F_{ep} (N)$	$F_{dep} (N)$	$v \text{ ratio}$
y=0	DNA l=400bp	17000	1.56E+14	-1.28E-16	6.20E-10	1.05E-25	-2.18E-12	-3.18E-20	-6.84E+07
	DNA l=23kbp	17000	1.56E+14	-7.36E-15	6.20E-10	1.00E-18	-1.25E-10	-3.03E-13	-4.13E+02
y=45	DNA l=400bp	21652	2.74E+14	-1.28E-16	6.195E-10	1.05E-25	-2.77E-12	-5.59E-20	-4.96E+07
	DNA l=23kbp	21652	2.74E+14	-7.36E-15	6.195E-10	1.00E-18	-1.59E-10	-5.33E-13	-2.99E+02

15V									
Location	DNA size	$E(V/m)$	$\nabla(E^2)$	$q(C)$	$\epsilon m (F/m)$	$r^3(m^3)$	$F_{ep} (N)$	$F_{dep} (N)$	$v \text{ ratio}$
y=0	DNA l=400bp	28593	3.50E+14	-1.28E-16	6.20E-10	1.05E-25	-3.66E-12	-7.14E-20	-5.12E+07
	DNA l=23kbp	28593	3.50E+14	-7.36E-15	6.20E-10	1.00E-18	-2.10E-10	-6.80E-13	-3.09E+02
y=45	DNA l=400bp	37333	1.08E+15	-1.28E-16	6.20E-10	1.05E-25	-4.78E-12	-2.20E-19	-2.17E+07
	DNA l=23kbp	37333	1.08E+15	-7.36E-15	6.20E-10	1.00E-18	-2.75E-10	-2.10E-12	-1.31E+02

Table D1: Force and velocity calculations for DNA molecules with two different sizes and two different locations in the sample channel. Parameter d is defined as the distance from the location to the sample channel wall as referred to [Figure 3.7](#) in [Chapter 3](#).

For red blood cells:

3V					
Location	$E(V/m)$	$\nabla(E^2)$	$\zeta(V)$	$r^2(m^2)$	v ratio
d=50	5897	1.77E+13	-0.0157	2.03E-11	1.55
d=5	7389	4.22E+13	-0.0157	2.03E-11	0.81
9V					
Location	$E(V/m)$	$\nabla(E^2)$	$\zeta(V)$	$r^2(m^2)$	v ratio
d=50	17000	1.56E+14	-0.0157	2.03E-11	0.51
d=5	21652	2.74E+14	-0.0157	2.03E-11	0.37
15V					
Location	$E(V/m)$	$\nabla(E^2)$	$\zeta(V)$	$r^2(m^2)$	v ratio
d=50	28593	3.50E+14	-0.0157	2.03E-11	0.38
d=5	37333	1.08E+15	-0.0157	2.03E-11	0.16

Table D2: Velocity ratio calculations for red blood cells at two different locations in the sample channel. Parameter d is defined as the distance from the location to the sample channel wall as referred to [Figure 3.7](#) in [Chapter 3](#).

Based on **Table D1**, the dominating force (F_{ep}) increases with increased voltages applied. **Table D3** illustrates the EP force ratio when voltage applied is increased from 3V to 9V (9V/3V), and from 9V to 15V (15V/9V).

Location	Voltage	<i>Fep ratio</i>
d=50	9V/3V	2.88
	15V/9V	1.68
d=5	9V/3V	2.93
	15V/9V	1.72

Table D3: EP force ratio calculations for DNA molecules at two locations. Parameter d is defined as the distance from the location to the sample channel wall as referred to **Figure 3.7** in **Chapter 3**.